MULTI-HOP AND CHANNEL MODELLING FOR WIRELESS BODY AREA NETWORKS AT 60 GHZ

BY

XIAO LI

A thesis submitted to

the University of Birmingham

for the degree of

DOCTOR OF PHILOSOPHY

School of Electronic, Electrical & Systems Engineering

College of Engineering and Physical Sciences

University of Birmingham

March 2015

ABSTRACT

This thesis presents work on antennas and propagation for WBANs at 60 GHz. First, a compact, wearable Vivaldi antenna and Vivaldi antenna array covering the whole unlicensed band from 57 to 64 GHz are proposed to overcome the shadowing due to human movements. Second, multi-hop channels for on-body communication at 60 GHz are investigated through applying the proposed antennas, and it is found that multi-hop wireless network adaption can increase reliability when the separation between sensors exceeds 40 cm compared to single-hop. Radiation pattern diversity is selected among different diversity techniques for providing stable links for 60 GHz WBANs. Results show that radiation pattern diversity enlarges the signal coverage area on the human body, which compensates for the narrow beamwidth antenna, thus more stable links can be established. Finally, a representative channel model for 60 GHz on-body network with an appropriate power control method is presented. With this model and power control method, it has been proved in this thesis that a multi-hop method for on-body communication at 60 GHz is feasible to establish a stable network for different applications.

ACKNOWLEDGEMENTS

My first debt of gratitude must go to my supervisors Dr. Costas Constantinou and Professor Peter S. Hall. The vision, encouragement and advice provided by them enabled me to proceed through the doctoral program and complete my thesis, especially Dr. Costas Constantinou. I appreciate all their unflagging encouragement and serving as role models to me.

I would also like to thank my colleague, Dr. Yuriy I. Nechayev, who has been generous in sharing his knowledge. I want express my gratitude to Mr. Alan Yates and Mr. Warren Hay for providing the technical support. Special thanks go to my nice friends, Dr. Xianyue Wu, Mr. Mofei Guo, Mr. Yasin Kabiri, Mr. Yineng Wang and Mr. Xiang Gao, for their kind friendship.

I also want to thank the School of Electrical, Electronic and Systems Engineering for providing me partial funding to pursue my PhD degree.

Lastly, I want to express my deep love to my parents and brother, for their endless support and understanding.

ACRONYMS

BAN Body Area Network

BSN Body Sensor Network

CDF Cumulative Distribution Function

CIR Carrier to Interference Ratio

FCC Federal Communications Commission

FDTD Finite Difference Time Domain

ISM Industrial Scientific and Medical

LCR Level Crossing Rate

LTCC Low Temperature Co-fired Ceramic

MICS Medical Implant Communication Service

MBAN Medical Body Area Network

RSSI Received Signal Strength Indicator

RMS Root Mean Square

SAR Radiation Absorption Rate

SINR Signal to Interference plus Noise Ratio

SIW Substrate Integrated Waveguide

SNR Signal to Noise Ratio

UWB Ultra-wide Band

VNA Vector Network Analyzer

WBAN Wireless Body Area Network

WLAN Wireless Local Area Network

CONTENTS

LIST OF FIGURES

LIST OF TABLES

CHAPTER 1

INTRODUCTION

1.1 WBANs

Body area networks (BANs), also referred to as wireless body area networks (WBANs) or body sensor networks (BSNs), are a new type of wireless network architecture for wearable computing devices mounted in/on the human body. Generally speaking, the network consists of one central unit (e.g. a base unit) and several sensor units covering the whole body area. All communication is restricted on, near, and around the human body. WBAN technology was proposed around 1995 based on wireless personal area network (WPAN) technologies [1].

With the rapid growth in physiological low power sensors, integrated circuits, systems-on-a-chip and wireless communication technology, it is possible to realise the promise of BANs. Through mounted sensors, a ’ y y
Therefore, information on health status and motion pattern is fairly helpful to realise various novel and interesting applications such as healthcare, entertainment, interactive gaming, as well as military applications. The wireless body area network (WBAN) concept has been noticed by many industries a long time ago. Companies such as Apple and Heapslylon have been trying to explore the possibility of wearable devices for recording daily human body activity. Some impressive wearable products have made it to market, such as Google Glass® and Fitbit®. Among all these applications, healthcare is the most attractive application due to the trend of world population age growth. According to the population

report from US Bureau of Census, the number of retired people (65-84 year olds) will be up to 81 million in 2050. That will cause tremendous pressure to the existing health care systems, thus affecting the quality of life [2]. Furthermore, it is estimated that the overall health care expenditure would increase to $6 trillion in 2020 [3]. Therefore, WBANs technology is a good candidate to help solve the impending health care crisis. A WBAN can provide inexpensive and long term health monitoring with ' y . Through integrated sensors, fatal diseases can be detected at an early stage and health recovery from surgery can also be supervised easily.

1.2 WBANs Applications

Some WBAN technologies have drawn a lot of attention for military, health care, and entertainment applications y ' q y of life or safety, and have specific requirements. Some promising and popular WBAN applications are discussed below:

A. Medical applications

WBANs can be used to continuously monit ' W development of advanced medical sensors and wireless technology, the service model of healthcare might be changed fundamentally and the detection and management of diseases will become more easy and convenient. Some vital signs such as body temperature, blood pressure and heartbeat can be monitored at any time and any place and all such information can be synchronised to a cellular network where users themselves and doctors can implement a timely treatment. By using these applications, some fatal diseases such as hypertension,

diabetes and cardiovascular can be prevented at an early stage. Further classification of WBANs medical applications are shown following:

1) Wearable WBAN: Some wearable medical applications used in human performance management have been recently publicized. For instance, athletes can tune their training schedule according to parameters captured by the sensors, thus unscientific training and unnecessary injuries can be prevented. Moreover, sleep disorders have caused inestimable losses to people, so sleep monitoring has received much attention. Some WBANs applications have been developed to help users improve their sleep qualities.

2) Implant WBAN: Implanted nodes are always put underneath the skin and can monitor the ’s physiological function, thus reducing the risk of potential illness and even provide the information about proper dosing of medication. With the help of these implanted nodes it is possible to monitor, treat or prevent some illness such as cardiovascular or kidney diseases.

3) Remote monitoring: WBAN ’ , therefore, patients who are in the recovery process can send their real time feedback to their own doctors without showing up at the hospital. Internet connectivity thus eliminates the distance between patients and their doctors.

B. Other applications

There are many interesting applications of WBANs, which can be categorised as follows:

1) Real time data streaming: Many applications can bring people convenience on different occasions: For instance, video streaming can be used when a video clip is captured by a phone and audio streaming can be realized through voice communication between different headsets e.g. providing guidance in a museum or schedule information at a train station. Finally, stream transfer can be used to control body-based entertainment devices.

2) Entertainment: The most popular applications are gaming and social networking. Many wearable entertainment devices, such as microphones, cameras and other advanced appliances, can be integrated in WBANs used for game controlling, item tracking, information exchanging, etc.

3) Emergency: Off-body sensors can send people an alarm when some serious problems are happening. For example, if an empty room is on fire, people in another room can be notified by sensors installed in the house and this can reduce the impact of a fire.

4) Emotion detection: With the help of advanced bio-sensor and sensing technologies, it is possible to detect human emotion through temperature, pulse, respiratory and blood pressure. For instance, advanced sensors may be able to justify small changes of human emotion when people are telling lies.

5) Security: The applications about security issues have always been the most important part of WBANs utilization. Given these applications, some unique body characteristics or behavior can be used for secure authentication.

1.3 WBANs Classification

Generally, a WBAN can be divided into two parts: in-body and on-body area network. In-body area networks rely on the feasibility of implanting biosensors that allow communication between inside and outside the body, while on-body area networks allow communication between wearable sensors and a base station.

1) In-body: There are many basic requirements for the In-body antennas to avoid causing unexpected side effect to human body. First of all, the material being implanted in the body must have some certain properties, such as being bio-compatible and having non-corrosive chemistry [4]. Secondly, according to the FCC, the first licensed band for in-body Communication is in the frequency range of 402-405 MHz, called Medical Implant Communication Service (MICS). Conventional antennas operating at this frequency will be too big to put into the human body. Therefore, designers have to confront these serious challenges.

Investigations of in-body signal propagation characteristics are quite difficult because measurements can only be conducted in a human phantom which can simulate the human tissues approximately. The authors in [5] have done several investigations on the performance of various antennas inside a phantom, and it was found that the penetration depth and polarization of antennas affects the propagation pattern significantly. Although the in-body link was evaluated by using a phantom, the results were still indicative of in-body propagation characteristics.

2) On-body: To design an on-body antenna, two things have to be considered first; antenna radiation pattern; and antenna sensitivity to body tissues. Loop, patch, patch

array antennas and monopole antennas were designed just for on-body communication in [6]. They were compared according to the path loss performances, and it was found that the scenario of monopole to monopole possesses the least path loss and the highest path gain. The directional patch antennas were found to reduce multi-path fading caused by the surrounding environment.

The signal propagation characteristics of on-body communication systems seem more complex because the signals propagating across the body surface may contain surface waves, creeping waves, diffracted waves, and scattered waves [7], which also indicates that the placements of antennas are also crucial to the channel propagation characteristics. Unlike the case of in-body, antennas for on-body communication are required to have an end-fire radiation pattern, as well as an appropriate polarisation.

1.4 Research Challenges

Much research has been carried out based on both measurement and simulation to support the development of wearable antennas with better radiation pattern, and link performance prediction for different sensor placement scenarios. Various frequency bands, such as 400 MHz, 900 MHz, 2.4 GHz and 3.1~10.6 GHz introduced in Chapter 2, have been investigated for on-body sensors. However, there are still problems and challenges in WBAN ' realization:

1) Environmental influences: WBANs always suffer from high path loss which may be caused by body absorption or other reasons, especially at millimetre band frequencies. Moreover, different environments will have different effects on WBAN performance. For instance, WBANs in a typical office room will experience more multi-path than that those used in open spaces. Also, human movement and interference from adjacent

WBANs may result in interruption of operation or errors in the reported sensor data. To avoid these problems, many sensors should be mounted on or implanted in human subjects at various positions forming multi-hop networks. Therefore, sensor design is a very important issue because the effect of the human body needs to be considered carefully in variety of scenarios and this is very complex. Additionally, some WBAN applications may have specific requirements that will constraint the design in terms of material, size and RF environment.

2) Power consumption: Appropriate wireless technology protocols that enable WBANs to consume less power are a big challenge. Designers have to achieve further advancement on radio hardware and channel sensing algorithms to decrease power consumption. According to [8], the peak power consumption when a WBAN is in a stand-by mode cannot exceed 0.1mW, while the power can be up to 30mW when the WBAN is in a fully active mode.

3) Interference: It is one of the main shortcomings of WBAN technology. With the development of wearable devices, more and more WBANs will coexist, thus interference ' j WBAN y P designers have to consider how to minimize or avoid such interference. Furthermore, as mentioned above, the control of transmit power is not only crucial to the power consumption but also to the generated interference level. In the vicinity of a WBAN low power transmission can minimize interference efficiently. Lastly, the interference may come from the sensors in the same WBAN, so the designers need to consider how to arrange the positions of sensors to eliminate this effect as much as possible.

4) Security: So far, most the of existing security protocols for other wireless communication networks cannot fully satisfy the security requirement of WBANs because they need to enable data transmission that is secure, private and accurate among various WBANs. For instance, patient information detected by sensors needs to be sent to a doctor in a manner which is secure and clearly identifiable and only available to specific authorised people. Moreover, WBANs are facing some non-technical factors such as social acceptance, regulatory, ethical and legal issues, which may slow down their adoption.

5) Data transfer: WBANs mounted on/in the human body may be employed in different applications, so information exchange between different applications can lead to a very complex data transfer procedure. To ensure consistent data transfer, the transmission frequency, data rate and transmit power should be designed for specific applications. In addition, due to the limited memory and battery life, protocol information on retransmission and efficient reception acknowledgment are required during data transfer.

These challenges have driven wireless system researchers to find a solution in the Extra High Frequency (EHF) bands starting from 30 GHz to 300 GHz. It has been identified that the 60 GHz band is more suitable for short-range (< 100 m) wireless communication due to its unique propagation characteristics such as high free space loss, oxygen absorption and rain attenuation. Although the coverage range is limited, it allows a high level frequency re-use. Applications such as high-speed data exchange between portable devices and a base station and uncompressed high definition television can be realised with increased speed by 60 GHz technology.

1.5 WBANs at the Millimetre Band

The millimetre band has the advantages to face above challenges, which are small RF components, low visibility and interference, a wide available spectrum (57-64 GHz), high data rates and so on. Although the cost of producing devices at this frequency is still high, with the development in chipsets manufacturing the band has been opened by some leading authorities (INTEL and IBM), and various standards have been made such as IEEE 802.15.3c [9] and 802.11ad [10].

Compared to microwave frequencies, the unlicensed free spectrum from 57-64 GHz is a good candidate for next generation wireless communication systems. Samsung has announced that the development of a system based on 60 GHz for the future 5G mobile communications [11], and some WLAN device manufacturers have also proposed their hybrid WLAN solution having 60 GHz for short distance and line-of-sight communications.

However, research into on-body antennas and propagation at 60 GHz band is still limited, and no explicit standards appeared, which motivate the author to do research on both on-body antennas and propagation at 60 GHz.

1.6 Layout of the Thesis

This thesis consists of 7 chapters:

Chapter 2 provides a background on wireless body area networks, focusing on the antennas and propagation aspects. First, the state of art on wearable antennas at different frequencies

for different applications for WBANs is presented. Then, the on-body channel investigations at various frequencies are reviewed

Chapter 3 presents the measurement methodology, and the advantages and limitations of used equipments are discussed.

A new proposed antenna for on-body communication at 60 GHz is introduced in Chapter 4. The applications of the proposed antenna are also given in this section.

Chapter 5 involves the investigations on multi-hop on-body channels for 60 GHz WBANs. A simple thresholding algorithm and the channel modelling are described in this chapter as well.

Chapter 6 discusses the diversity at 60 GHz. The results show that the diversity technology is very helpful to form a reliable link in WBANs at 60 GHz.

Chapter 7 presents a representative network model to describe the states of multi-hop 60 GHz on-body channels in different movement scenarios. Also, a power control algorithm is proposed to extend the lifespan of the sensors. By using this model, it shows that networks performed with better reliability than using simple fixed threshold.

The final Chapter 8 arrives at conclusions and proposes possible future work on this topic.

CHAPTER 2

LITERATURE REVIEW OF TECHNOLOGIES IN WBANS

2.1 Introduction

There are many unlicensed frequency bands for use by WBANs developed by the IEEE 802.15.16 group, such as 403 MHz for medical implant communication services, ISM bands (434 MHz, 915 MHz and 2.45 GHz) and UWB band (3.1 GHz to 10.6 GHz) [12-48]. Therefore, research has been conducted at various frequencies on antennas and propagation for WBANs. It has been found that the requirements, as well as performance, on antennas and propagation varied significantly with different frequency bands, thus the advantages and disadvantages of each band are still being debated. For instance, the desired signals always suffer less attenuation at a lower frequency comparing to a higher frequency, but there are some shortcomings at the same time such as more interference from surrounding environment, lack of radiation control and lower data rates.

Wearable antennas are different from other kinds of antennas, because there are some specific requirements , , ,
they must be compact, light weight, low profile and conformal to the human skin. These requirements can be met by employing printed antennas fabricated on thin and flexible substrates. Moreover, wearable antennas cannot be sensitive to proximity to the human body,

and their properties must be stable when they are mounted on the body surface. A ground plane or an electromagnetic band-gap surface can be used to meet this requirement. Finally, it is advantageous that wearable antennas can improve the channel performance and reduce the surrounding interference. To satisfy this demand, directional antennas or tuneable antennas can be used. Additionally, the positions where antennas are placed are also important, which may excite differing propagation modes for the EM waves.

Existing investigations on antenna design and propagation characteristics at various frequencies will be introduced in the following sections, and the reasons of adopting 60 GHz technology for WBANs will also be given.

2.2 Relevant Concepts and Parameters

There are some relevant concepts and parameters that are used in the following chapters. Therefore, these concepts and parameters are introduced before any research on WBANs technologies are discussed.

2.2.1 Path loss and path gain

Path loss is one of the most important parameters in wireless communications, because it can be used to estimate the channel performances between transmitters and receivers. According to the definition of free-space path loss, in an ideal condition the path loss only depends on the distance between the transmitter and receiver and the signal frequency. The equation for free-space path loss is:

$$FSPL = (\frac{4\pi df}{c})^2 \quad (2\text{-}1)$$

Where *d* is the distance between transmitter and receiver, *f* is the signal frequency, and *c* is the speed of light. However, in a real life environment many situations can cause path loss. The environment is very important to signal path loss, because refraction, diffraction and reflection may occur besides the free-space loss.

For the case of on-body communication, the path loss is used to describe the on-body channels. Parameters related to the location of antennas as well as the activities that the human subject is conducting are all important. Path loss (P_L) in dB is the ratio of the sum of transmit power (P_t) and the transmitter antenna gain (G_t) to the sum of receiver antenna gain (G_r) and receive power (P_r):

$$P_L = P_t + G_t + G_r - P_r \text{ in dB} \tag{2-2}$$

While path gain (P_G) is the reverse of path loss and which is:

$$P_G = P_r - (P_t + G_t + G_r) \text{ in dB} \tag{2-3}$$

2.2.2 Diversity

Fading in wireless communication channels can be categorised as long-term and short-term fading and is unavoidable because in real life the channel is always affected by the surrounding environment which causes various path loss as mentioned above. Under certain circumstances whose many obstacles exist between transceivers and channel fading may affect the quality of service and even destroy the reliability of the channel. Therefore, diversity is employed to improve the channel performance and overcome the fading. The

principle is to combine two or more uncorrelated branches, thus fading can be minimized and a reliable channel can be established.

Antenna diversity is one of the most popular ways of implementing diversity reception. To realise antenna diversity, multiple antennas are adopted at the transmitter end or receiver end in the wireless communication system.

2.2.3 Diversity Combining

Signal to noise ratio (SNR) can be improved through combining the multiple signals from those branches. Usually, there are four ways to realise this combining, which are Switched Combining (SWC), Selection Combining (SC), Equal Gain Combining (EGC), and Maximal Ratio Combining (MRC).

In general, the receiving branches will be weighted and added, which can expressed by the following equation:

$$y(t) = \sum_{i=1}^{N} a_i r_i(t) \tag{2-4}$$

Where y (t) is combined signal, a_i is the weight of the i^{th} branch and $r_i(t)$ is the received signal level of the i^{th} branch. Figure 2.1 can help to visualize the combining process.

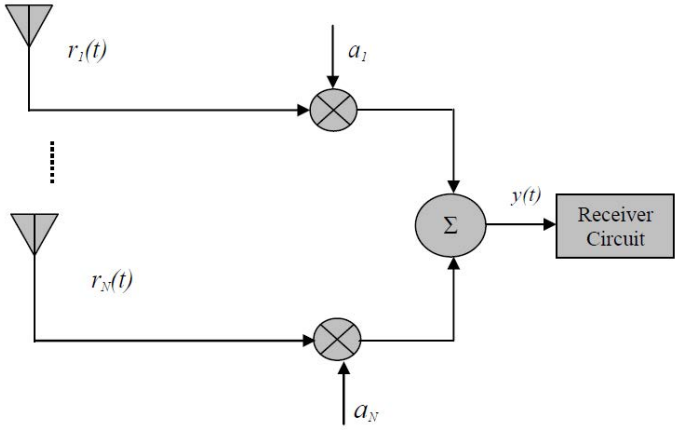

Figure 2.1 Demonstration of diversity combining

For switched combining, a pre-defined threshold referring to SNR is required to justify which branch of the received signal should be picked out of all branches. However, it is hard to measure the SNR value in a practical system, instead, the signal strength plus noise is used [49]. After the comparison among all branches, the highest value is selected and the weight of this branch is 1, while the remaining branches are ignored.

The method of selection combining is very similar with that of switched combining. The only difference is that it does not require a pre-defined threshold. The branch with highest SNR will be chosen and its weight will be 1, while the weight of the other branches will be 0.

The other two combining methods MRC and EGC require signal co-phasing, thus the cost of system and complexity will increase. Due to the particularity of human activities, these two combining technologies will not be involved in our research. More details about co-phasing, MRC and EGC are given in [49-51].

2.3 Antennas and Propagation at Lower Frequencies for WBANs

Different types of antennas have been found suitable for being mounted on the human body, such as top loaded monopoles, patch antennas, slot antennas and aperture coupled patch antennas. Details can be found in [52-69].

So far most studies have focused on the 2.45 GHz ISM band because a wide range of applications work at this frequency. Therefore, this band is chosen as a benchmark for the investigation of antennas and propagation at 60 GHz. It is found in [70, 71] that signals are much stronger with the polarisation perpendicular to the body surface. Tangentially polarised waves attenuate much quicker than the perpendicularly polarised wave. In addition, a creeping wave is used to describe azimuthally propagating waves and details about creeping wave and surface waves are referred in [70, 72].

Fading is more complex in WBANs compared to cellular communications. Human body movements and the surrounding environment cause short-term fading and long-term fading, including shadowing in WBAN channels. Researchers have proved that Rician or Nakagami-m distribution describes the short-term fading at 2.45GHz, and the log-normal or gamma distribution describes the long-term fading. Details can be found in [14, 16, 17, 19, 21, 27, and 28]. In addition, to overcome the fading in WBANs diversity reception can be adopted, and the full study about diversity for WBANs at various lower frequencies is presented in [25].

Finally, interference is always one of the most vital factors in a wireless body area communication system. Unlike the cellular system, the variable nature of WBANs might give rise to unexpected interference. For instance, mutual interference between BANs can occur

frequently in a crowded environment such as a shopping mall, school and hospital. For this case, the interference arises from adjacent WBANs. However, interference can also come from the environment, especially at some bands where many standards are co-located. To solve the interference problems, it is common to consider this issue at higher layers of OSI model [73]. However, it is preferable to minimise these problems at physical layer.

Researchers in [74-76] have presented co-channel interference investigations at 2.45 GHz. All kinds of factors which might cause interference were considered in an indoor environment, and SIR was employed to evaluate the received signals. It was found that interference caused by various body movements was much stronger than that caused by increasing the distance between persons.

2.4 Antennas and Propagation at 60 GHz for WBANs

Recently, due to advantages in millimetre wave radio communication, such as the allocation of large amounts unlicensed spectrum, high data rate (up to 5 Gb/s), higher security and lower interference, many types of antenna operating at the millimetre band were proposed. Unlike the wearable antennas at microwave frequency, the antennas' performance at the millimetre wave band can be easily affected by the feeding structure. Therefore, an investigation on the influence of feeding structure was included in [77]. Two patch antennas, a microstrip patch antenna and an aperture coupled patch antenna, were compared both in free space and on a phantom. It was found that there was rarely any adverse influence of the human body on both of these antennas, and their performance was quite stable as well. However, they were quite different with respect to their SAR. The aperture coupled patch antenna suffered much more

absorption than the microstrip patch antenna. Therefore, it is better to avoid the aperture coupled feeding structure in wearable antenna design.

Textile antennas at this frequency band are very difficult to fabricate on a textile surface. The technological fabrication process was introduced in [78, 79]. Instead of cutting the metallic part separately, the process mentioned in the references is to carve the desired shape in one piece and then remove the undesired part.

On-body antennas must be light-weight, low profile and conformal to the human body. An end-fire radiation pattern and medium gain are also necessary to minimise the losses and high attenuation. In [80], an end-fire wearable Yagi-Uda antenna was proposed. It was found that although the reflection coefficient of antenna remained below -10dB, its radiation pattern was strongly affected by the proximity of the human body. As end-fire antennas, which always provide good directivity and gain, seem to be the best choice for on-body communication, other types of antennas having end-fire radiation patterns, such as antipodal antennas and Vivaldi antennas, were proposed in [81,82]. This thesis also proposes a SIW Vivaldi antenna for on-body communication in the following chapter.

It is noticed that although the dimension of the radiator element is small, the entire antenna size is still bulky for mounting on the human body during experimental work using a VNA due to the big adapter used to connect the cable to feeding structure, e.g. as in [83]. Therefore, to minimise the entire antenna size, an adapter designed for the proposed SIW Vivaldi antenna is presented in appendix II this thesis.

To establish reliable communication in WBAN systems and design efficient transceivers and protocols, the properties of wave propagation in the WBAN channel are crucial, especially for

communication at 60 GHz. Given the severe influence of the human body, the positions where antennas are placed also play an important role, as well as the movements conducted and the surrounding environment.

So far, many investigations of on-body channels have been done in both indoor and outdoor environments [14, 15, 17, 22, 27]. Most of them were completed with the help of a network analyser because of its high accuracy. Fibre optic cables can be used in the measurement procedure for eliminating unwanted wave scattering caused by the conventional coaxial cable [84, 85].

Compared to the body of work on the characteristics of BAN channels at 2.45GHz and the UWB band, there are only a small number of groups who are working on 60 GHz WBANs. Research in [86-89] showed that fading at 60 GHz was always a strong influencing factor on body channels. Unlike the separation of short-term and long-term fading at microwave frequencies, it was very difficult to distinguish between these two types of fading. Some researchers have started to use wideband channel sounders to extract long-term fading and study the body shadowing effect at this frequency. Furthermore, the group at Queens University, Belfast [90], has been studying the channel characteristics between soldiers in the field. Researchers at the University of Birmingham have conducted work on both simulation and measurement: A 3D phantom was developed by using animation software, POSER, to simulate the body movement in the simulator [91]. However, it is hard to use at 60 GHz because of the computational overheads of modelling.

Interference at 60GHz is much less than that at lower frequencies, because the signal attenuates very quickly with distance. The study in [75] proved that 60 GHz technology could

improve the carrier-to-interference ratio although body movements were not considered. Also, multiple antenna technology can be used to eliminate interference in WBANs [92].

Finally, based on the ' k , y GH z different applications in body area networks are very rare so far, so in Chapter 5 investigations on diversity reception at 60 GHz for WBANs are provided.

2.5 Summary

In this chapter, studies on antennas and propagation for wireless body area networks at various frequencies are reviewed. It seems that solutions for WBANs at lower frequencies have become more mature and even some commercial products have come out, but there are still many challenges on highly efficient antenna design and reliable WBANs channel modelling.

Finally, it can be argued that UWB is likely to be superseded by 60 GHz wireless technologies because of not only the failed adoption of UWB, but also the technical advantages of adopting the 60GHz band. So far not many studies on on-body channel at 60 GHz have been proposed, especially the issues of multi-hop channel modelling at this band. Therefore, in this thesis Chapter 5 to 7 will present original contributions on antennas and propagation for WBANs at 60 GHz.

CHAPTER 3

MEASUREMENT METHODOLOGY

3.1 Introduction

In this thesis measurement is one of the most important aspects of the work, not only for the on-body channel characterization, but also for checking the performance of the proposed antennas. Simulation can only be used to design some small components in body area networks at 60 GHz, such as antennas and adapters, because it is impractical to characterise on-body channels in any commercial simulator at 60 GHz, as the human body is electrically large, which requires infeasibly extensive computational effort. Usually, there are several ways to measure the channel data. The first method is that a vector network analyser is used to measure the S_{21} parameter between transmitters and receivers. Coaxial cables are indispensable for the connection between VNA and antennas in this method. The second method is that dedicated commercial transceivers that contain both transmitter module and receiver module are used to collect the channel data. Cables can be avoided with this method. Also, dedicated channel sounders, some of which have electro-optical converters, can be used to replace the cables by optical fibres, and thus minimise unwanted scattering. However, mature transceivers at 60 GHz are fairly rare in the current market; in addition, the first method is more simple, flexible and intuitive. Therefore, the first method was adopted in this work.

3.2 Equipment

The equipment used during the measurements is introduced below.

3.2.1 Vector Network Analyser

A four-port Rohde&Schwarz© vector network analyser was employed in all measurements with working frequency up to 67 GHz as shown in Figure 3.1. The direct access ports were used during all the measurements in order to eliminate the extra loss from the front end directional couplers. In addition, the dynamic range is one of the most important factors that may affect the measured results, and it can be controlled by varying the IF bandwidth and the output power as well. In most measurements in this thesis, a 1 kHz IF bandwidth and 10 dBm output power working at 60 GHz were adopted. It is able to record 1000 points per second, which is fast enough to capture the time variation caused by body movements. The trade-off among sweep time, noise level and dynamic range depends on the requirements of the specific channel under study. The above parameters were adopted in the entire thesis.

Figure 3.1 Four-port Rohde&Schwarz© vector network analyser

3.2.2 Cables

The cables working at this frequency are very expensive, relatively lossy and their assemblies are also fragile after repeated flexing. Therefore, extra attention should be paid to these cables. There are two types of cable used to connect the VNA and antennas, which are plastic-shielded and ruggedized metal-shielded cables, respectively. The latter was used in all the measurements although they are heavier when mounted on the human body. The metal-shielded cables used are 2 m long, which enables the test subject to conduct movements without too many restrictions, but they introduce about 10 dB of insertion loss each (shown in Figure 3.2). A half piece of semi-rigid coaxial cable (Anritsu V086MM-30cm) introducing about 1 dB insertion loss at 60 GHz was used to connect the antenna and 2 m long cable for releasing the direct stress from the flexible cable, thus enabled the placement of antenna more easily as shown in Figure 3.3. In addition, to minimise the unwanted scattering and re-radiation, the cables should be carefully routed on the human subject, making them more static.

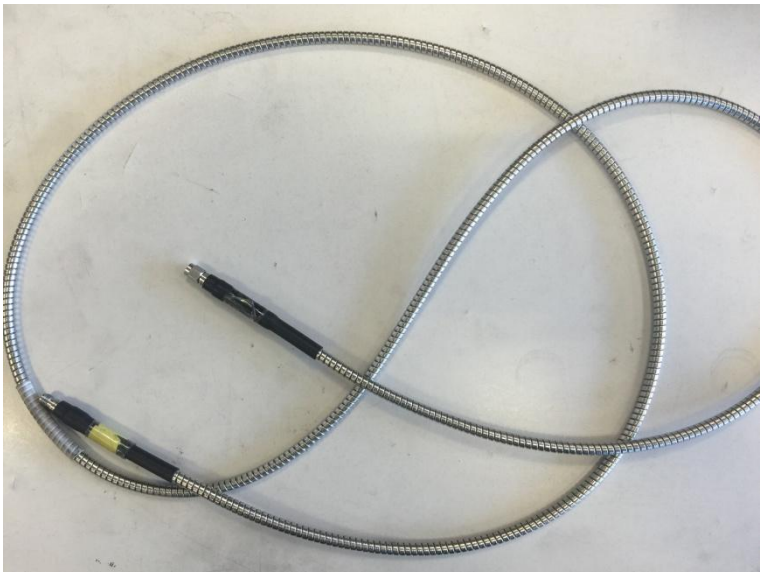

Figure 3.2 The metal-shielded cable

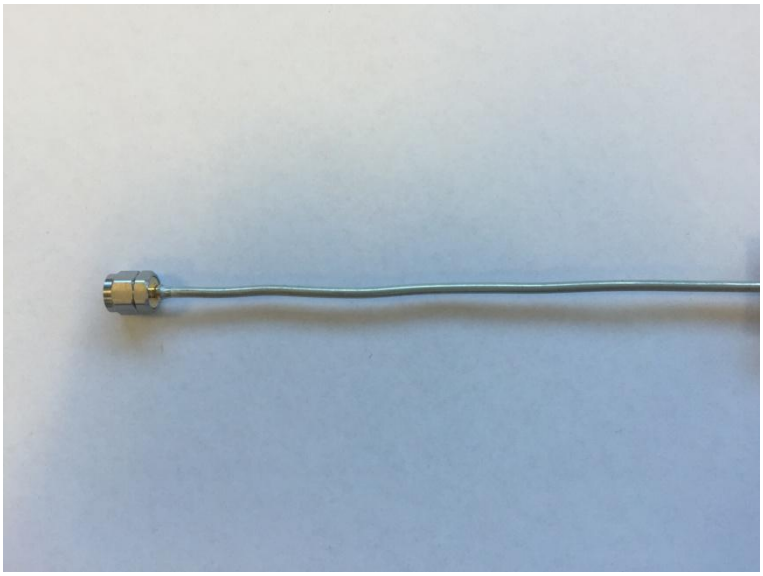

Figure 3.3 The semi-rigid coaxial cable

3.2.3 Channel Measurement Method

Channel measurements at 60 GHz are much more complex than those at lower frequencies, especially when human bodies are involved. Firstly, the body movements will cause many changes to the measured channel, such as varying the separation between transmitter and receiver, altering the receive signal polarization significantly and shifting the angles of arrival due to a shifting bore-sight direction. Therefore, the measurements should capture the desired changes of channels. Secondly, to only investigate the channel characteristics antennas should be de-embedded from the measured data, which is very difficult. Moreover, it is unrealistic to require the test subject to repeat their movements exactly.

All measurements were conducted on the floor of an open university laboratory environment. The test subjects were surround by shelves, tables, chairs and computers as shown in Figure 3.4.

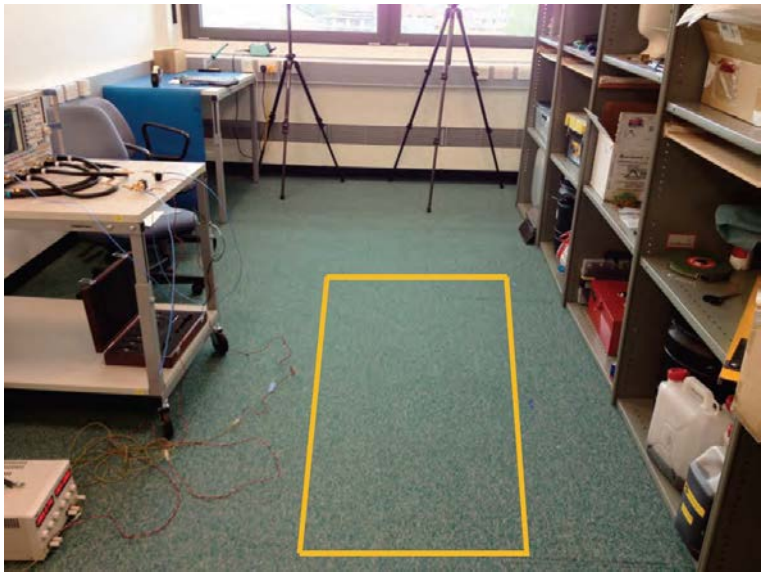

Figure 3.4 Laboratory environment

The metal-shielded cables can cause a measurement magnitude error when they were twisted or bent due to rapid movements as shown in Figure 3.5. The metal-shielded cable was tested five times, and various movements were conducted in each test, but the measurement magnitude error maintains in a range of ±1 dB.

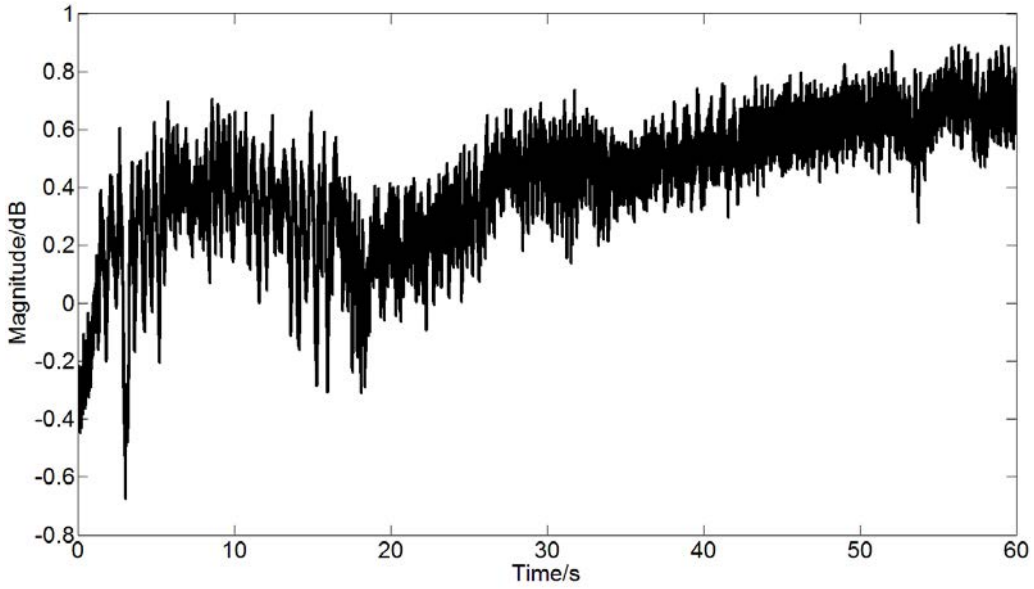

Figure 3.5 Measurement magnitude error of metal-shield cable during movement

Moreover, in all on-body measurement setup, to avoid the influence of the 2 m coaxial cables normalization was implemented before and after each measurement. The normalization process was as follows:

First, a through calibration was used to connect the input and output cables. Then, the parameter of S_{21} was recorded with consistent random cable movements. Finally, the mean value of S_{21} was used to normalise the measured channel data. Thus, under this condition the RMS noise level of the analyser was found to –92.6 dBm when no cables were connected to any port. This noise floor applies to all measurement setting in Chapter 5, 6 and 7, unless it needs to be changed for specific cases.

The test subject during all the measurements is a 70 kg male of a 1.75 m height. The antennas were mounted on the body with the help of 2 cm × 2 cm × 5 mm Styrofoam block, because the antennas are not only too fragile to fix on the body directly, but also their radiation pattern, and efficiency significantly deteriorate for smaller spacings than 5 mm. In addition, in a real BAN the sensors and electronics will separate antennas from skin. The distance between the antennas and body surface is around 5 mm, which is the best choice as shown in [80]. The designed SIW to coaxial transition block introduced in Appendix II reduces the dimension and bulk of the whole antenna unit significantly compared to earlier work in [83].

3.3 Summary

This chapter introduces all the devices and the channel measurement methods that were adopted in all measurement for wireless body area networks. Although all the devices had limitations, they were adequate to capture various movement changes in body area networks with proper settings and post processing.

CHAPTER 4

DIRECTIONAL ANTENNAS AND SINGLE HOP LINKS FOR BODY AREA NETWORKS AT 60 GHZ

4.1 Introduction

Although it has been shown that omni-directional (monopole) antennas are the best candidates to cover the vicinity of the body at 2.45 GHz [93], this kind of antennas have low gain property which is a shortcoming for security because other antennas in adjacent WBANs may cause interference if the coverage area is too wide. In addition, due to the high free space loss in millimetre wave bands and significant path loss in shadow areas, it is very difficult to establish reliable communication links, such as between belt-wrist and wrist-chest. Therefore, to overcome these shortcomings directional antennas with high gain are required. As discussed in the introduction chapter, the various directional antennas such as the common horn antenna can improve both the reliability and security of the on-body channels. However, they are too bulky to be suitable to mount on the human body, and for commercial body sensors such antennas are unsuitable for integration into chip packages. Wearable antennas should be low- , ' movement. Ideally body-worn antennas should possess an end-fire radiation pattern because the main beam of the antenna should be parallel to the body surface. Furthermore, to offset the high path loss at 60 GHz, at least 10 dBi gain at both transceivers is needed according to

the requirements for on-body communication antennas in [98]. The work in [129] has shown the antenna beamwidth requirements and thus directivity through motion capture. In this chapter, antenna in [94] for BANs at 60 GHz is presented for comparison purpose to the proposed antenna. Taking into account these requirements, the printed Vivaldi antenna is a strong candidate for satisfying them because of its merits mentioned in Chapter 2, but also for its excellent in-situ beamwidth and bandwidth performance. Therefore, a broadband, low profile, low cost Vivaldi array antenna with an integrated substrate integrated waveguide (SIW) power divider feeding network and an element isolation wall made of metallised vias is proposed. The SIW technology is chosen to feed antenna element because it is an emerging approach for the implementation of compact, low-loss, circuits, and antennas at millimetre band. The method is similar to that of [95], but is implemented at a much higher frequency band. Also, this antenna is much smaller than other directional antennas and is more suited to mounting on the body. The structure of the antenna and the isolation via wall is introduced. Then comparison between antennas with and without the via-wall is given, which demonstrates that the existence of the via-wall is critical for both return loss and insertion loss. Subsequently the performance of this antenna is discussed. Finally, two arrangements of two-element Vivaldi antenna arrays are proposed to investigate multi-hop communication and networks.

4.2 Substrate Integrated Waveguide Vivaldi Antenna at 60 GHz

The technology of SIW has drawn a lot of attention recently due to its merits of low cost, low insertion loss and high density layout. It is an especially promising candidate for use in millimetre wave bands. It is widely used to design integrated active circuits, planar antennas, filters, etc [96]. The structure of SIW is composed of metallised vias, which can be

manufactured by using PCB or LTCC technology. The details about how to determine the parameters of this structure to avoid the extra losses due to the energy leakage through gaps or other reasons are presented in [99].

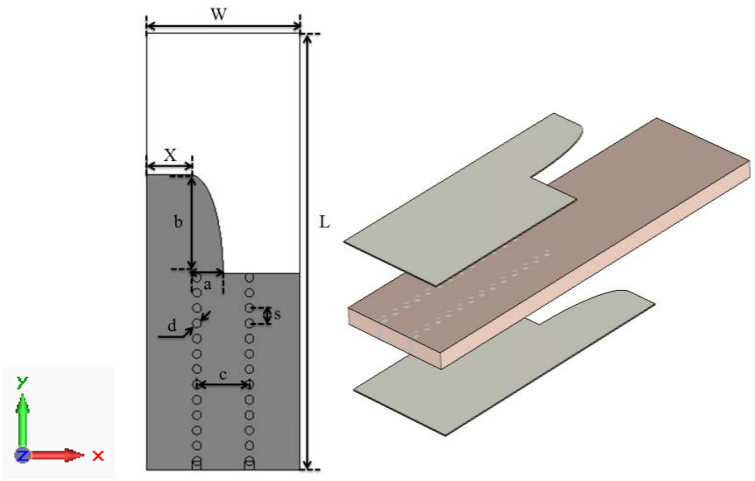

Figure 4.1 Geometry of proposed SIW Vivaldi antenna at 60GHz

Table 4.1 Dimensions of proposed structure

Parameter	a	b	c	d	s	X	L	W
Value(mm)	1.5	4.5	2.4	0.4	0.7	2	20	7

The Vivaldi antenna is a uniplanar tapered slot antenna that can be integrated on the both sides of a single substrate. Because of its advantages, such as high element gain, wide bandwidth, etc, it is highly suitable to be integrated into millimetre-wave systems. Firstly, the geometry of the SIW Vivaldi antenna working at 60GHz band is shown in Figure 4.1. The antenna is etched on a 0.508 k R / 5 $\varepsilon_r = 2.2$). The dimension of each parameter will be shown in Table 4.1.

According to [97], the main working frequency range always depends on the opening width of two flares, while the taper length can control the beamwidth and gain. As this antenna will be used for investigating the on-body communication system, the size of antenna should be small enough to mount on body. At the same time, for on-body communication, the ideal beamwidth and antenna gain are meant to restrict the power around the human body as much as possible.

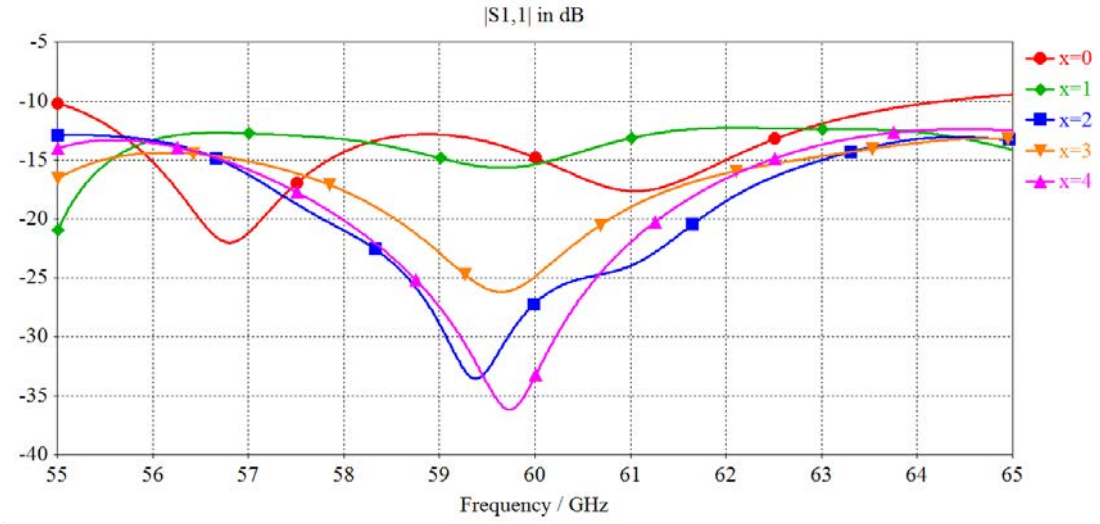

Figure 4.2 Numerical optimization of parameter X

The adopted optimization procedure optimises one parameter at a time to achieve an approximation of the desired performance. Moreover, it was determined that the extension dimension, X, improved not only the reflection coefficient but also the front-back ratio of radiation pattern. First, the reflection coefficient optimization of X is shown in Figure 4.2. Then the E-planes were given with 5 different lengths of X as well as the information about gain, side lobe and beamwidth in Figure 4.3. According to Figure 4.2, almost all five lengths can achieve a wide bandwidth from 55 GHz to 65 GHz except X = 0, but impedance matches are better when X = 2, 3, and 4 mm at 60 GHz.

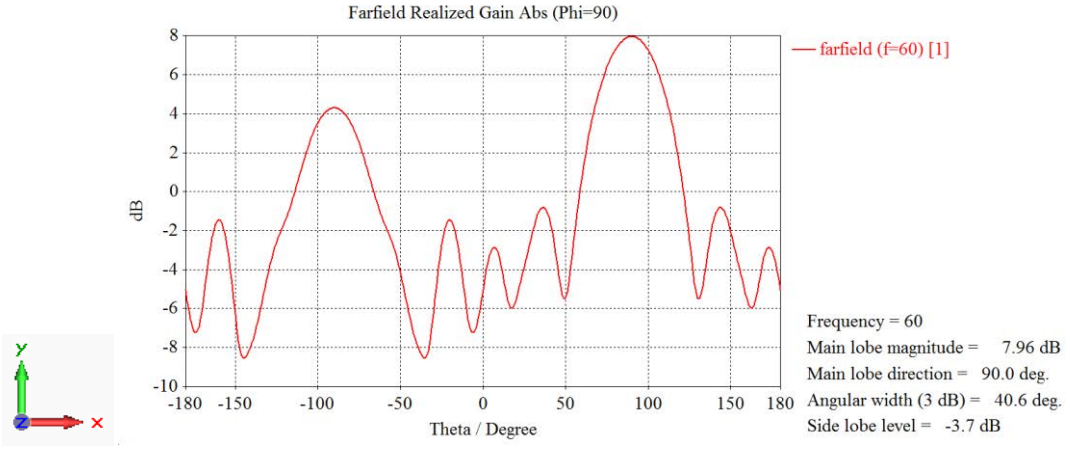
Farfield Realized Gain Abs (Phi=90)
farfield (f=60) [1]
dB
Theta / Degree
Frequency = 60
Main lobe magnitude = 7.96 dB
Main lobe direction = 90.0 deg.
Angular width (3 dB) = 40.6 deg.
Side lobe level = -3.7 dB

(a)

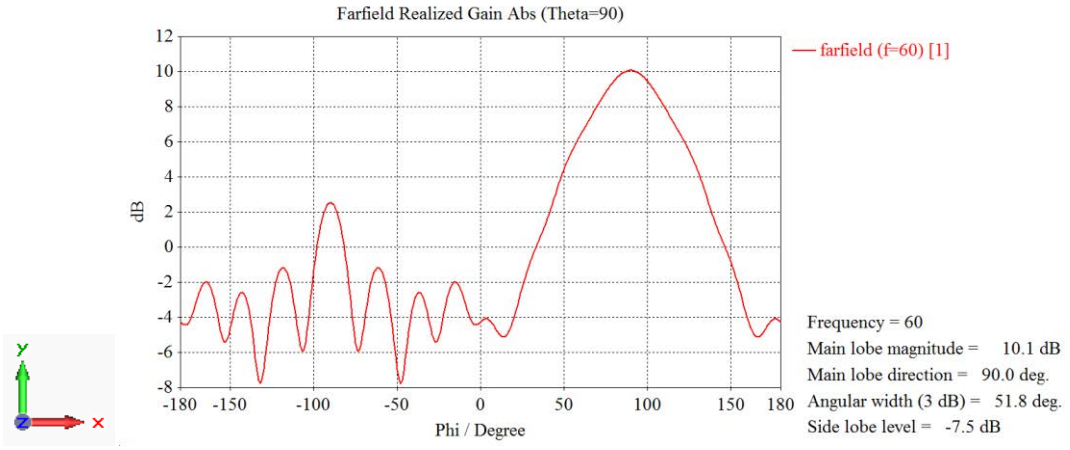
Farfield Realized Gain Abs (Theta=90)
farfield (f=60) [1]
dB
Phi / Degree
Frequency = 60
Main lobe magnitude = 10.1 dB
Main lobe direction = 90.0 deg.
Angular width (3 dB) = 51.8 deg.
Side lobe level = -7.5 dB

(b)

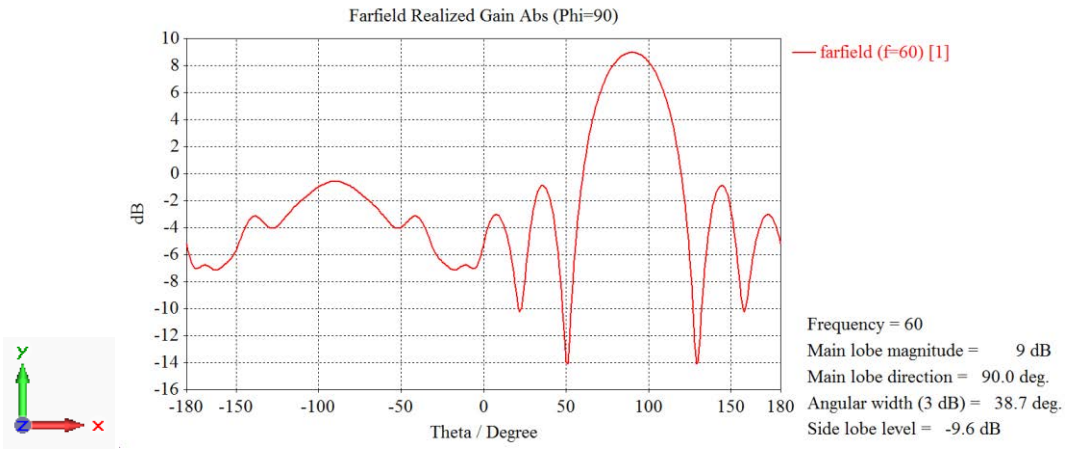
Farfield Realized Gain Abs (Phi=90)
farfield (f=60) [1]
dB
Theta / Degree
Frequency = 60
Main lobe magnitude = 9 dB
Main lobe direction = 90.0 deg.
Angular width (3 dB) = 38.7 deg.
Side lobe level = -9.6 dB

(c)

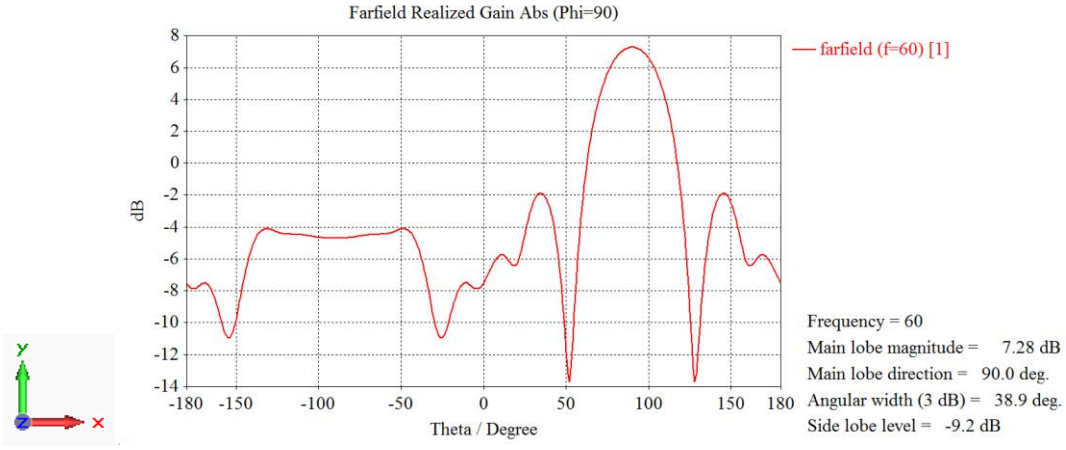

(d)

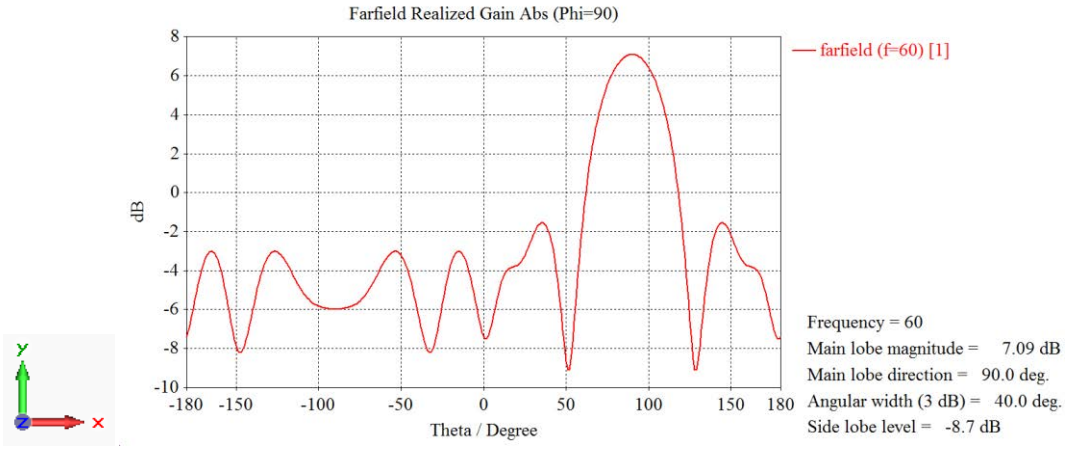

(e)

Figure 4.3 Comparison of radiation pattern when (a) x = 0 (b) x = 1 mm (c) x = 2 mm (d) x = 3 mm (e) x = 4 mm

In addition, according to Figure 4.3 the rear lobes when X = 0 and 1 mm are much stronger than the other cases. Therefore, X = 0 and 1 mm won' A other cases, it is observed from Figure 4.3 that the case, X = 2 mm, has the highest gain, lowest side lobe and approximate beamwidth comparing to the other two case. Therefore, X = 2 mm is chosen finally.

It was found that the proposed antenna above can satisfy the requirement defined in [98] for on-body communication at 60 GHz, which has a broadband covering the unlicensed band from 57 GHz to 64 GHz, a 9 dBi gain and an appropriate beamwidth that not only can focus the energy at the subjective sensors, but also protect the on-body links from external interference.

In addition, for the purpose of facilitating on-body VNA measurements, a broadband SIW to coaxial cable adapter is proposed. Various transitions from conventional transmission line technologies to SIW structures have been proposed [100-104]. Among them, the coplanar waveguide (CPW) seems to be a good option for the 60 GHz frequency band because of its compatibility with MMICs. In [100], a current probe positioned at the end of a feed line is employed to transfer power and in [101] an elevated-coplanar waveguide is proposed for an intermediate section of a coplanar waveguide to SIW transition. However, both of these solutions increase the complexity of fabrication. In [102], the author uses SMA connectors that have been attached to the top wall of post-wall waveguide. The center conductor is fed through a hole in the top wall and is electrically connected to the bottom wall, forming a current probe. However, the SMA connectors are perpendicular to the waveguide, while our application may requires a conformal structure. Therefore, the author proposes a new 60 GHz coaxial to SIW adaptor that is low cost, compact, lightweight and easy to manufacture and optimize. Figure 4.4 shows the feeding structure and 3D cut-out of supporting block. Further details about this adapter are presented in Appendix II.

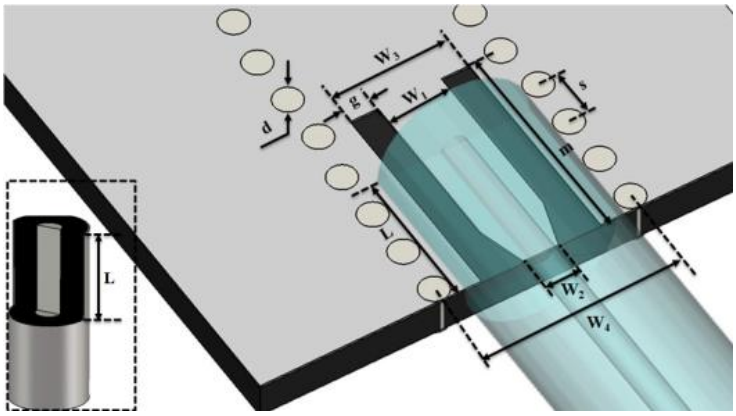

(a)

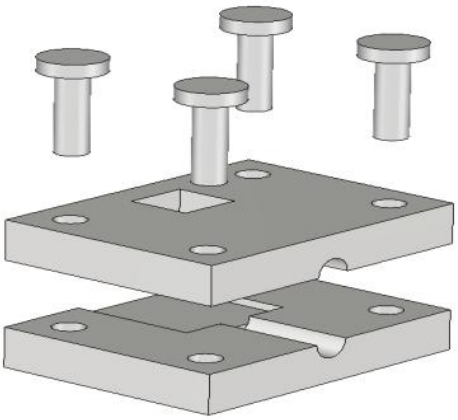

(b)

Figure 4.4 (a) modified coaxial cable and feeding structure (b) 3D cut-out supporting block

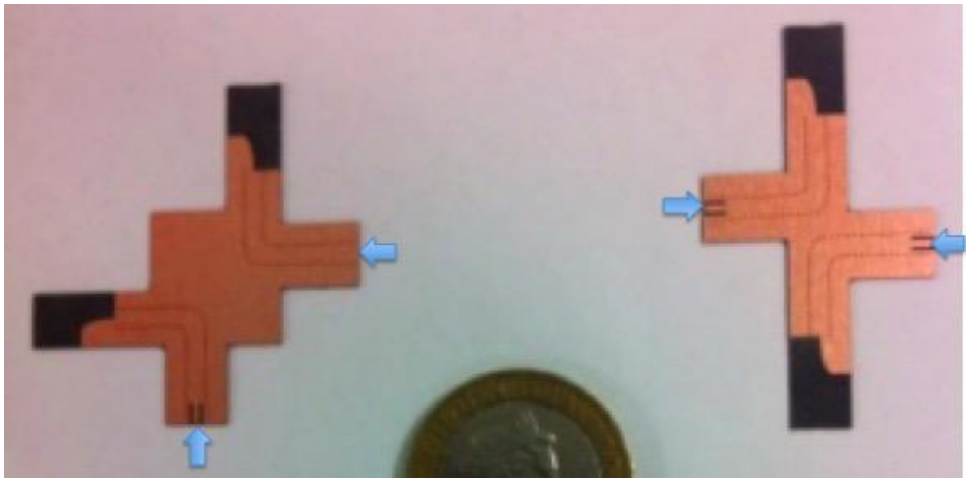

Figure 4.5 SIW fed Vivaldi antenna

Finally, the fabricated antenna is shown in Figure 4.5. As previously mentioned, the proposed antenna will be used for on-body measurements, thus the antenna element is combined into the specific layout that will satisfy the specific requirements of on-body links shown in Figure 4.6. In addition, the sizes of these antennas are a little bigger than one Euro coin that it is very suitable to on-body communication investigation.

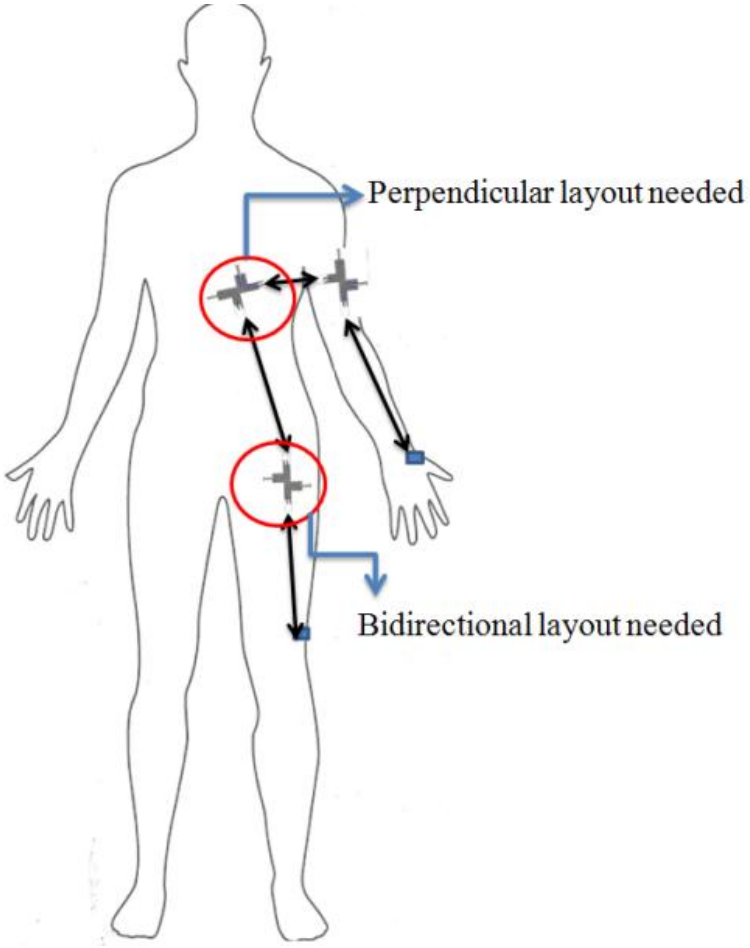

Figure 4.6 On-body channel types

Figure 4.7 shows the simulated and measured antenna reflection coefficient. Results indicate that the simulation achieves a good agreement with the measurement on the -10 dB impedance bandwidth, except that there are more ripples in the measured results compared to

the simulated results, which is believed it may be caused by the reflection from the via wall due to poor manufacturing.

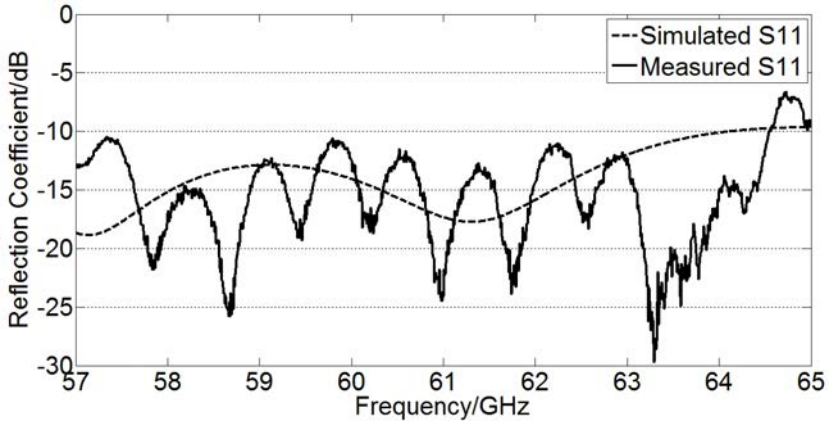

Figure 4.7 Simulated and measured reflection coefficient of SIW Vivaldi antenna

Figure 4.8 Measurement setting up in a small chamber

Figure 4.8 shows the setting up of the radiation pattern measurement. Figure 4.9 shows the measured radiation pattern of SIW Vivaldi antenna in the E-plane at 58 GHz, 60 GHz, 62 GHz and 64 GHz, respectively. The solid line represents the co-polarised pattern, while the dashed line shows the Cross-polarised pattern. The measured cu

y , . We can observe that in the E-plane the side lobe at 60 GHz is the smallest comparing to the other frequencies and information about beamwidth and difference between polarizations are also given in the Figure.

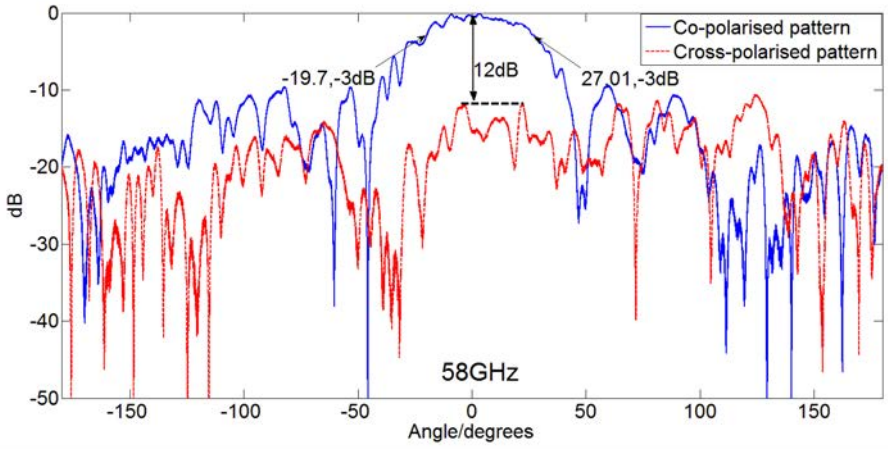

(a)

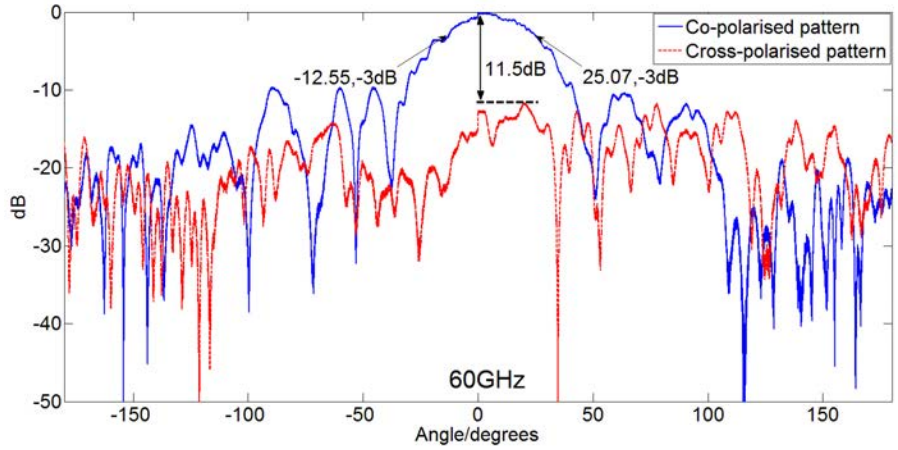

(b)

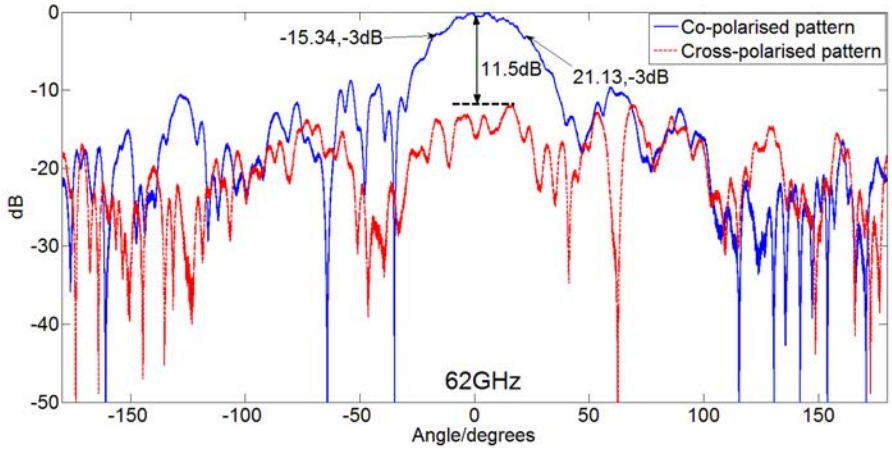

(c)

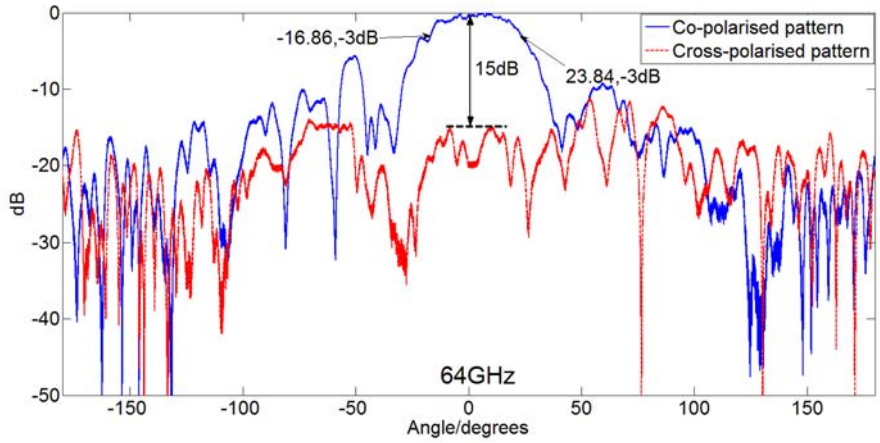

(d)

Figure 4.9 Radiation pattern of SIW Vivaldi antenna element in the E-plane

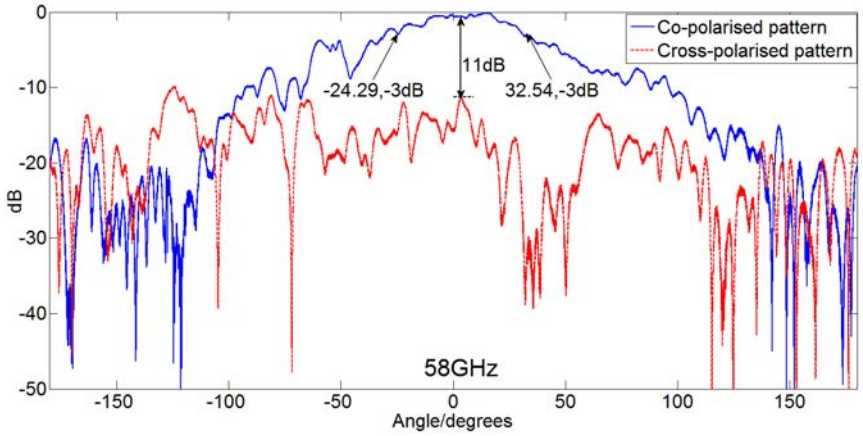

(a)

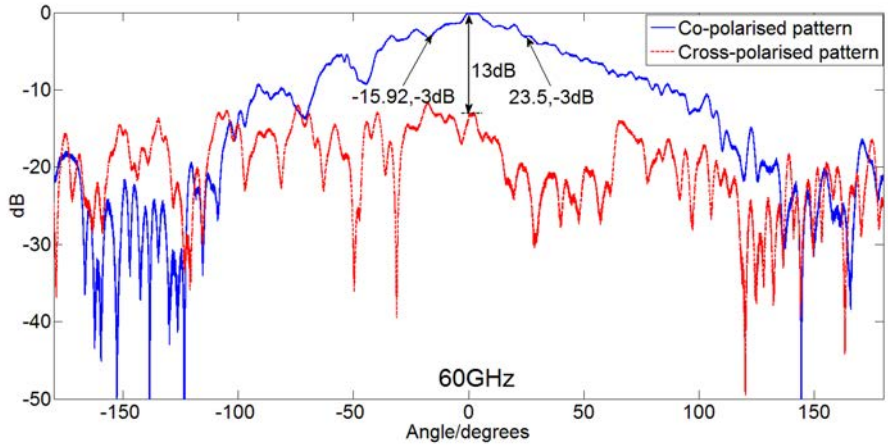

(b)

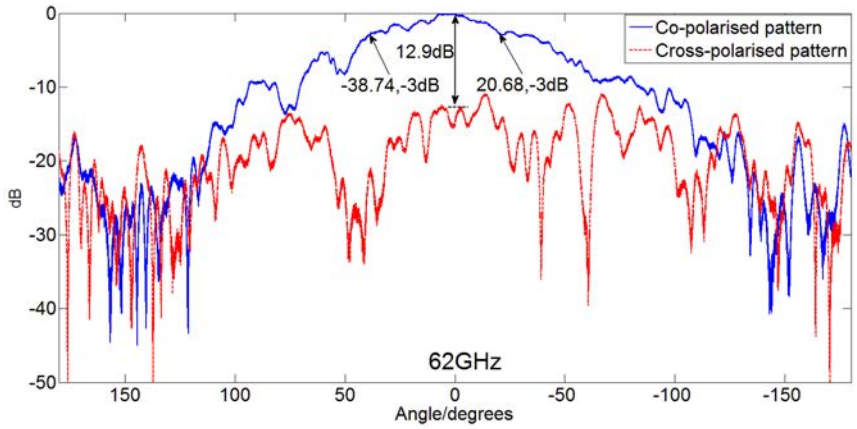

(c)

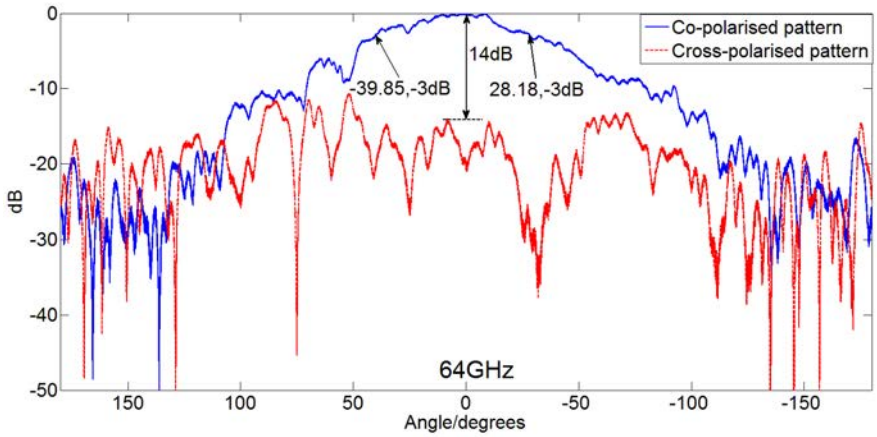

(d)

Figure 4.10 Radiation pattern of SIW Vivaldi antenna element in the H-plane

Figure 4.10 shows the H-plane radiation pattern at the aforementioned frequencies. As observed, the 3 dB beamwidth in the H-plane is much wider than that of E-plane. Overall, the main beam maintains a good pattern over the entire 60 GHz band.

Furthermore, the gain was measured by using a substitution method [105] that compared the proposed antenna to a standard 20 dBi-gain pyramidal horn antenna over 57~64 GHz. The measured gain is 8.1 dBi at 60 GHz, which is consistent with 1 dB less than the simulation results. It is believed that the 1 dB loss is from the proposed adapter mentioned in appendix II.

According to the requirement of on-body antennas in millimetre bands [98], the antenna gain is required to be at least 10 dBi. The proposed SIW Vivaldi antenna satisfies almost all the requirements except the requirement for antenna gain. Therefore, a Vivaldi antenna array is employed to achieve the target performance.

4.3 Two-element Vivaldi Antenna Array

A SIW fed Vivaldi array antenna has been proposed in [106] working at the millimetre-wave Ka-band. A single element Vivaldi was found not to provide sufficient gain to overcome the on-body path losses at 60 GHz, while a two element Vivaldi array is likely to have increased gain. Unlike at Ka-band, the difficulty of designing a Vivaldi array antenna at the 60 GHz band is that antenna performance deteriorates dramatically without any isolation between Vivaldi elements due to mutual coupling between them.

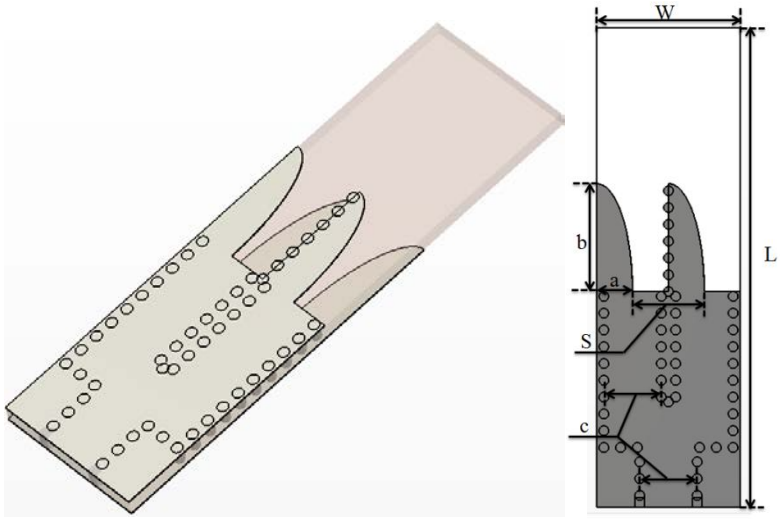

Figure 4.11 3D view and geometry of proposed antenna array

Figure 4.11 shows the 3D view and geometry of the proposed 60 GHz Vivaldi array and the E-field distribution with and without the isolation wall is shown in Figure 4.12 from a CST simulation at 60 GHz. The antenna is etched on a 0.508 mm thickness RT/Duroid 5880 ($\varepsilon_r = 2.2$). A 50 Ω -backed Co-planar waveguide is used to feed signal from cable to the SIW structure. A two-way SIW power divider is deployed to feed each Vivaldi element. To suppress potential sidelobes, the spacing between two elements should satisfy [96]

$$S < \frac{\lambda}{1+|\cos\phi|} \tag{4-1}$$

where S , λ GHz, ϕ is the main beam angle which is 90 degrees in our case. Therefore, the spacing should be smaller than 5 mm. The dimensions of parameters are shown in Table 4.2.

Table 4.2 Dimensions of proposed antenna array

Parameter	a	b	c	S	L	W
Value(mm)	1.5	4.5	2.4	3	20	6

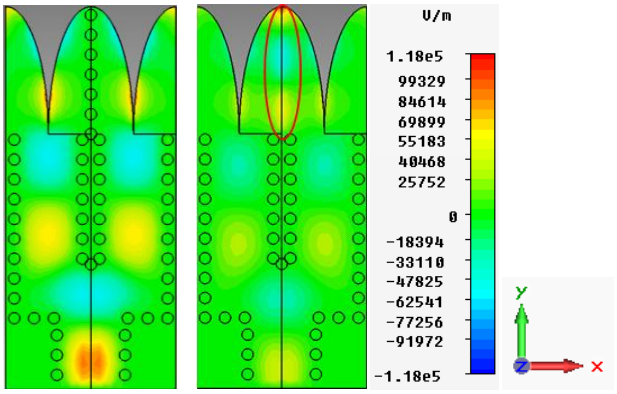

Figure 4.12 The E-field at Z-axis of proposed Vivaldi array antennas with and without isolation wall

Figure 4.12 shows the simulated electric field distribution. The TE_{10} mode is the dominant mode propagating in the SIW structure. The signal is equally divided between the two elements and it can be observed that the field intensity with the isolation wall is much stronger than that without. This is a consequence of the power reflected at the excitation port when the wall is present being much less than that when it is not. Furthermore, the coupling effect between the two elements is much stronger in the case of without the wall as shown in Figure 4.12.

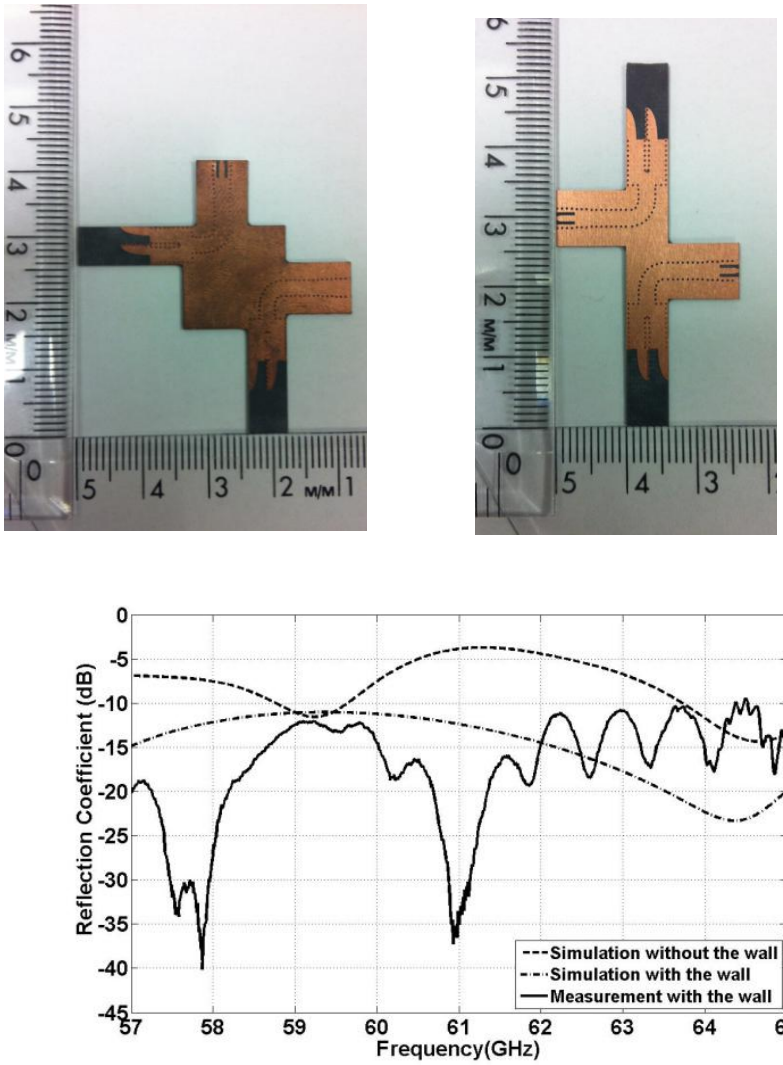

Figure 4.13 Fabricated antenna array and comparison between simulation and measurement results

Figure 4.13 shows the fabricated antenna array and the comparison of reflection coefficient between two cases. Without the isolation wall, the impedance match is very poor around 60 GHz band. In contract, the reflection coefficient is -10 dB over a broad band from 57 GHz to 65 GHz with the isolation wall. The large discrepancy between the simulation and measurement with the wall may caused by the reflection from the via wall. In addition, the adapter proposed in Appendix II may also cause impedance mismatch.

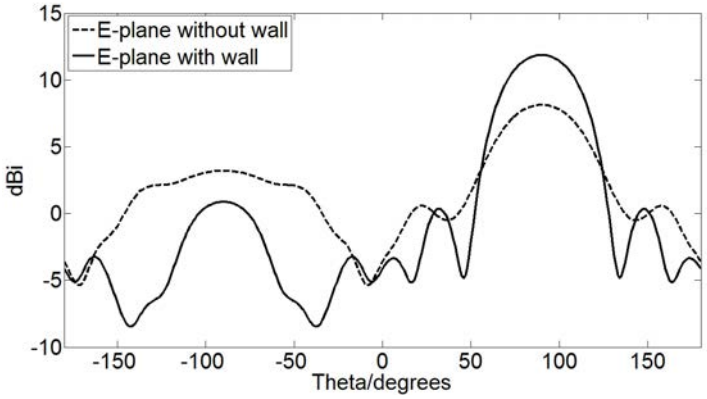

(a)

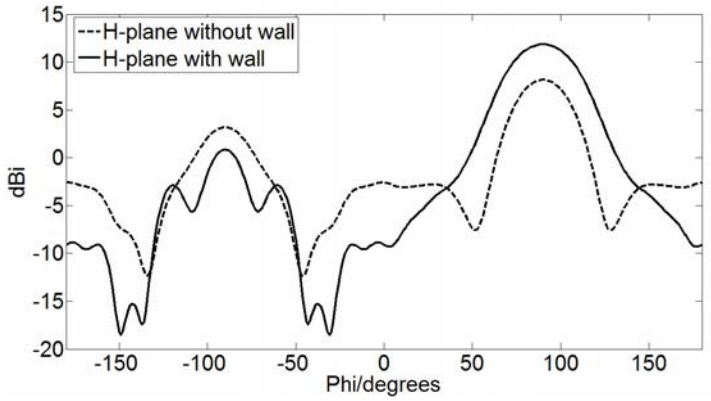

(b)

Figure 4.14 Comparison of simulated radiation pattern (a) with isolation wall (b) without isolation wall

The radiation pattern comparison is also shown in Figure 4.14. The simulated gain and front-back ratio of the array with the post-wall are much better than that of array without the post-wall. The gain is improved from 8.1 dBi to 11.9 dBi, and the front to back ratio is improved over 10dB.

An array with more Vivaldi elements can be designed, such as 4-elements as shown in Figure 4.15, however, although the gain of the antenna array will increase, the beamwidth in the desired E-plane will also get narrower , which is unacceptable for on-body communication

due to movement induced misalignment errors. Therefore, only a two-elements Vivaldi antenna array is considered in our experiments.

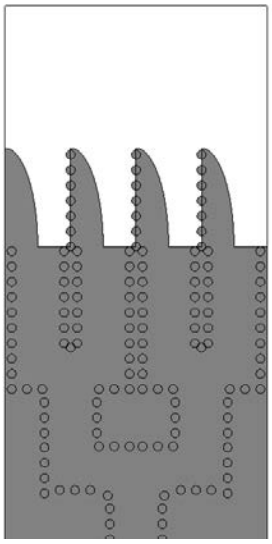

Figure 4.15 4-element Vivaldi antenna array

Figure 4.16 presents the E-plane radiation pattern of the proposed two-element Vivaldi antenna array at 58 GHz, 60 GHz, 62 GHz, and 64 GHz, respectively. The 3dB beamwidth is also marked in the figure and it is found that the E-plane beamwidth for two-elements is almost the same as one-element shown in Figure 4.9, however, the cross-polarization is stronger.

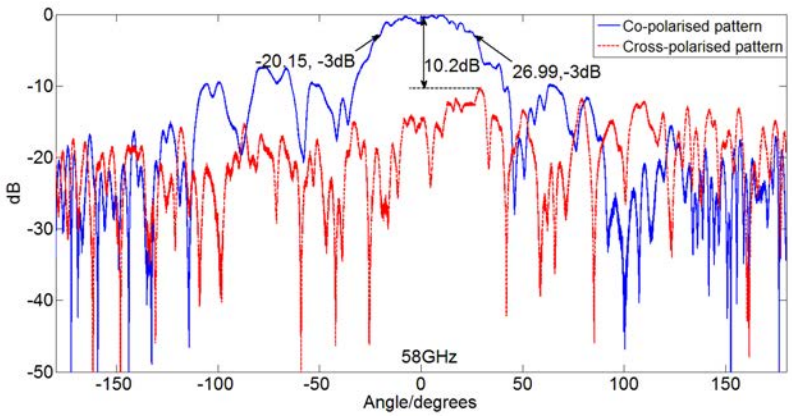

(a)

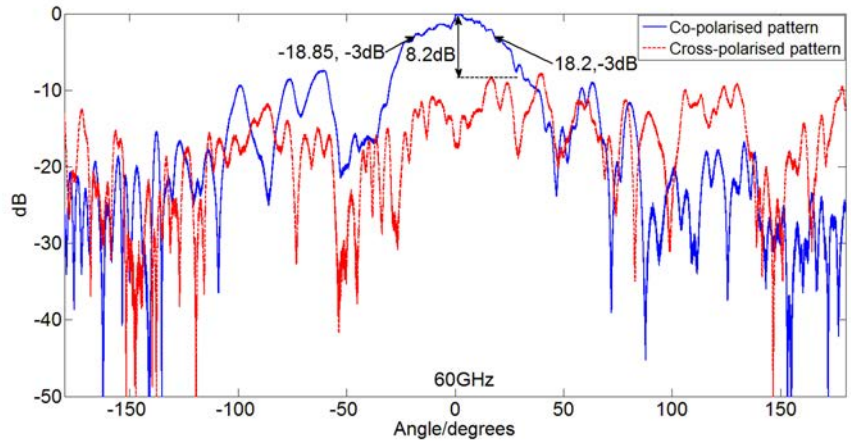

(b)

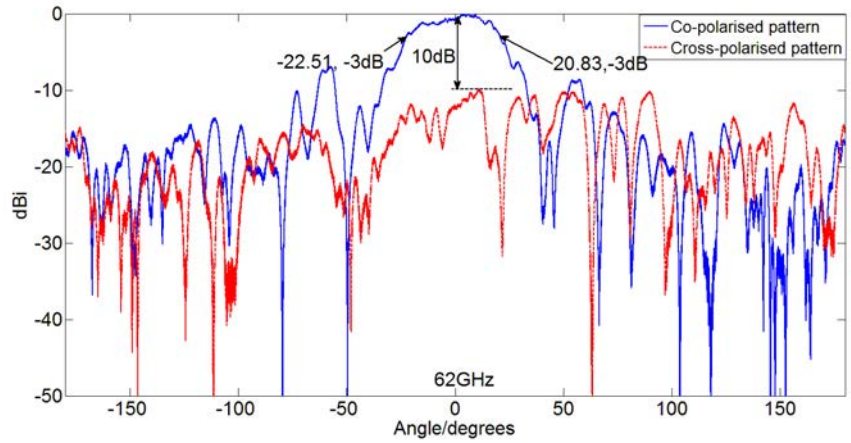

(c)

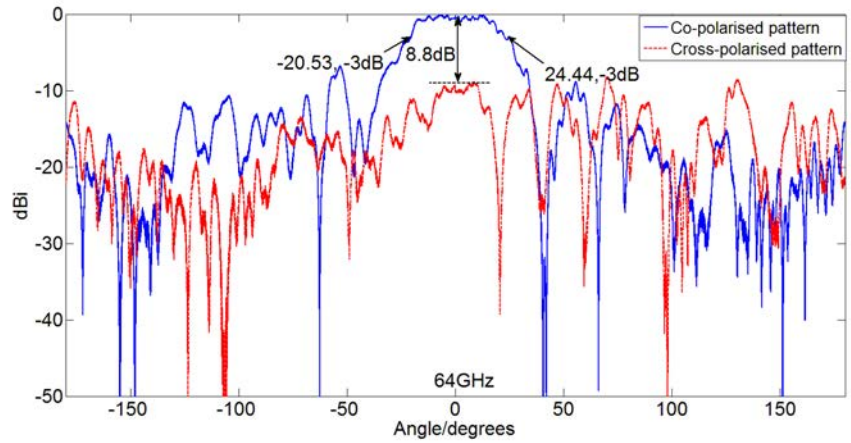

(d)

Figure 4.16 Radiation pattern of Vivaldi array in the E-plane

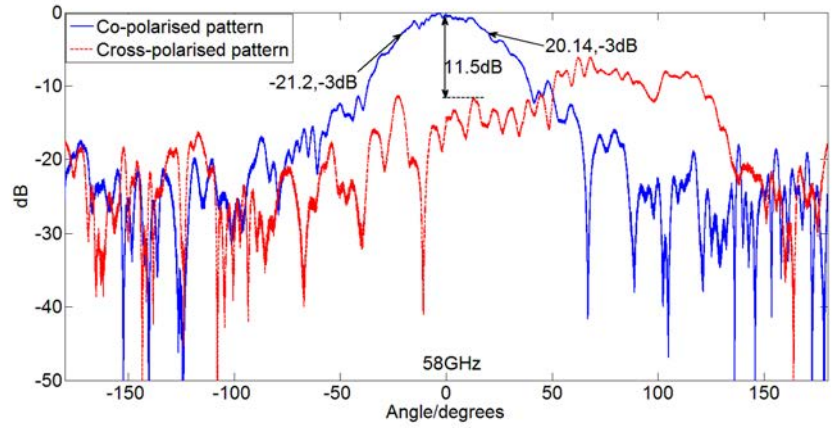
Co-polarised pattern
Cross-polarised pattern
-21.2,-3dB
11.5dB
20.14,-3dB
58GHz
dB
Angle/degrees

(a)

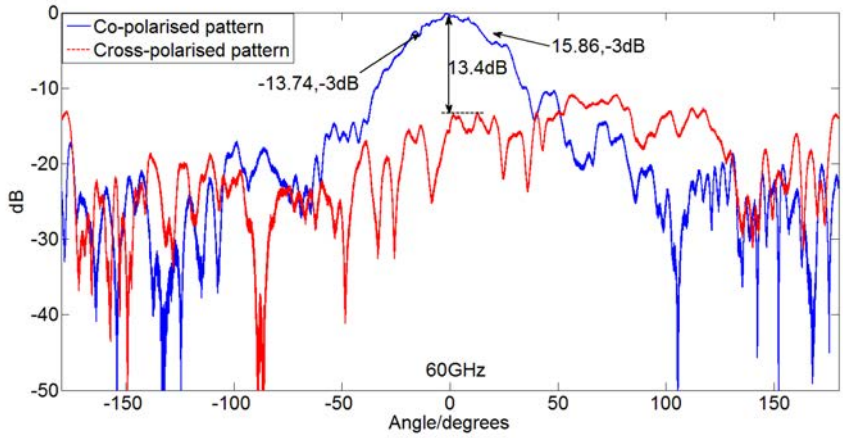
Co-polarised pattern
Cross-polarised pattern
-13.74,-3dB
13.4dB
15.86,-3dB
60GHz
dB
Angle/degrees

(b)

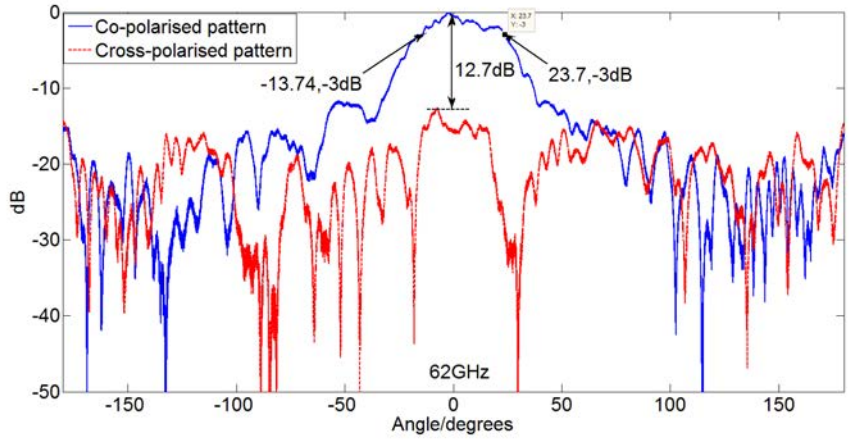
Co-polarised pattern
Cross-polarised pattern
-13.74,-3dB
12.7dB
23.7,-3dB
62GHz
dB
Angle/degrees

(c)

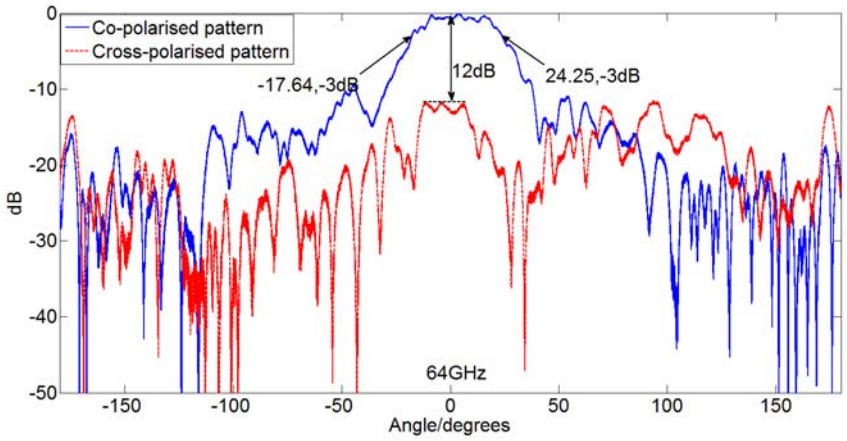

(d)

Figure 4.17 Radiation pattern of Vivaldi array in the H-plane

Figure 4.17 shows the H-plane radiation pattern of the proposed two-element Vivaldi antenna array at the same frequencies shown for the E-plane. It is observed that the beamwidth becomes much narrower than that of one element. For instance, the H-plane beamwidth for one-element at 60 GHz is 40°, while for two-element is 30°.

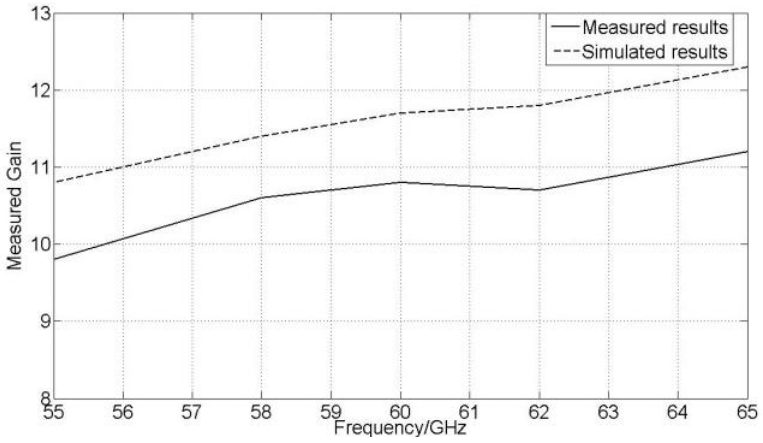

Figure 4.18 Comparison of simulated and measured gain

Finally, the simulated and measured gain of two-element Vivaldi antenna array is shown Figure 4.18. It can be seen that the measured gain is always 1dB lower than the simulated gain,

which is caused by the coaxial to SIW adapter insertion loss we built for this antenna. The precise loss due to the adapter is shown in Appendix II.

4.4 Multi-hop BAN measurements with Vivaldi antennas

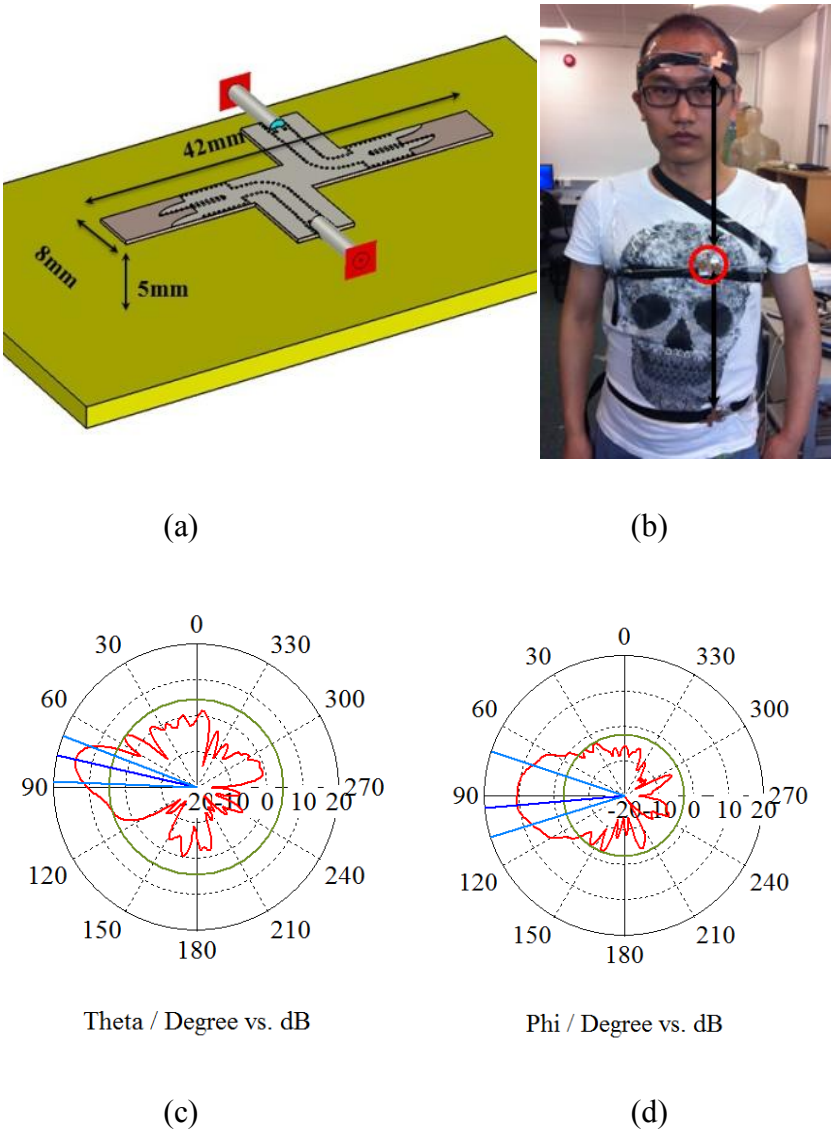

Figure 4.19 Simulated radiation pattern above skin (a) schematic diagram above wet skin (b) position mounted (c) E-plane (d) H-plane

Figure 4.19 shows the bidirectional antenna proposed for multi-hop communication on the body. Usually, it is placed between the transceivers as a repeater. The simulated radiation

pattern with the antenna situated 5 mm above the skin surface is shown in Figure 4.19 (a) because a 5 mm thick polystyrene foam block is used in practice to support the antenna shown in Figure 4.19 (b). Wet skin permittivity is used in the simulation to simulate the condition when antennas are mounted on human skin in practice. As concluded in [94], the antenna will experience radiation pattern distortion, impedance mismatch and also power absorption especially in the millimetre wave bands due to the close proximity of human tissue. The effect caused by human tissue at 60 GHz has been studied in [80].

Figures 4.19 (c) and (d) show that the H-plane pattern of the Vivaldi antenna remains unaffected, and the main beam in the E-plane (perpendicular to the skin) is raised by approximately 10° relative to the skin surface. Meanwhile, the maximum gain increases up to 13.8 dBi in the E-plane.

In the measurements, the proposed antennas are used to investigate the link of head to chest and chest to belt with five possible postures for different potential applications: standing with the antennas mounted at the front of the body, standing with the antennas mounted on the back of the body, a soldier in the slightly lifted prone position shooting with the antennas mounted at the front of the body, soldier in the slight lifted prone position shooting with antennas mounted on the back of the body and a patient lying down in a supine or lateral position on the bed with antennas mounted at the front of the body. The aim of this measurement is to identify whether the proposed antennas can establish some specific and stable on-body multi-hop channels.

Each measurement lasted 10 seconds and 1001 sample points were collected. The output power was set as 10 dBm and the measurement bandwidth was adjusted at 100 Hz to capture the effects of movements on tested channels in such a short time.

4.4.1 Standing with the Upright Antennas Positioned At the Front of the Body

Figure 4.20 shows the antenna placements in the case of standing still with the antennas mounted at the front of the body. The distance from head to chest and chest to belt was 39 cm and 32 cm, respectively, which ensured that the antennas were in the far-field of each other, which was $2D^2/\lambda =$

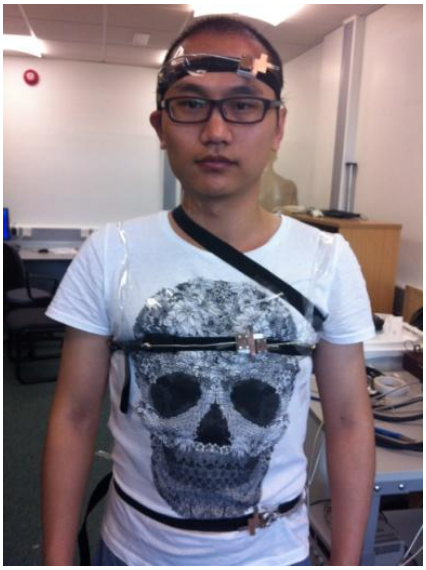

Figure 4.20 Antenna placements of standing still

Figure 4.21 presents the received signal level of the two hops. It was observed that both of the links were almost at the same strength level, but unlike the chest-head link being in a static state, the chest-belt link has regular peaks and troughs which are believed to be caused by breathing. In addition, the free space path loss of chest-head link and chest-belt link is 39.8 dB and 38.1 dB, respectively.

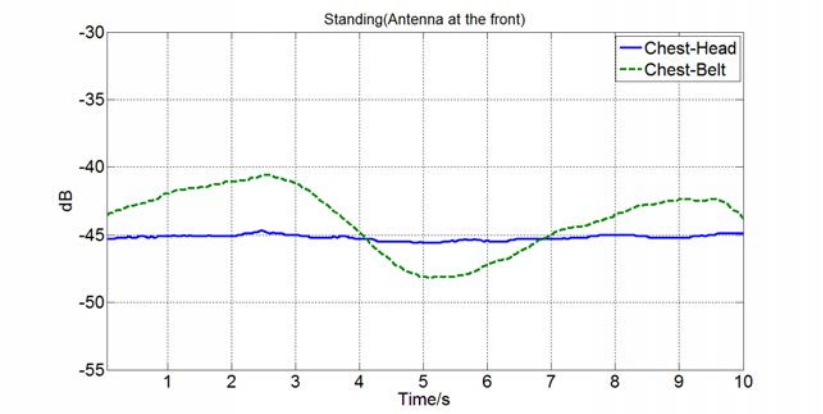

Figure 4.21 S_{21} of two hops with standing (antenna at the front)

4.4.2 Standing with the Upright Antennas Positioned On the Back of the Body

As shown in Figure 4.22, the case of standing upright with the antennas mounted on the back was investigated. Next, the relative positions of the antennas were almost the same as the front case. The distances from head to shoulder blade and shoulder blade to belt were 40 cm and 33 cm, respectively.

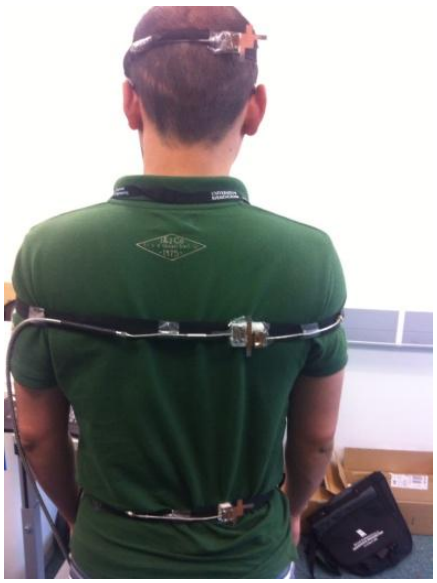

Figure 4.22 Antenna placements of standing with antenna at the back

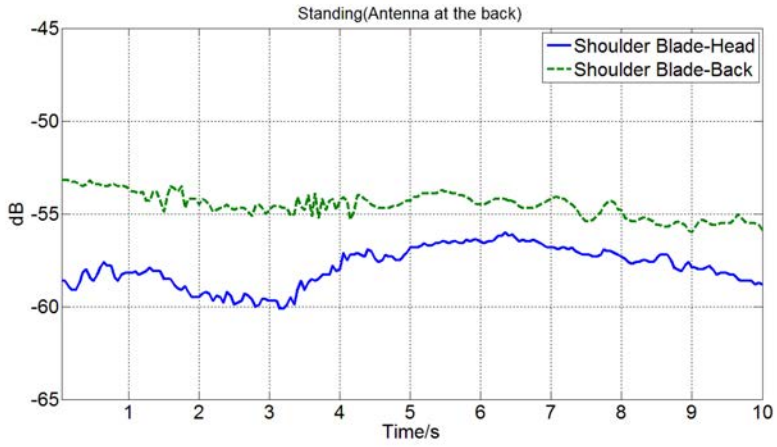

Figure 4.23 $S_{21}$of two hops (antennas at the back)

Figure 4.23 indicates that both links are not as strong as the case of the antennas mounted at the front of the body. Although the slightly longer separation between the transceivers will cause more path loss, it is likely that the most of the extra loss is due to the diffraction caused by the geometry of the human body, especially in the shoulder blade-head link. However, both the links are more stable than the front case, which means the effect of breathing does not affect the channel at the back. The free space path loss of head to shoulder blade and shoulder blade to belt is 40 dB and 38.4 dB, respectively.

4.4.3 Soldier Shooting In the Slightly Lifted Prone Position with the Antennas Mounted At the Front of the Body

As shown in Figure 4.24, the case of shooting in the slightly lifted prone position with the antennas mounted at the front was investigated. The relative positions of the antennas were the same as the case of standing still with the antennas mounted at the front of the body. However, the distances from head to chest and chest to belt were elongated to 50 cm and 39 cm, respectively.

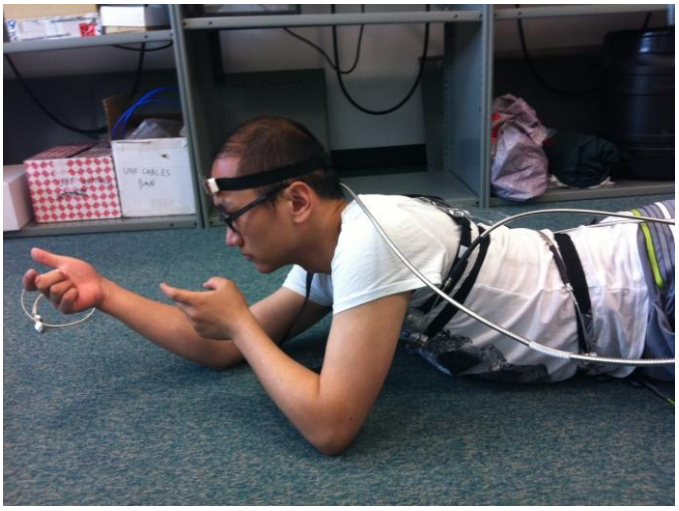

Figure 4.24 Antenna placements for shooting like a soldier (at the front)

Figure 4.25 shows that the link of chest-belt is still as strong as the case of standing with the antennas mounted at the front of the body, but not the link of chest-head. The free space path loss of chest-head and chest-belt is 42 dB and 39.8 dB, respectively. However, the link of chest-head suffers over 20 dB extra path loss according to Figure 4.25. It is likely that of the extra path loss is due to the antenna misalignment caused by the raised head and lifted body.

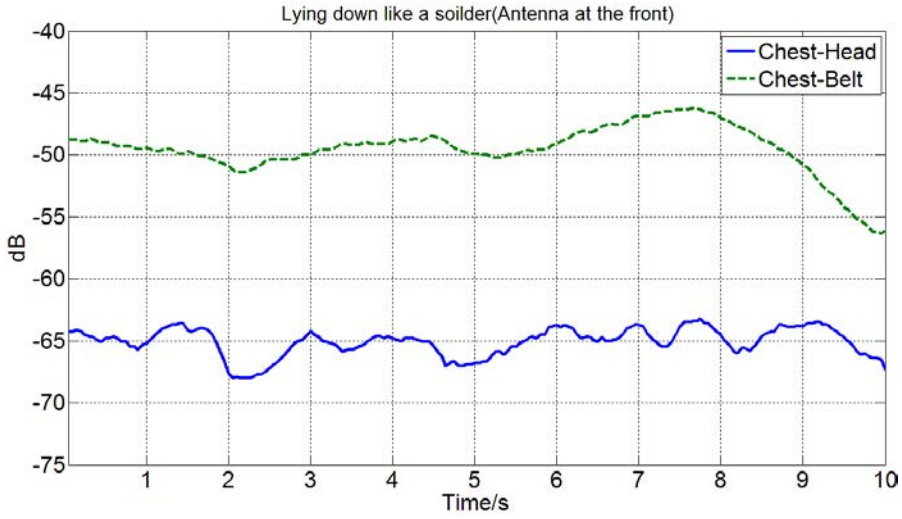

Figure 4.25 $S_{21}$of two hops with shooting (at the front)

4.4.4 Soldier Shooting In the Slightly Lifted Prone Position with the Antennas Mounted on the Back of the Body

As shown in Figure 4.26, the case of shooting in the slightly lifted prone position with the antennas mounted on the back of the body was investigated. The relative positions of the antennas were the same as the case of standing upright with the antennas mounted on the back. The distances from the back of head to shoulder blade and shoulder blade to belt were 38 cm and 35 cm, respectively.

Figure 4.26 Antenna placements for shooting like a soldier (on the front)

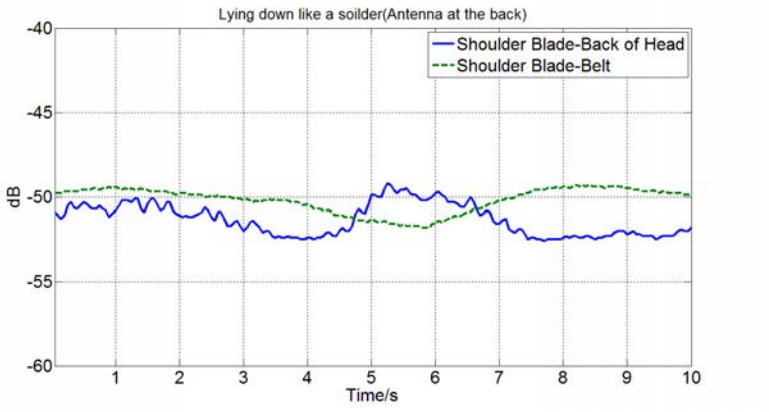

Figure 4.27 $S_{21}$of two hops with shooting (on the back)

Figure 4.27 indicates that both of the two links are as strong as the case of standing with the antennas mounted at the front of the body. Unlike the chest-head link in the case of shooting with the antennas mounted at the front of the body, the link of shoulder blade to the back of head is much stronger because the lifted body and raised head shorten the distance between transceivers and enable this link work under a good light-of-sight condition. The free space path loss of head to shoulder blade and shoulder blade to belt in this case is 39.6 dB and 38.9 dB, respectively.

4.4.5 A Patient Lying Down In A Supine or Lateral Position on the Floor

Figure 4.28 shows the case of a patient lying down in a supine or lateral position on the floor with the antennas mounted at the front of the body. The antenna placements of this case are at typical positions for medical applications. The distance between antennas remained the same as in the upright standing case. The distance from head to chest and chest to belt was 42 cm and 32 cm, respectively

Figure 4.28 Antenna placements of two hops (lying down like a patient)

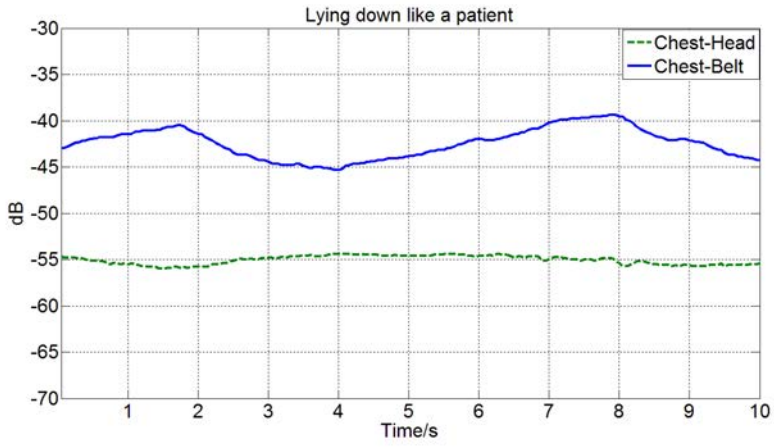

Figure 4.29 Received signal level of two hops (lying down like a patient)

It was observed in Figure 4.29 that both of these two hops were strong, and the regular long term changes were also caused by the breathing movement. The link of head-chest suffered 10 dB more than the other link, and this is likely to be due to antenna misalignment when not using a pillow.

4.5 Summary

In this chapter, a substrate integrated waveguide antenna and antenna array are described and characterised. These were proposed for use in on-body communication channel investigation at the 60 GHz band. It has been demonstrated that the substrate integrated waveguide Vivaldi antenna meets the criteria for on-body antennas that require good gain, end-fire radiation pattern, and wide bandwidth. The human tissue does not affect too much antenna performance, except the E-plane radiation pattern.

The compact low profile features make for easy integration in body sensors compared to other traditional antennas. According to the specific antenna requirements for on-body communications, the proposed antenna can meet the requirements [98], and it is quite easily

integrated in the PCB broad. Finally, these antennas make multi-hop on-body links and even on-body network investigation possible.

CHAPTER 5

MULTI-HOP ON-BODY CHANNEL INVESTIGATION FOR 60 GHZ WBANS

5.1 Introduction

On-body channels are totally different from any other mobile communication channels, because they are extremely affected by body movements, antenna positions and surrounding environment. For the on-body channel, the single hop channel working at various frequencies has been well-studied in [28, 29]. It was found that the single hop channel could provide stable links in different movement scenarios, and the channel characterization at 2.45 GHz has been done in [19, 27, 107].

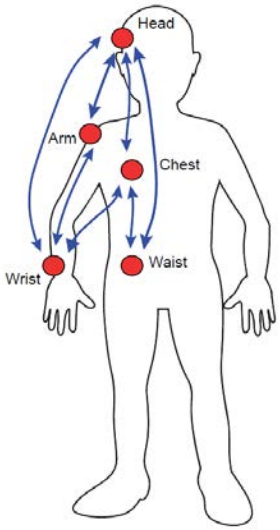

Figure 5.1 Possible antenna positions and channels

Figure 5.1 demonstrates some of the possible antenna positions and channels between different antennas. Every single link among these links aims to represent a practical application, such as mobile phone or smart watch on the wrist, headphones or Google glasses® on the head, a heartbeat monitoring node on the chest, and so on. Thanks to the development of integration technology, products working at low microwave frequencies have been pushed out to the market for serving people in daily life. At microwave frequencies, due to the limited bandwidth and strong interference among different devices, complex coding processes to tell apart the desired signal and interference are required. Therefore, to avoid this complication 60 GHz bands could be employed. However, due to the severe on-body path loss at 60 GHz bands, unlike single hop link at lower frequencies, the single hop link at 60 GHz for on-body communication is very unstable if the distance between the transceivers is much more than 40 cm [108] and in some particular cases the channel will be strongly attenuated due to shadowing. Thus it is necessary to place a repeater node in-between the original link endpoints to increase reliability, which makes the link become part of a multi-hop channel.

In addition, as concluded in [107], the single hop link at 60 GHz is more sensitive to human movements than those at microwave frequencies, which can be considered as both disadvantage and advantage. Although the signal strength level is much lower at 60 GHz bands, it can provide additional information such as the posture or type of movement of the human subject that is not easily identifiable at lower frequencies.

It is well established that on-body radio transmissions at 60 GHz only provide adequate signal coverage over 30-35 cm [108]. This is due to high diffraction losses and small antenna effective aperture areas, in conjunction with the time-variability caused by human movement.

Therefore, to overcome these shortcomings and establish reliable on-body links, high gain reconfigurable antennas are required. However, the design of compact reconfigurable antennas is challenging and their beam steering/switching control can be very complex, making them unsuitable for their intended applications. Therefore, restricting 60 GHz on-body radio links to short distances and adopting a multi-hop radio network approach by employing repeater nodes with fixed beam antennas across the body is a good candidate solution to these problems. However, to the best of the author's knowledge there is no reported research on modeling on-body multi-hop links at 60 GHz.

5.2 Two-hop On-body Communication Investigation

As mentioned before, there are many potential two-hop combinations in a wireless body area network, but this research focuses only on a subset of combinations that could have some practical applications. Therefore, three representative two-hop combinations are discussed here, these being the Head-Chest-Belt, Hand-Belt-Chest and Hand-Arm-Head, respectively. Additionally, only the upright movement scenario, which is a common human position in practice, is investigated for the above three combinations, firstly to see their performances under the same movement scenario in this section. The other movement scenarios will be considered in the following section using just the Head-Chest-Belt link only to see what effect different movement scenarios can cause. Two types of directional SIW Vivaldi array antennas designed for multi-hop communications as discussed in Chapter 3 were used. Figure 5.2 shows the structure of the antennas.

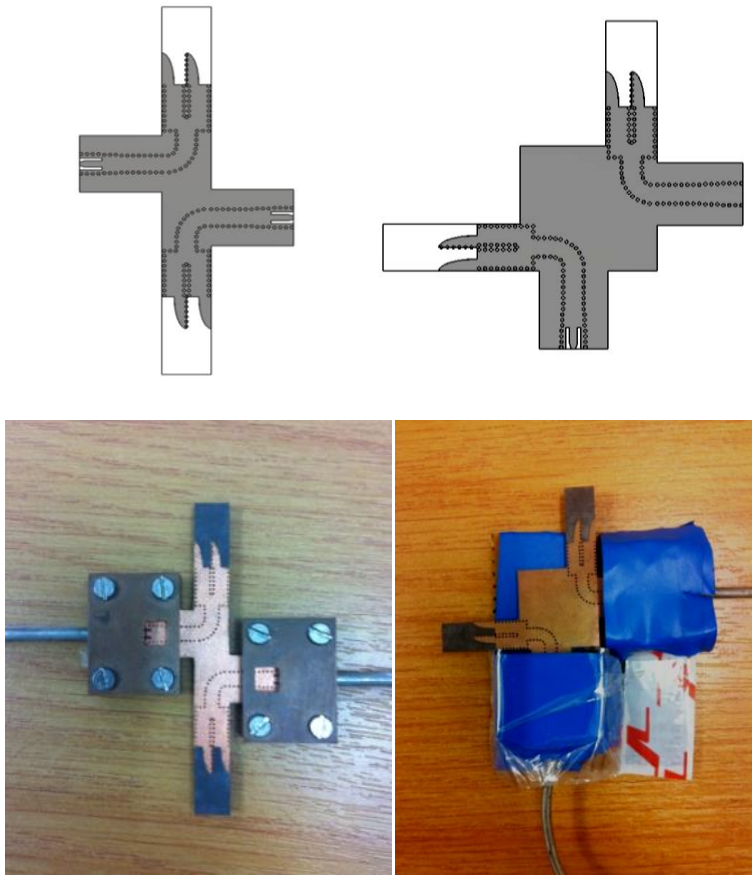

(a) (b)

Figure 5.2 Structure of mounted antennas

5.2.1 Head-Chest-Belt Link

In the measurements, all three antennas were placed on the left side of the body where sensors might be put. The static posture distances between antennas were 39 cm and 32 cm, respectively, and antenna (a) was used as shown in Figure 5.3. The upright movements adopted included walking, eating, typing, turning and bending body. This set of movements was repeated 5-6 times within 60 seconds, and the movement scope remained the same. Each individual movement lasted around 2 seconds to ensure that the VNA recorded the changing of movement.

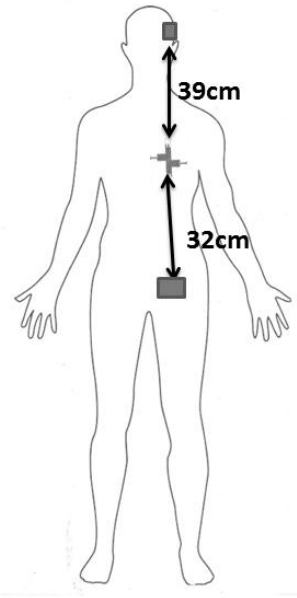

Figure 5.3 Head-Chest-Belt link using proposed antenna (a)

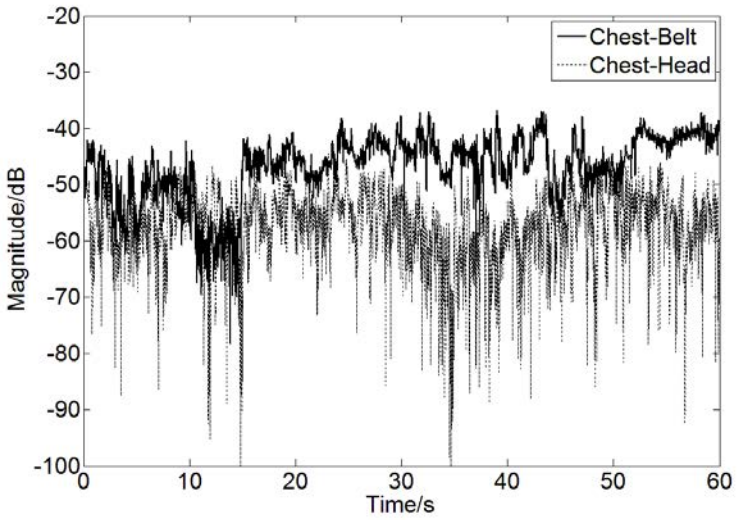

Figure 5.4 Normalised S_{21} of the Head-Chest-Belt link

According to Figure 5.4, the Belt-Chest link is strong and remains within a small range because no matter what movement is adopted the relative position of the two antennas mounted on the chest and belt is static. However, it is observed that the movements cause more fading to the link of Chest-Head than the link of Belt-Chest. This is because the relative position of the antenna on the head is not as static as that on the belt, and also the distance

between head and chest is larger than the distance between chest and belt, which also accounts for the signal level of the Chest-Head link being always weaker than that of Chest-Belt link.

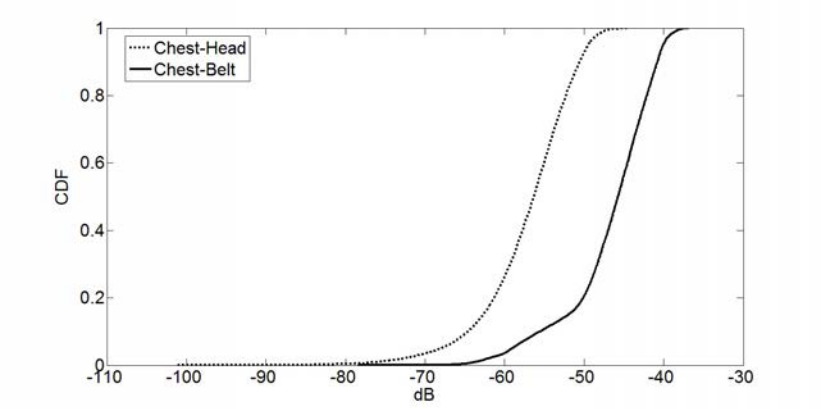

Figure 5.5 CDF of the Head-Chest-Belt link

Figure 5.5 presents the CDF of the Head-Chest-Belt link. It indicates that the Chest-Belt link is about 10 dB (median value) better than the Chest-Head link, and the signal of Chest-Head falls below the noise floor only at 12s, 14s and 34s, but the Chest-Belt link is never below the noise floor. In addition, the wider the CDF curve expands, the wider range the signal changes within.

5.2.2 Head-Arm-Wrist

As seen in Figure 5.6, the static posture distances between antennas were 40 cm and 35 cm, respectively. The repeater node was mounted on the upper part of the left arm, and the upright random movements were introduced as well. Antenna (a) was used in this measurement.

Figure 5.7 shows the received signal level of the Head-Arm-Wrist link. It shows that the wrist-arm link is more stable than the arm-head link, because the relative positions of

antennas on wrist and upper arm are less variable with body movement, while the arm-head link suffers from more rapid variations because of the polarization mismatch caused by turning the head or raising the arm.

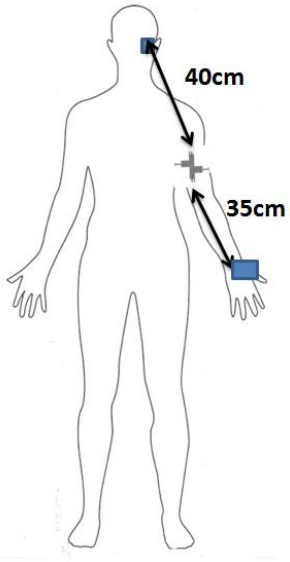

Figure 5.6 Head-Arm-Wrist link using proposed antennas

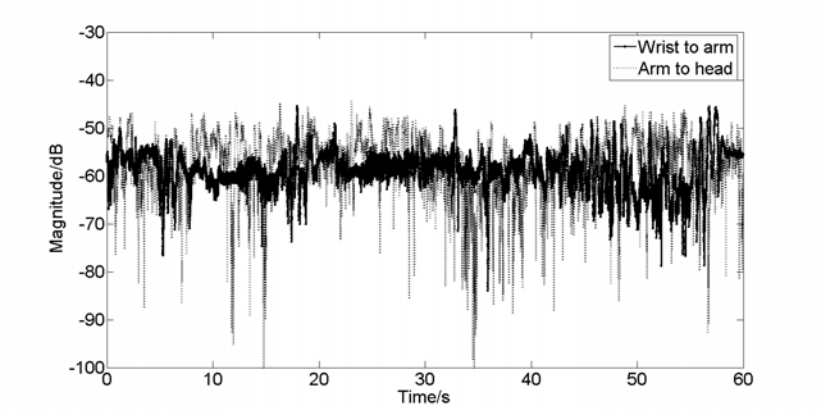

Figure 5.7 Normalised S_{21} of the Head-Arm-Wrist link.

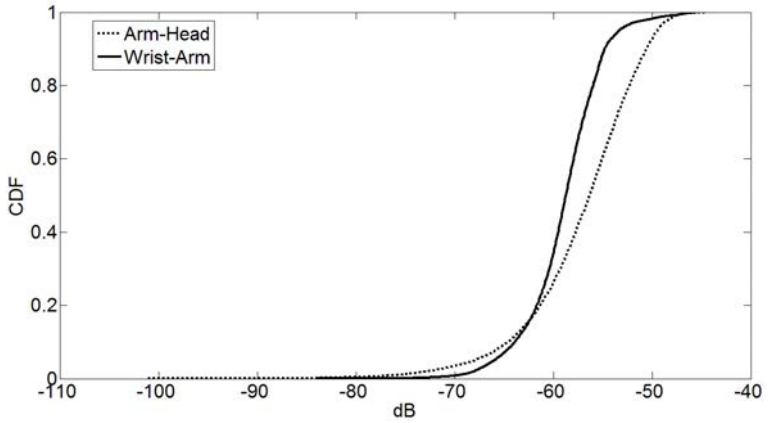

Figure 5.8 CDF of the Head-Arm-Wrist link

Figure 5.8 shows the CDF of the Head-Arm-Wrist link. Although the average strength level of each single link is almost the same, the signal range of the Wrist-Arm link is much smaller than that of the Arm-Head link.

5.2.3 Belt-Chest-Wrist

In this case, the antennas were mounted on the belt, chest and wrist, respectively shown in Figure 5.9. The static posture separation between the chest and belt remained the same as before, and the distance between the wrist and belt was much shorter than any link studied in the other measurements. However, because upright random movements were conducted, the Belt-Wrist link was the most variable link with distance ranging from up to 100 cm down to 15 cm when the test subject started moving. In addition, antenna (b) was used in this measurement.

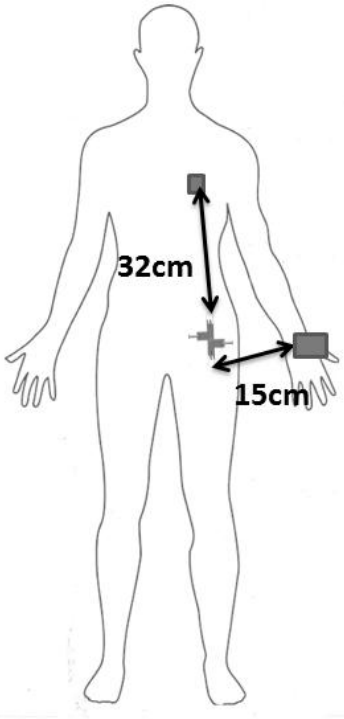

Figure 5.9 Chest-Belt-Wrist link using proposed antenna (b)

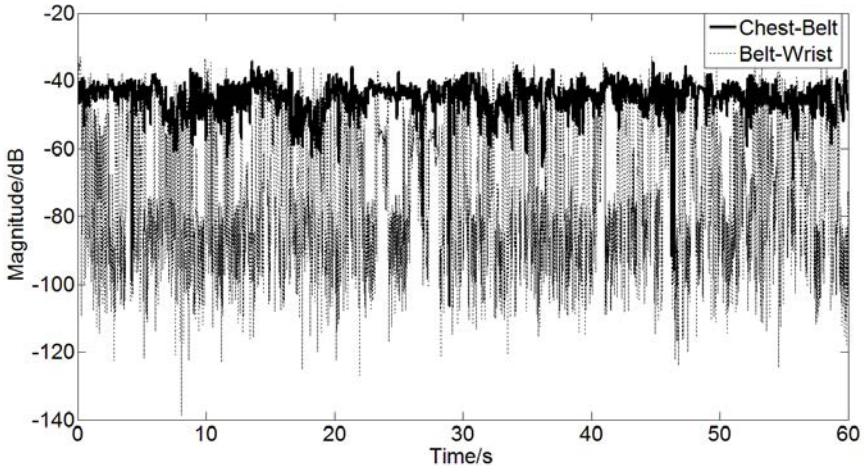

Figure 5.10 Normalised S_{21} of the Chest-Belt-Wrist link

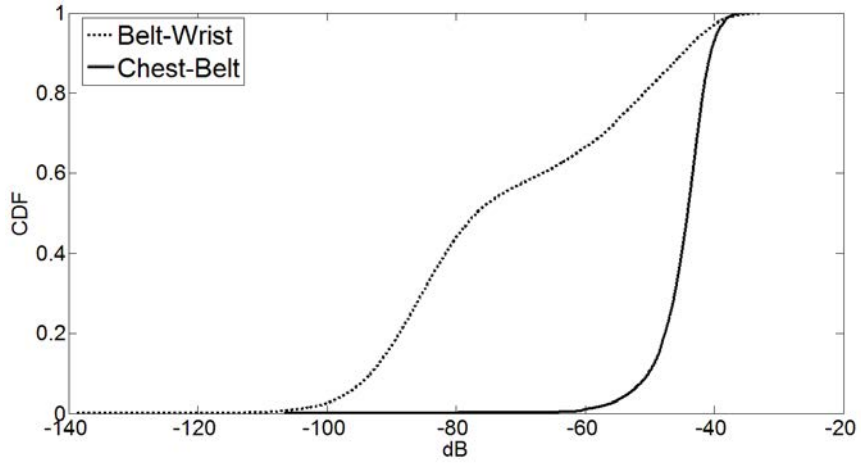

Figure 5.11 CDF of the Chest-Belt-Wrist link

As shown in Figure 5.10, although the separation between belt and wrist was the shortest among all the links studied when there were no movements introduced, the received signal level of Belt-Wrist was the most unstable link when the upright random movements were introduced. Additionally, shadowing kept occurring in the belt-wrist link due to the non line-of-sight condition caused by arm swinging behind the body during movement, while the Belt-Chest link remained stable as expected. Figure 5.11 also indicates that 99% of the Belt-Chest link is over -60 dB, but only about 30% of the Belt-Wrist link is over -60 dB. In addition, nearly 20% of Belt-Wrist signal is below the noise floor.

5.3 Simple Thresholding and Modelling

Most on-body communication network investigations have been focused at microwave frequencies bands such as the 2.45 GHz industrial, scientific, and medical (ISM) frequency band and the 3.1 – 10.6 GHz ultra-wide band (UWB). The propagation channel at 2.45 GHz is comprehensively described in [109]. A three-state Frichman model was proposed through the analysis of dynamic path loss characteristic of on-body channel. Research at 60 GHz has

previously concentrated on the empirical characterization of single links [108], where a Markov process was used to model the intermittency of 60 GHz on-body channels.

This studies focus on modelling the characteristics of multi-hop on-body channels in three different movement scenarios, such as duration of joint-state, and transition probabilities between different states. A single two-hop link was chosen to represent a basic BAN on the human body with end nodes located on the belt (e.g. wearable computer) and head (e.g. , G ®), j ’

Three movement scenarios were investigated: random movements performed in an upright position (e.g. walking, eating, typing, and turning and bending body), crawling on the ground like a soldier (back and forward), and lying on a hospital bed like a patient (adopting a semi-reclined position, lying down, and turning side to side on the laboratory floor). Figure 5.12 shows the node placements and investigated scenarios. The adopted node placements are typical of a wide range of BAN applications. For example, the head node is representative of an infrared visor head-mounted display in military applications, an electro-encephalogram aggregation node in medical applications, or a head-worn display (e.g. Google Glass®) in infotainment applications.

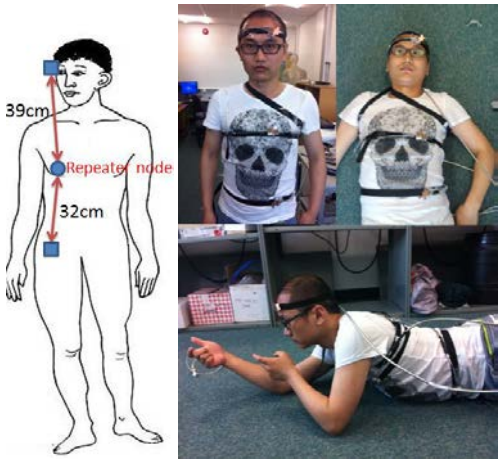

Figure 5.12 Node placements and movement scenarios

Figure 5.13 shows the measured data obtained for the three movement scenarios. For each measurement, the two individual links of the investigated multi-hop network are measured simultaneously. In the case of crawling, shown in Figure 5.13 (a), the chest to head link is very weak due to the raised head position adopted, and the strength of the received signal is very close the measurement noise floor. In contrast, the chest-belt link is much stronger, because the relative position of the endpoint antennas is relatively static, with a near line of sight condition being met most of the time. In addition, compared to the other two cases, it is observed that there exists a more rapid temporal variation in the received signal in the crawling case. It is believed that this is caused by multipath fading because the test subject is crawling with the antennas in close proximity to the ground, introducing a strong ground reflected path. System link thresholds – dB below the median path loss, imitating transmit power control aiming to extend the node battery lifespan. It is a simple way of thresholding to help to justify the state of the channel, and more details about thresholding method can be found in Chapter 6. The only exception is the chest-to-head link, where this threshold would be very close to the noise floor, thus degrading severely the bit error ratio (BER) of a 60 GHz radio module. In this case it is assumed that a typical Vubiq® receiver is used and the threshold is set

to be its 10^{-6} BER quadrature phase shift keying (QPSK) modulated receiver sensitivity – 5 dBm). The threshold levels are summarized in Table 5.1.

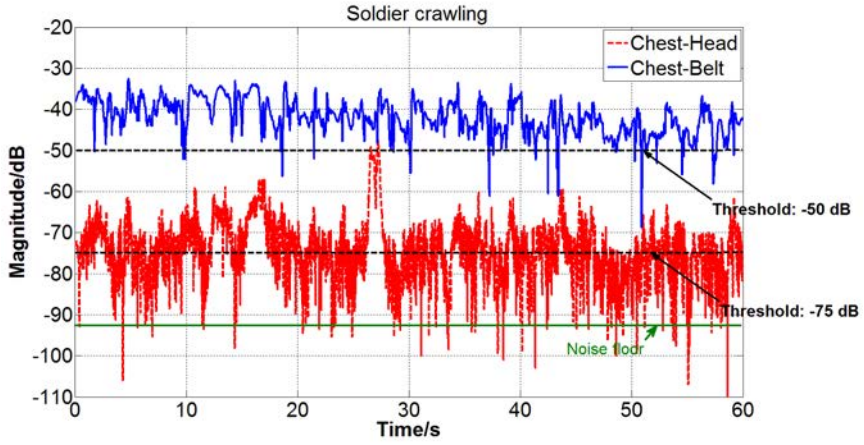

(a)

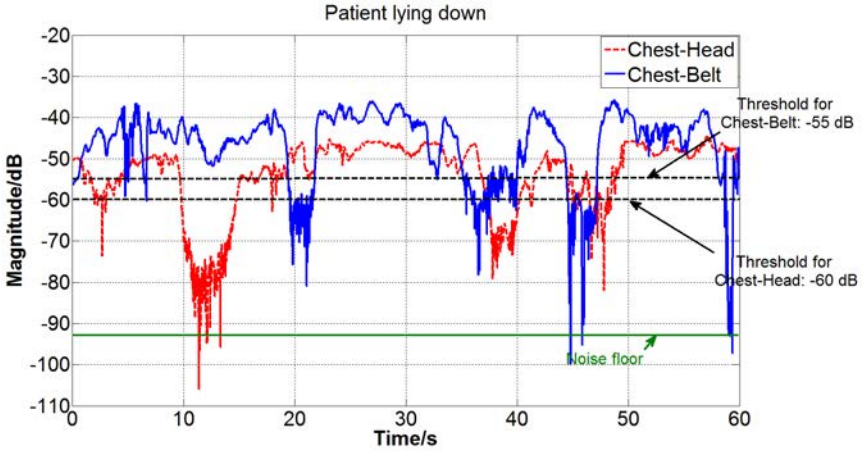

(b)

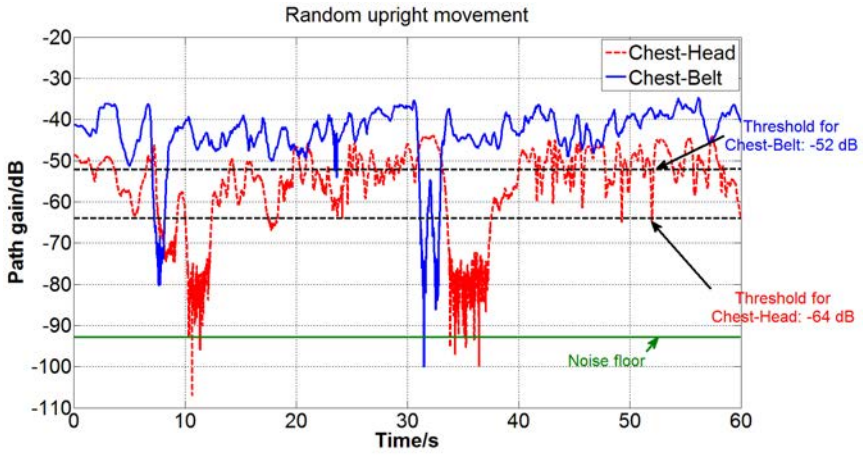

(c)

Figure 5.13 Measured signals with time variation: (a) soldier crawling, (b) patient lying down and (c) random upright movements

Table 5.1 Link State Threshold Levels

Link	**Thresholds (dB)**		
	Crawling	***Patient***	***Random***
Chest-Head	–75	–60	–64
Chest-Belt	–50	–55	–52

Given the choice of thresholds discussed above, the state of the two-hop WBAN channel in terms of four combinations of individual binary link states are described as:

- On-On:- both links are on;
- Off-On:- chest-head link is off and chest-belt link is on;
- On-Off:- chest-head link is on and chest-belt link is off;

• Off-Off: - both links are off.

The channel state probabilities for each of the three scenarios are given in Table 5.2. The table indicates that in all the three movement scenarios, the On-On state occurs most frequently, while the Off-Off state happens very infrequently. This naturally occurs by design due to the choice of the thresholds. However, the frequency of the states in which only one of the links is off, is fairly significant, especially in the case of the crawling movement for the Off-On link, which occurs almost as often as the On-On state. Thus, a store and forward switch with a suitably dimensioned memory buffer is needed in the repeater node on the chest as well as the head node to hold the received data during the On-Off and Off-On periods in order to transmit it later, when the Off link transitions into the On state again.

Table 5.2 The Probabilities of Channel States for the Three Movement Scenarios

Channel state	**Movement scenarios**		
	Crawling	***Patient***	***Random***
On-On	0.5358	0.6958	0.8087
Off-On	0.4358	0.1276	0.1346
On-Off	0.011	0.1323	0.0433
Off-Off	0.0147	0.044	0.013

The empirical cumulative distribution functions (CDFs) of the durations of each of the four states are shown in Figure 5.14. As the measured data sets were limited to time spans of only about 60 s, and most states happen fairly infrequently, the available data is not sufficient to derive reliable statistics. Therefore, most plots in Figure 5.14 do not look smooth and are only a rough estimate of the CDFs. However, they do provide a reasonable indication of the

expected durations of the channel states, and they are enough to tell the different effects caused by different movement scenarios.

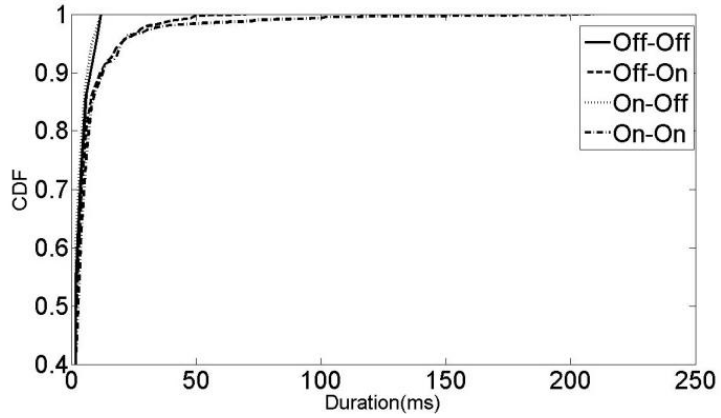

(a)

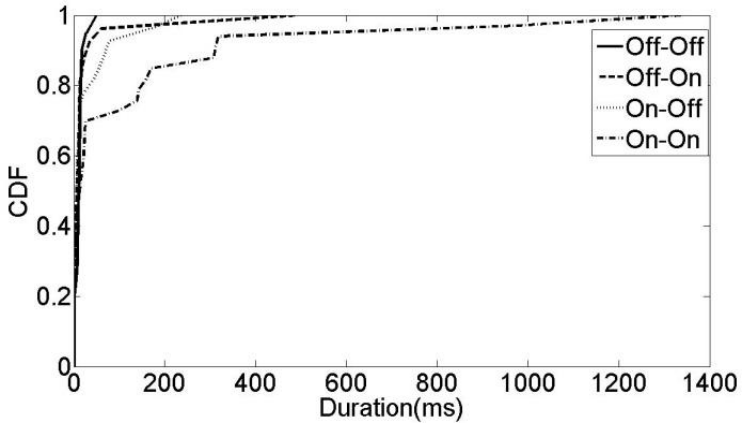

(b)

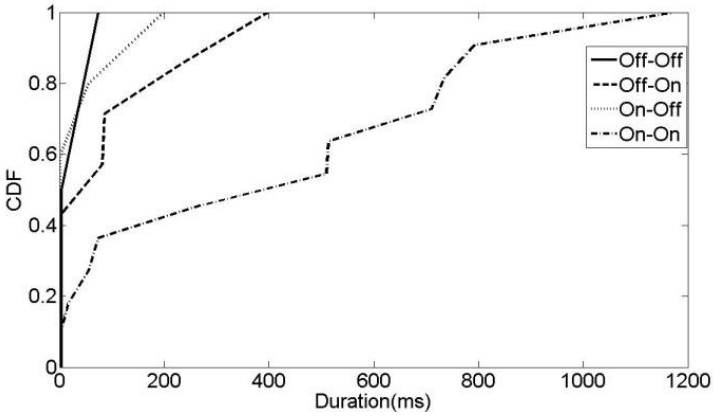

(c)

Figure 5.14 CDF of the duration of four states in the case of (a) crawling (b) patient lying down and (c) upright random movements

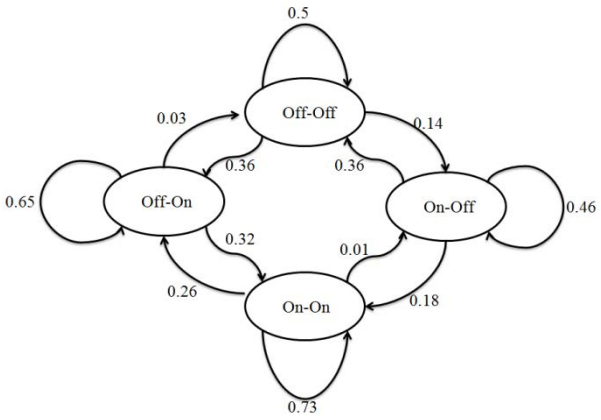

(a)

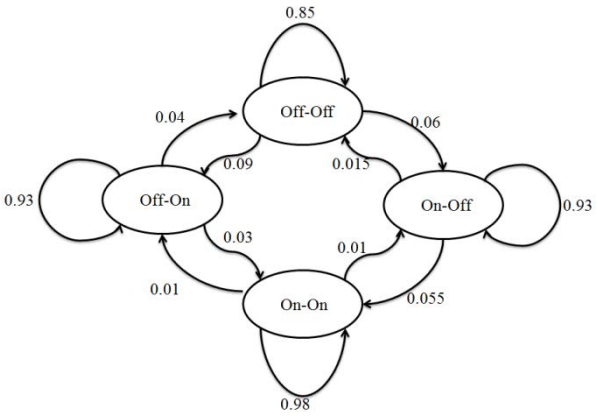

(b)

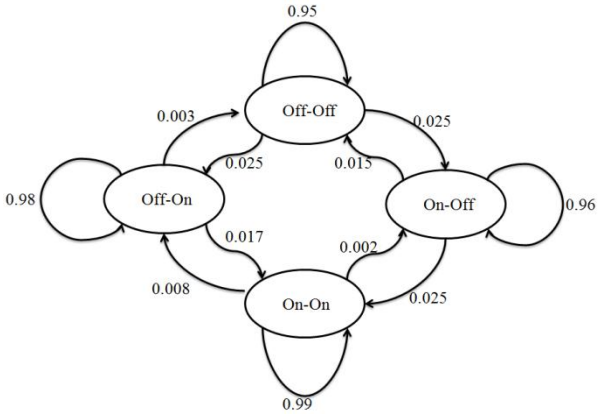

(c)

Figure 5.15 Transition probabilities of four-state model for (a) soldier crawling (b) patient lying down and (c) random upright movements

Figure 5.15 depicts the state transition probabilities of the four-state model. Each state will either be maintained or transited to the other three states. The arrow starts from one state and end at another, and the number above the arrow represents the transition probability from one state to another. It is observed that the crawling case is the most unstable scenario among the three, with the most short-lived states and relatively small probability of staying in a stable On-On state. The state of the channel keeps switching mostly between the On-On and the Off-On states. Transition to the On-Off state is unlikely, but when it does happen, it is more likely to switch to the Off-Off state than to return back to the On-On state. For the other two types of movement, the On-On state dominates and transitions to the other states happen infrequently and for relatively short durations. It is worth mentioning that there are no direct transitions between the Off-Off and On-On states during the whole process, as switching the states of the two links simultaneously is very unlikely and has never been observed.

Table 5.3 The durations of Channel States for the Three Movement Scenarios

Channel state	**Movement scenarios (ms)**		
	Crawling	***Patient***	***Random***
Off-Off	8	50	70
Off-On	44	490	380
On-Off	16	200	180
On-On	76	1200	1100

Table 5.3 shows the durations of channel states for the three movement scenarios. In the case of crawling, the duration of the On-Off and Off-Off states is very short compared to the Off-On and On-On states. Moreover, 99% of the On-Off and Off-Off state durations are shorter than 16 ms. Similarly, in the case of patient movements and upright random movements, the Off-Off state hardly ever lasts longer than about 50 ms and 70 ms, respectively. However, the states in which only one link is in the Off state (i.e. On-Off and Off-On) last significantly longer, up to about 490 ms. Table 5.2 shows that the probabilities of such states are also quite significant, mostly around 0.13 but being as high as 0.44 for the Off-On state in the crawling movement. Moreover, the On-On state in the case of patient movements and upright random movements can live over 1000 ms, and even in the case of crawling it is still the longest lived state. Finally, according to all above discussions, it is easy to find out that these two-hop links provide much more information compared to single links at either the 2.45 GHz [108] or the 60 GHz bands. This extra information, such as data in Table 5.3, can be made use of indentifying posture and activity in a BAN wearer. Moreover, the duration of the joint link states can inform the dimensioning of store and forward memory buffers in the repeater nodes.

5.4 Summary

In this chapter, first, an investigation on three two-hop links under the same movement scenario is given. It is found that static two-hop links can be achieved using the proposed antennas in Chapter 3 except the most variable Belt-Wrist link. Then an initial experimental assessment of the applicability of a four-state model for multi-hop on-body communications at millimetre-wave frequencies is presented. This model reveals that, protocol designers need to adopt a disruption tolerant network approach in creating protocols capable of end-to-end data transport that is reliable, despite the link intermittency observed. It must be stressed that the presented results are *indicative* of on-body channel intermittency at 60 GHz. However, as they have been conducted on a single subject over a restricted number of antenna placements and stylized movements, they cannot be considered as a comprehensive reliable statistical model.

CHAPTER 6

ON-BODY LINK DIVERSITY AT 60 GHZ

6.1 Introduction

Channel fading is usually categorised into short-term and long-term fading. Short-term fading is mainly caused due to multipath propagation, while the long-term fading, also called shadowing, is mainly caused by the changing separation between the transceivers, or a relatively electrically big obstruction moving into position along the propagation path. For the case of on-body communication, the short-term fading usually comes from the scattering from the surrounding environment (furniture, humans and so on), while the long-term fading is often caused by human movements. Figure 6.1 shows a typical example of signal variation, with the short-term fading separated from the long-term fading by adopting a sliding window averaging process over a short-time period. Details of the data analysis can be found in [108].

Diversity is considered as a powerful technique that can overcome the channel fading. According to the definition of diversity, the received signals can be improved through using two or more uncorrelated branches. If the branches are sufficiently independent in time, space, frequency, polarization and/or radiation pattern, the fading in each branch will be independent. The application of the diversity technique for on-body communication at lower microwave frequencies has been studied in [110]. It was found that through applying space, pattern and polarization diversity at lower frequencies, up to 10 dB diversity gain can be achieved in most

on-body channels. In addition, different combining technique can also affect the performance of combined signal.

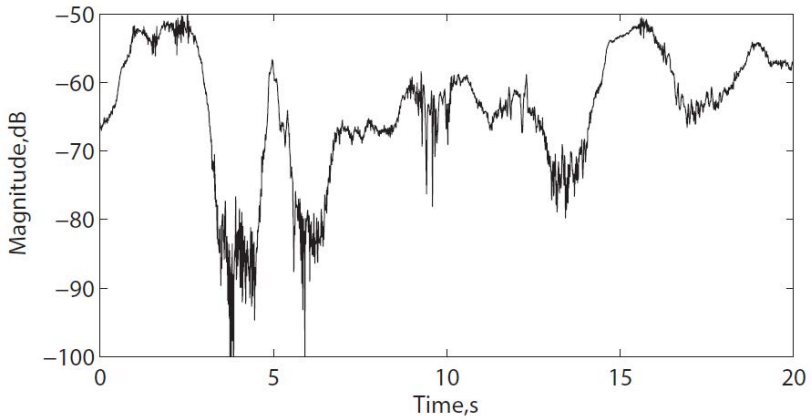

(a)

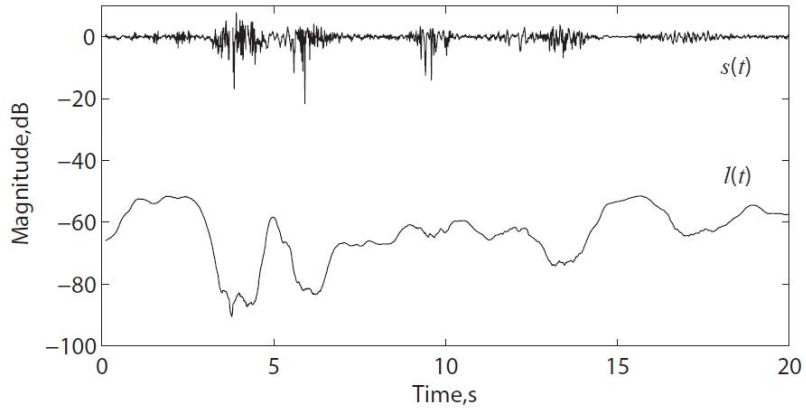

(b)

Figure 6.1 Time variation of measured signals (a) measured signal envelope (b) Long-term, *l(t)*, and short-term, *s(t)*, components

However, on-body channels at 60 GHz are very different from those channels at lower frequencies. For some variable channels, such as the Belt-Wrist and Chest-Head, deep shadowing occurs frequently due to the non-line-of-sight condition caused by human movements, which is much less severe at lower frequencies. Therefore, not all diversity techniques are able to improve the performance of on-body channels at 60 GHz. For instance,

if space diversity is applied in the Belt-Wrist channel at 60 GHz, all branches are likely to suffer the same shadowing when the line-of-sight condition is lost due to the wrist movements, Thus, none of the branches are useful in contributing to the combined signal. After comparing the disadvantages and advantages of all diversity methods, it is found that radiation pattern diversity is the best choice at 60 GHz because each branch under this method can cover its own district propagation path that has the potential to be experiencing uncorrelated shadowing to other paths. In another word, radiation pattern diversity enlarges the physical area over which energy can be transported between transceivers for some specific channels. In addition, among four combining methods, selection combining is likely to be the best option to work well with radiation pattern diversity, because only the strongest branches should be selected among all branches at certain moment and scattering environment. The four combining schemes considered have been discussed in Chapter 2.

6.2 On-Body Diversity Investigation at 60 GHz

Five scenarios are considered here, which are:

1. Transmitter on wrist with single antenna – Receivers on chest with two collocated antenna branches with orthogonal main lobes
2. Transmitters on wrist with two collocated antenna branches with orthogonal main lobes – Receivers on chest with two collocated antenna branches with orthogonal main lobes
3. Transmitters on wrist with two collocated antenna branches with orthogonal main lobes – Receivers on belt with two collocated antenna branches with orthogonal main lobes
4. Transmitters on wrist with two collocated antenna branches with back to back main lobes – Receivers on chest with two collocated antenna branches with orthogonal main lobes

5. Transmitter on wrist with two collocated antenna branches with orthogonal main lobes – Receivers on upper arm with two collocated antenna branches with orthogonal main lobes

The distance between the antenna and the body surface was about 5mm, and the separation between the transceivers would be discussed in the following analysis.

In addition, the success of diversity depends on the degree to which the different branches are uncorrelated. Therefore, to identify the degree of independence between different branches, cross-correlation is employed to describe the statistical independence of different branches. However, in some particular cases, even when the correlation coefficient is high, diversity still yields good improvement. The cross-correlation between branches will be discussed in each scenario below.

6.2.1 Single-transmitter (wrist) to Multiple-receivers (chest)

Figure 6.2 shows the case of Transmitter on wrist with single antenna – Receivers on chest with two collocated antenna branches with orthogonal main lobes. The proposed SIW Vivaldi antennas of Chapter IV were used in the measurement. The two sets of antenna elements on the chest are at 90°to each other to achieve orthogonal pattern diversity. This beams point to the upper arm and belt, respectively, while the transmitter on the wrist points toward the upper arm all the time. The distance between the transmitter and receiver was 37 cm when the test subject was standing still, and varied from approximately 10 cm to 60 cm when the upright movements were introduced during the entire measurement. Finally, the links were labelled as Branch 1 and 2 as shown in Figure 6.2

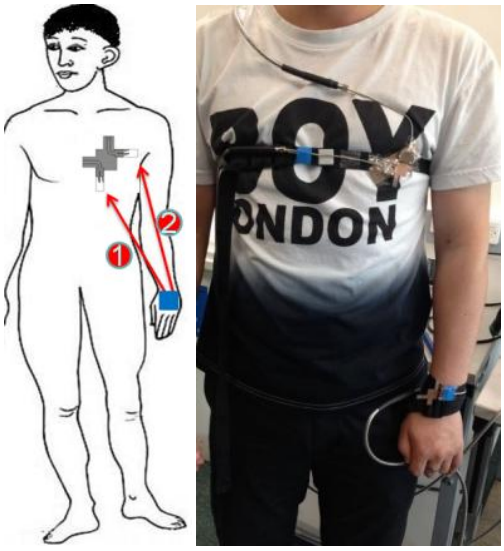

Figure 6.2 Single-transmitter (wrist) to Multiple-receivers (chest)

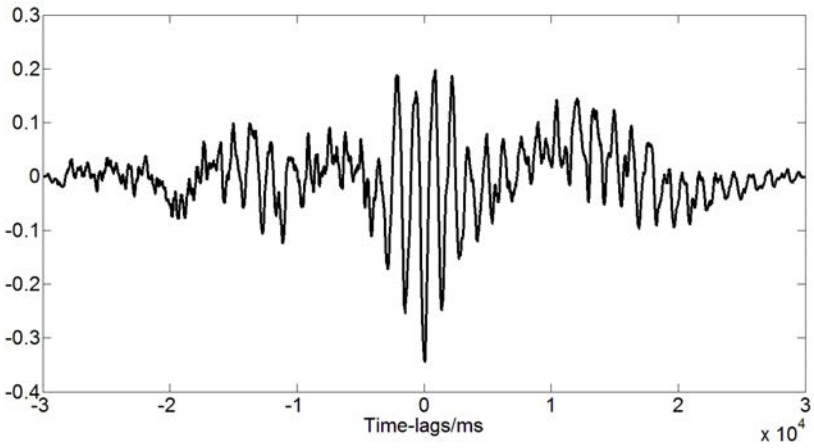

Figure 6.3 Cross-correlation between Branch 1 and 2

Figure 6.3 depicts the cross-correlation between Link 1 and Link 2. It indicates that the maximum cross-correlation coefficient of the two branches is about -0.35, which means they are anti-correlated to a small degree but not significantly. Therefore, these branches can be considered as sufficiently independent, and diversity can be employed to improve the link quality.

Figure 6.4 shows the received signal levels of each branch and selection combined signal. The mean value of Branch 1 and 2 in Figure 6.4 is -57.6 dB and -58.3 dB, respectively. They are at the same level and both of them cross the noise floor in a few instances. In addition, the environment of this measurement was different from the following cases. There is less short-term fading in this case, because the test human subject is surrounded by only few furniture

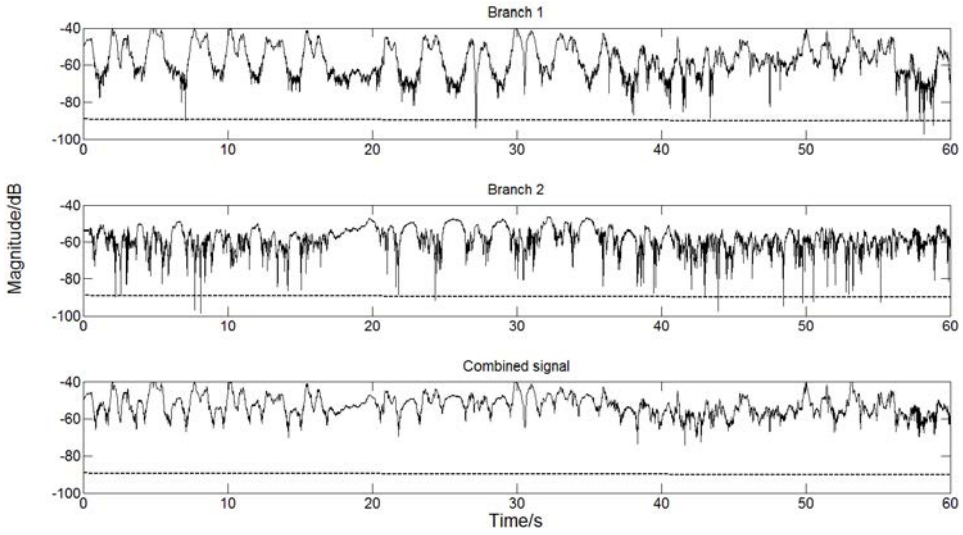

Figure 6.4 S_{21} of each branch and combined signal, noise floor indicated by dashed line

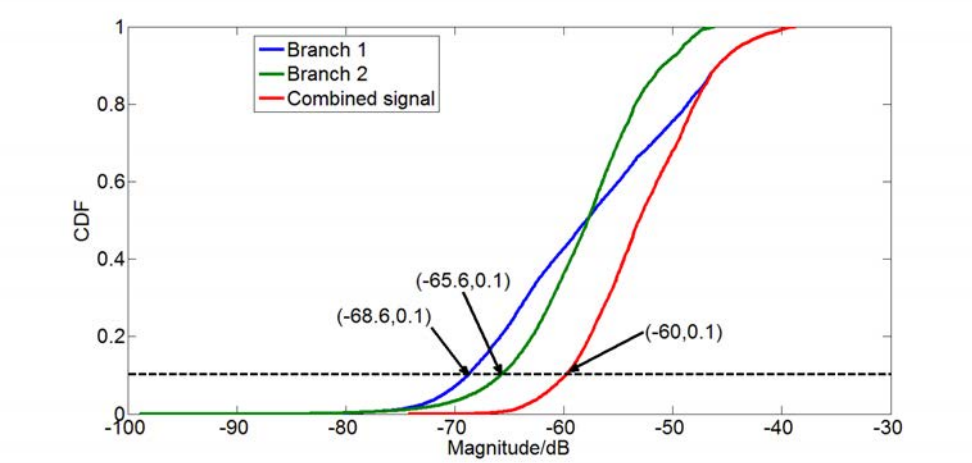

Figure 6.5 CDF comparison of each branch and combined signal path gain

Figure 6.5 shows the comparison of each branch and the combined signal path gain which is obtained by using the selection diversity method. The diversity gain is about 5.6 dB at the probability level of 10% (normal practice) according to Figure 6.5, which is such that fading is less severe and that the channel signal strength never crosses the noise floor. Therefore, signals can be improved by applying the selection diversity method in the case of Single-transmitter (wrist) to Multiple-receivers (chest).

6.2.2 Multiple- transmitter (wrist) to Multiple- receivers (chest)

The first case examined shows that Single-transmitter (wrist) to Multiple- receivers (chest) is able to improve the channel performance. However, only the case of transmitter pointing upward is considered, thus it was necessary to investigate the case of Multiple- transmitter (wrist) to Multiple- receivers (chest) to see whether this case can provide even better performance for a hightly volatile channel. Figure 6.6 shows the schematic diagram of Multiple- transmitter (wrist) to Multiple- receivers (chest), and the branches are labelled as Link 1, 2, 3 and 4, respectively. Upright random movements were still conducted in this case. The separation between transmitters and receivers were 37 cm when the test subject was standing still, but it could be up/down to about 70cm/10 cm when the test subject was moving.

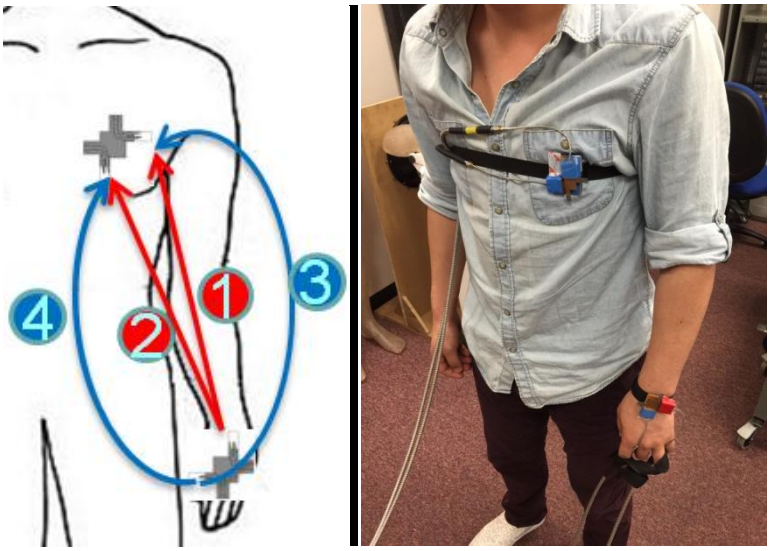

Figure 6.6 Multiple-transmitter (wrist) to Multiple- receivers (chest)

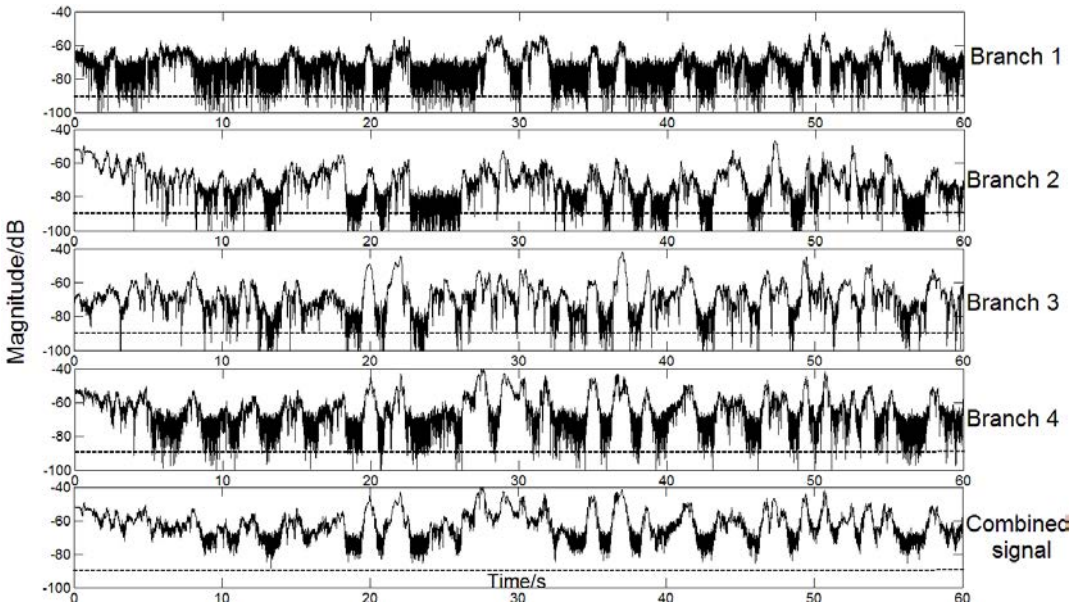

Figure 6.7 S_{21} of branch 1, 2, 3, 4 and combined signal (chest-wrist), noise floor indicated by dashed line

Figure 6.7 presents the branch and selection combined signals. The RMS noise floor is shown as a reference. Branch 1 and Branch 2 fall below the noise floor frequently, especially Branch 1 that exhibits a low signal level during the entire measurement. Both these branches suffer more multi-path fading compared to Branches 3 and 4, because it is believed that signals transmitted from the antenna element pointing toward upper arm are always affected by the

arm first, while signals transmitted from the antenna element pointing towards the torso propagate into space first. In addition, the mean value of each branch and combined signal is also given in Table 6.1 to show the improvement achieved bythe combined signal.

Table 6.1 Mean values of each branch and combined signal (chest-wrist)

Mean value (dB)				
Branch 1	Branch 2	Branch 3	Branch 4	Combined signal
-72.6	-72.8	-69.4	-65.6	-62.7

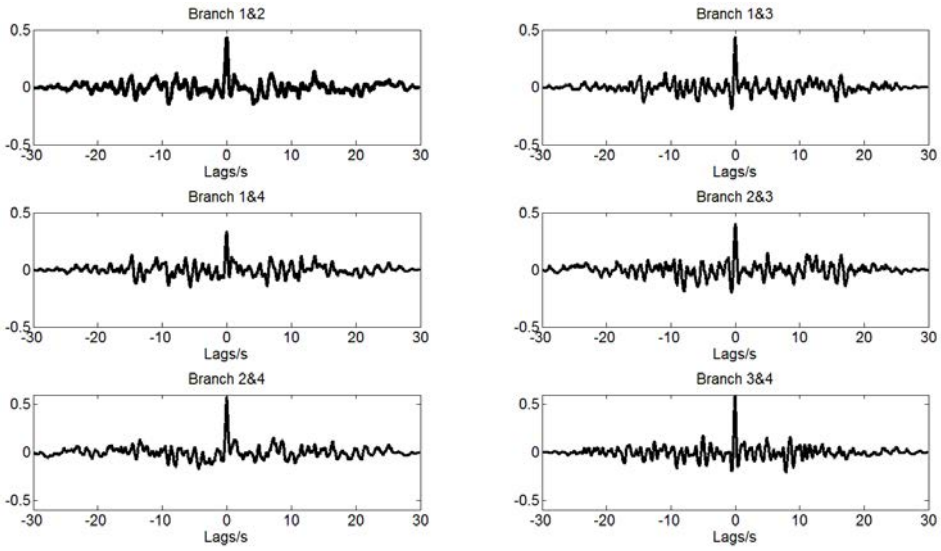

Figure 6.8 Cross-correlation between different branches (Chest-Wrist)

The Cross-correlation coefficients between different branches are shown in Figure 6.8. The cross-correlation at zero time lag between Branch 2 & 4 as well as Branch 3 & 4 are relatively high compared to the rest, which means in some instances the signal changing trend is same in

each branch. For instance, both Branch 3 and 4 received strong signals at around 22s. However, there are still some instances that only one branch can provide a reliable link. For instance, at around 24 s, only branch 3 recorded a strong signal. Therefore, employing a diversity technique is very useful in this case.

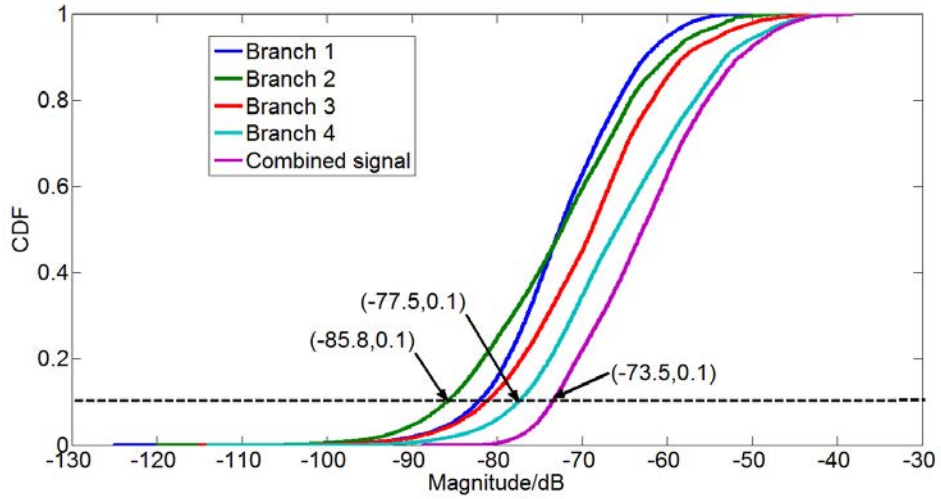

Figure 6.9 CDF comparison of each branch and combined signal (chest-wrist)

With the comparison of each branch and combined signal using selected diversity method shown in Figure 6.9, it indicates that at the level of 10% probability the minimum and maximum diversity gain are approximately 6 dB and 12.3 dB relative to individual branches.

6.2.3 Multiple-transmitter Formed 90 Degree (wrist) to Multiple-receivers (belt)

In this case, the receivers were relocated as shown in Figure 6.10, and branches were also labelled as 1, 2, 3 and 4. This arrangement is to justify whether reliable link can exist between wrist and belt where base station located usually. Upright movements were still conducted in this measurement. The minimum separation between transmitters and receivers was 11 cm

when the test subject was standing still, and the maximum separation was as much as 150 cm when the arm was raised over the head.

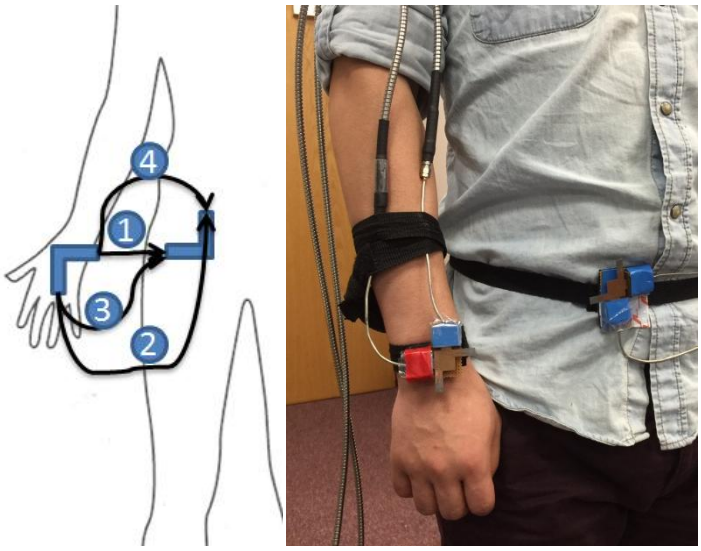

Figure 6.10 Multiple-transmitter (wrist-9) to Multiple-receivers (belt)

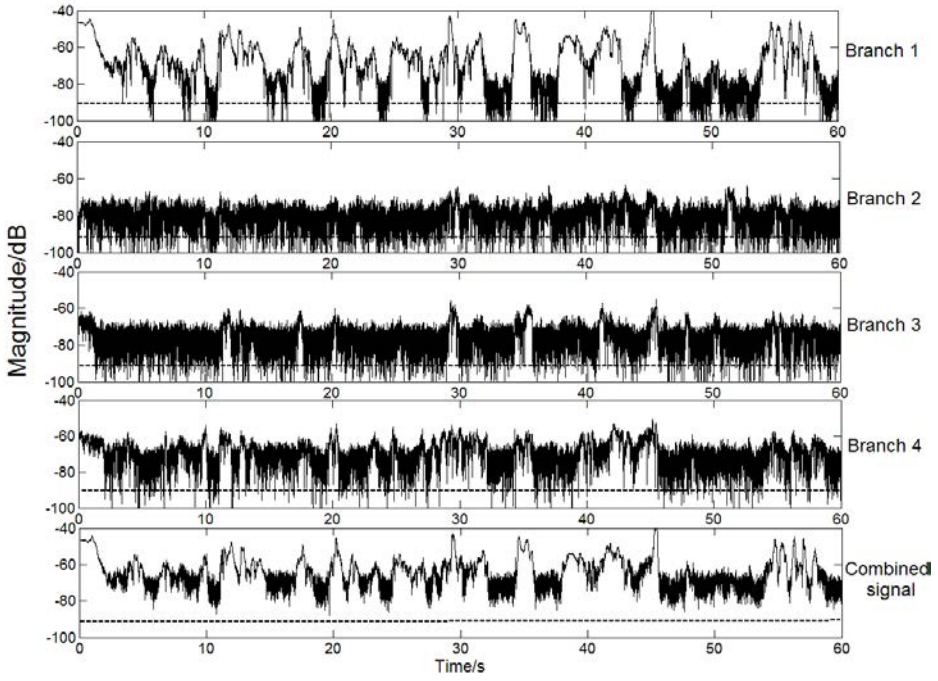

Figure 6.11 S_{21} of each branch an - to belt), noise floor indicated by dashed line

Figure 6.11 shows the received signal magnitude of each branch and selection combined signal in the case of Multiple-transmitter 90 degree (wrist) to Multiple-receivers (belt). It is found that only Branch 1 can provide a consistently strong signal during the entire measurement. Although the strength levels of Branches 2 and 3 are generally above the noise floor, they are not able to establish a reliable link individually, which indicates that the antenna element on the wrist pointing down is not helpful. Branch 4 also suffers from severe multi-path effect, but it still can provide a strong signal at some instances. For instance, at about 10s, all the other branches are at very low level, only Branch 4 still has a relatively high signal.

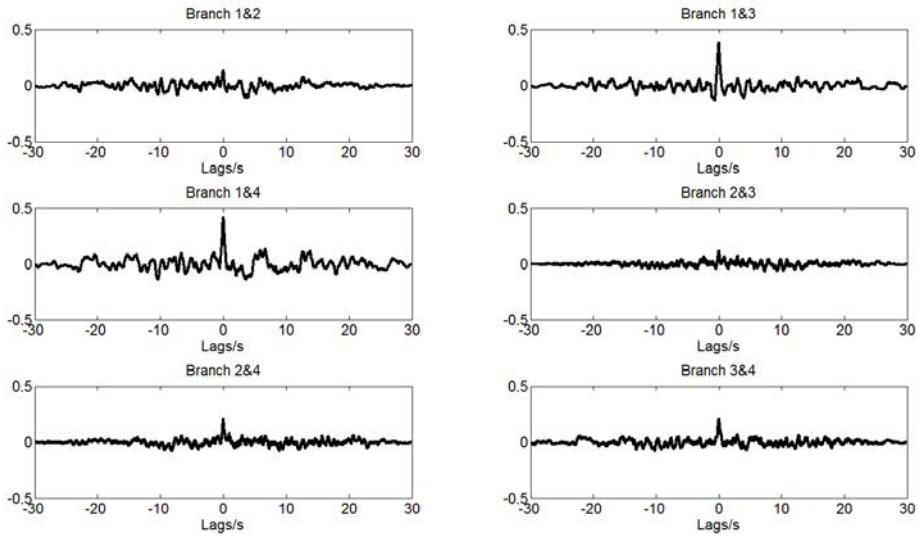

Figure 6.12 - - to belt)

Figure 6.12 presents the cross-correlation coefficient between different branches. It shows that only Branches 1 & 3 and Branches 1 & 4 exhibit a low correlation level for short time lags, and the other branches are independent to each other. Therefore, adopting a diversity technique is feasible in this case.

According to Figure 6.13, only Branch 1 varies over a big path loss range, while the other branches are less variable. In addition, at the 10% probability level the minimum and

maximum diversity gain are about 4.6 dB and 13.8 dB relative to Branch 2 and Branch 4, respectively. The mean values of each branch and combined signal are given in Table 6.2, which demonstrates the improvement achieved by combined signal.

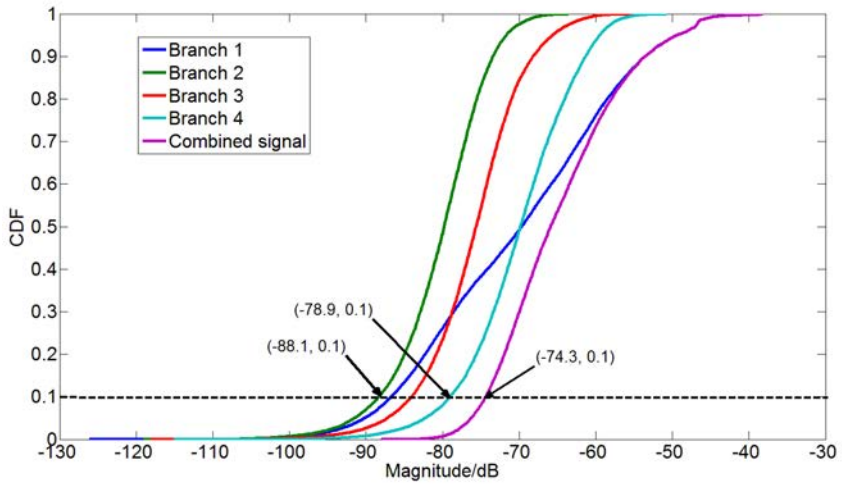

Figure 6.13 - to belt)

Table 6 - to belt)

Mean value (dB)				
Branch 1	Branch 2	Branch 3	Branch 4	Combined signal
-70.1	-80.4	-75.9	-70.1	-64.8

6.2.4 Multiple-transmitters Formed 180 Degree (wrist) to Multiple-receivers (belt)

y k ,

relative to each other is investigated in this section. Figure 6.14

shows the antenna placements and denotes schematically the diversity branches. Upright movements were also conducted in this measurement, and the separation between transmitters and receivers varied from 11 cm to 150 cm.

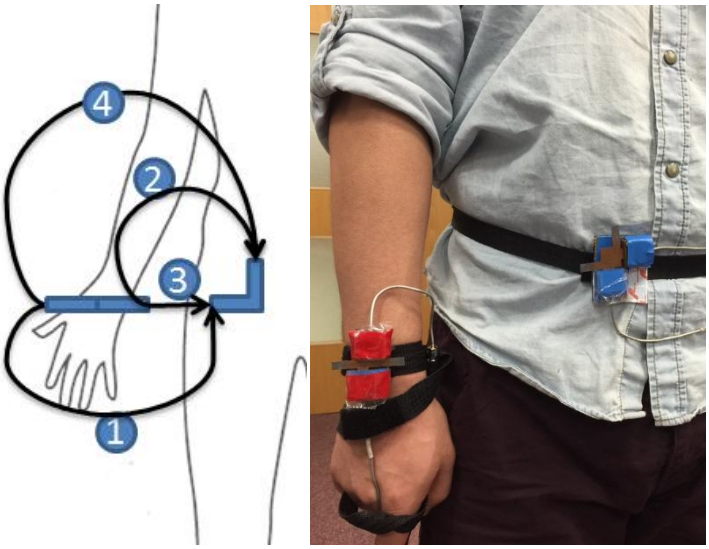

Figure 6.14 - -) to Multiple-receivers (belt)

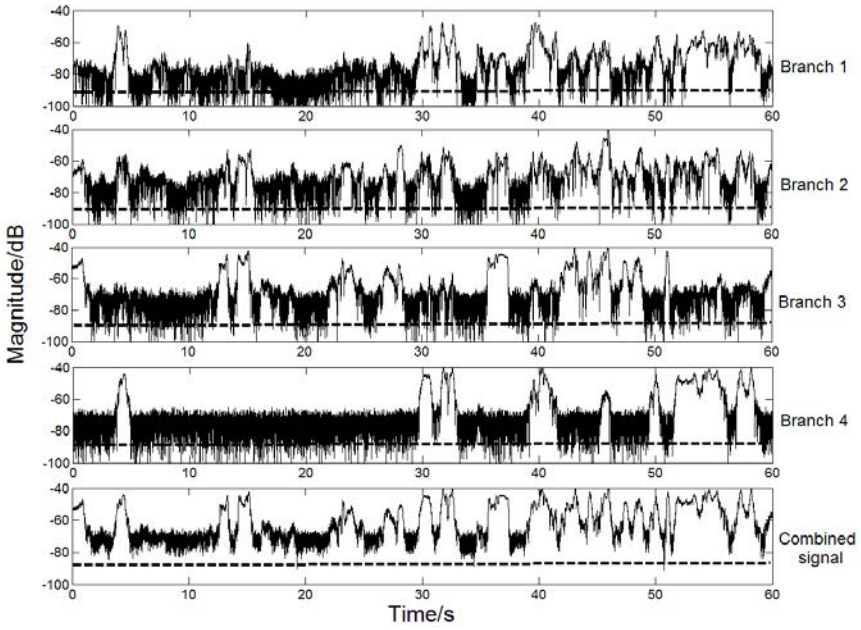

Figure 6.15 S_{21} - to belt), noise floor indicated by dashed line

Figure 6.15 shows the Received signal magnitude of each branch and selection combined signal in the case of Multiple-transmitters at 180^{o} on the wrist to Multiple-receivers (belt). It is observed that all branches exhibit strong signals at least some of the time. Branches 1 and 4 often reach their strongest signal at the same time, e.g. at 5 s, 30 s, 40 s, and 50 s and so on, but there are more variations recorded in Branch 1 compared to Branch 4, such as the period from 42 s to 45 s. Moreover, the changing signal trends are also similar to a certain extent in Branches 2 and 3, but there are some instances when only one branch exhibit a strong signal, such as at 55 s for Branch 2 and at 24 s for Branch 3.

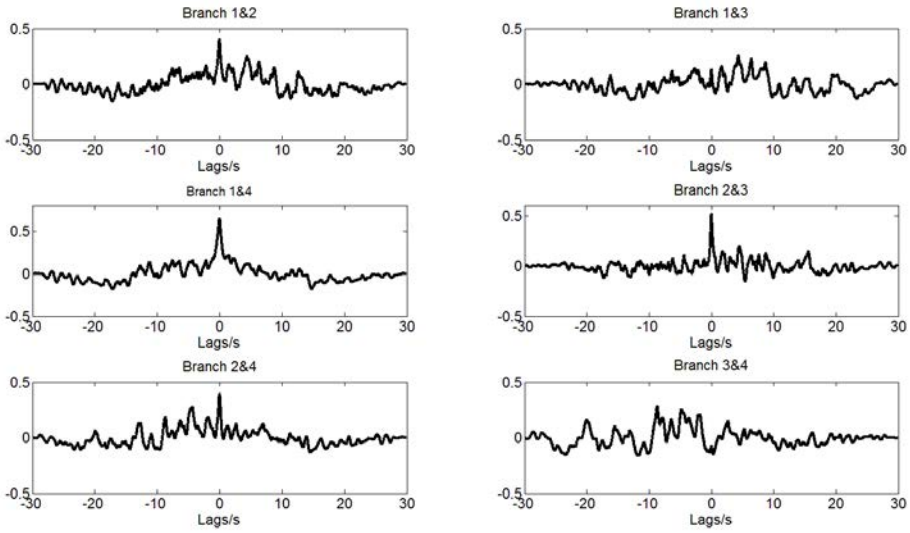

Figure 6.16 Cross-correlation between different branches (wri - to belt)

The cross-correlation coefficients between different branches in the case of Multiple-transmitters formed 180^{o} on the wrist to Multiple-receivers (belt) are shown in Figure 6.16. Only the cross-correlation between Branches 1 and 4 and Branches 2 and 3 is relatively high (over 0.5) according to Figure 6.16. However, as mentioned above, each branch can still contribute strong signal to combined signal at some moments. Therefore, employing a diversity technique is likely to be helpful in this case.

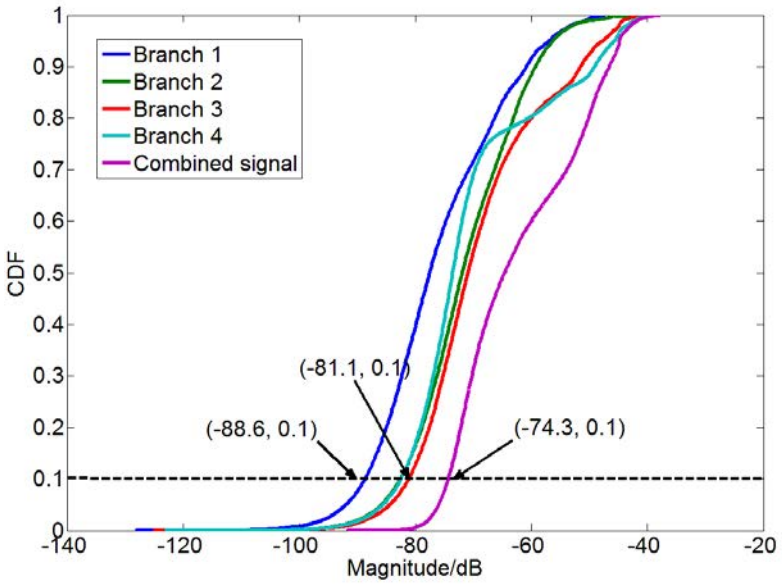

Figure 6.17 - to belt)

Figure 6.17 shows the CDF comparison of each branch and combined signal in the case of Multiple-transmitters formed 180 degree (wrist) to Multiple-receivers (belt). Among these four branches, it seems that Branch 4 experiences a big path loss range variation, with 75 % of the time staying between -70dB and the noise level, and 25 % of the time varying between -70 dB and -38 dB that is the maximum level. Finally, at the 10 % probability level the diversity gain achieved by the selection combined signal is at least 6.8 dB relative to Branch 3. The mean values of each branch and combined signal in this case are also given in Table 6.3 to show the improvements in signal level through the use of diversity technique.

Table 6.3 Mean values of each branch and combined sign - to belt)

Mean value (dB)				
Branch 1	Branch 2	Branch 3	Branch 4	Combined signal
-76.1	-71.3	-68.9	-70.6	-61.9

6.2.5 Multiple-Transmitters (wrist) to Multiple-receivers (upper arm)

In this case, the receivers were mounted on the left upper arm, while the transmitters were still kept on the wrist as before. The separation between transmitters and receivers was 38 cm when the test subject was standing still, and the shortest separation achieved during movements was about 20 cm. Figure 6.18 shows the various links between the antennas. As before, random movements were conducted during the measurement.

Figure 6.19 presents the received path loss for each branch, and it can be observed that Branches 1 and 2 are much stronger than the remaining two branches. Contrary to the case of the chest-wrist link discussed before where the antenna element pointed towards the torso and the link performance was affected strongly, in this case the element pointing towards the upper arm dominates the overall link performance.

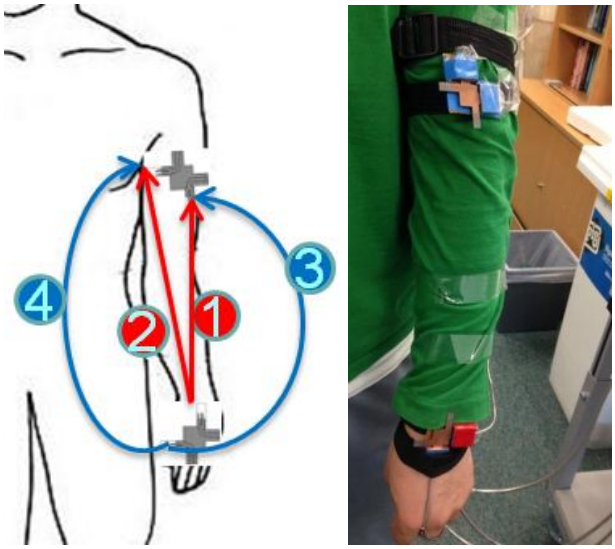

Figure 6.18 Multiple- transmitters (wrist) to Multiple- receivers (upper arm)

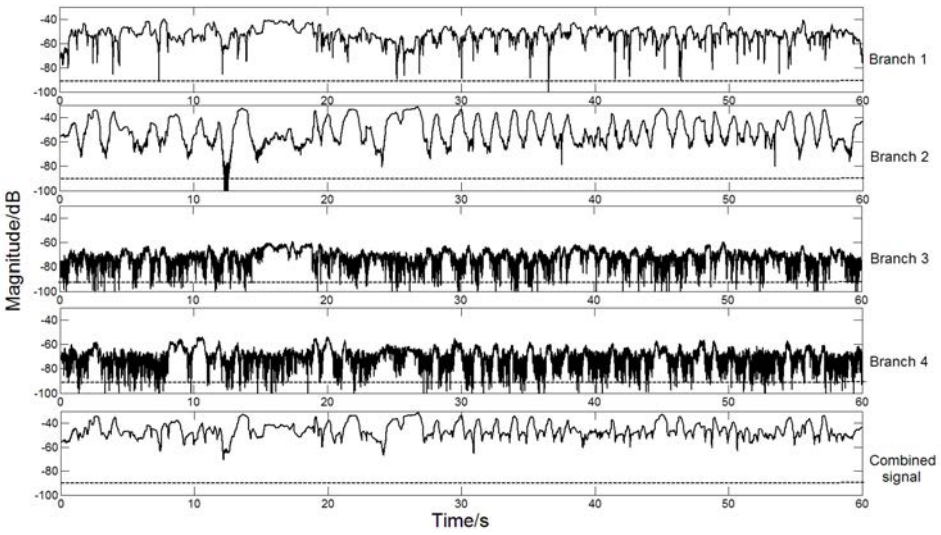

Figure 6.19 S_{21} of Branch 1, 2, 3 and 4 (upper arm to wrist)

Figure 6.20 shows the cross-correlation coefficient between different branches. Because the element pointing up dominates the entire measurement in this case, only the cross-correlation between Branch 1 and 2 is of practical relevance. According to Figure 6.20, Branch 1 is anti-correlated with Branch 2 for short time lags, which means if one branch provides a strong signal, the other one exhibits a weak signal, such as during the period from 30 s to 40 s in

Figure 6.20. Branches 1 and 2 are thus helpful in forming a strong combined link from the wrist to the upper arm. Therefore, employing a diversity technique is feasible in this case.

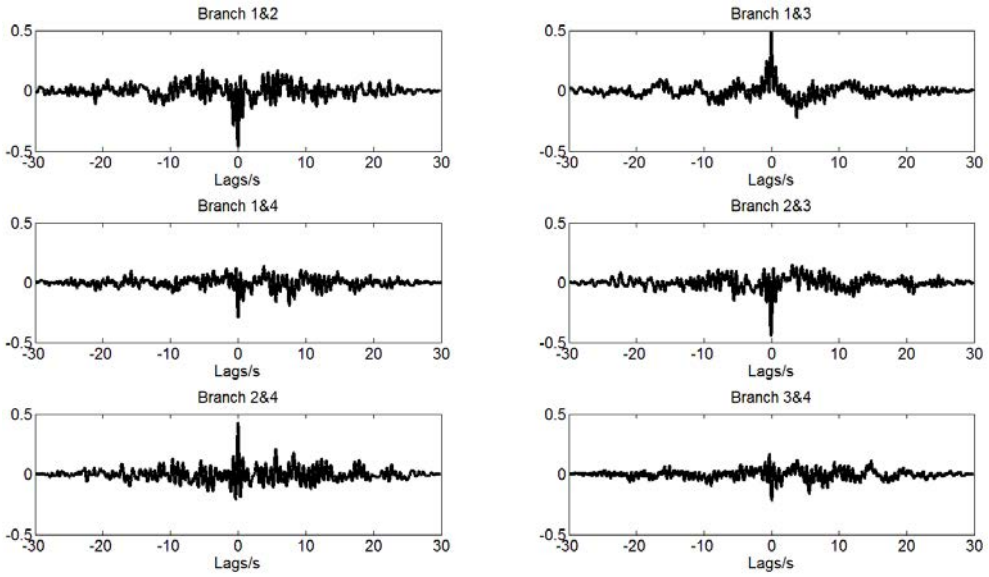

Figure 6.20 Cross-correlation between different branches (wrist to upper arm)

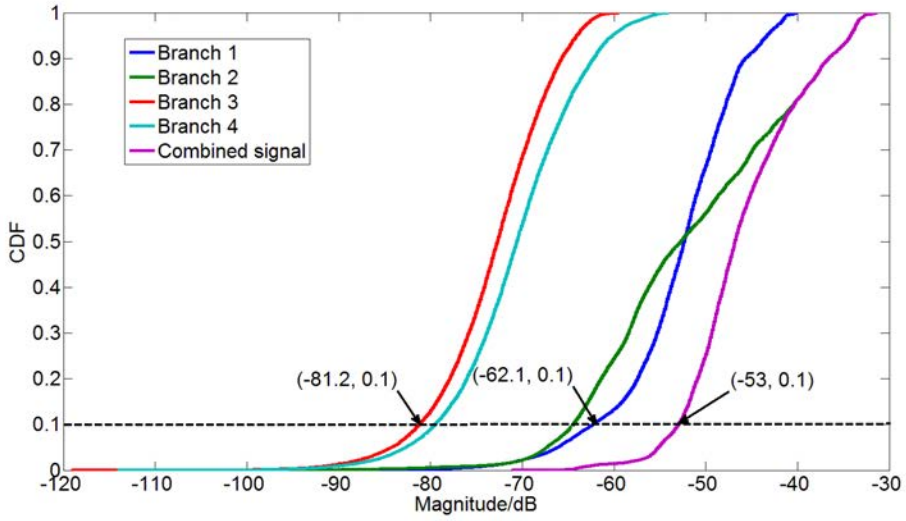

Figure 6.21 CDF comparison of each branch and combined signal (upper arm to wrist)

Figure 6.21 shows CDF comparison of each branch and combined signal in the case of Multiple- transmitters (wrist) to Multiple- receivers (upper arm). It also demonstrates that Branches 1 and 2 exhibit a much stronger signal on average than Branches 3 and 4. The

combined signal can achieve approximately 9 dB diversity gain related to Branch 1 and 2 at the level of 10% probability. Finally, the mean values of each branch and combined signal are given in Table 6.4.

Table 6.4 Mean values of each branch and combined signal (wrist to upper arm)

Mean value (dB)				
Branch 1	Branch 2	Branch 3	Branch 4	Combined signal
-53.1	-51.6	-73.2	-70.8	-45.9

6.3 Summary

In this chapter, the investigations on diversity for 60 GHz on-body channels are described. It is found that adopting two-branch orthogonal antenna pattern diversity is very helpful to establish a strong link in an on-body network. Although in some cases the movements conducted by the test subject enable the branches to be highly related, significant improvements can be still achieved through simple selection diversity combining. Overall, the diversity technique is very useful to overcome the severe path loss and shadowing caused by human movement in an on-body communication system, especially for highly volatile channels severely affected by human limb movements.

CHAPTER 7

BODY AREA NETWORK MULTI-HOP CHANNEL MODELLING AT 60 GHZ

7.1 Introduction

Wireless body area networks (WBANs) have drawn a lot of attention from researchers, systems designers and application developers. So far, the investigations on on-body communication at lower frequencies have become relatively mature in many respects. However, due to inherent shortcomings and limitations at lower frequencies, such as low frequency reuse, poor covertness, significant interference, limited bandwidth, and so on, the adoption of the 60 GHz band was proposed to overcome these, although the challenges on antenna design and channel characterization are not been fully solved yet. Wearable beam scanning antennas havenot been considered so far because of their complexities at 60 GHz. Instead, compact, low cost antennas are ideal candidates, thus multi-hop communication are required to establish stable links. However, all existing studies referred to various single links, and for some links it is hard to achieve the reliability at 60 GHz. Reasons for path loss can be categorised into:

- Long separation between transceivers： Results in [111] showed that the relationship between the path loss and separation of transceivers for the on-body channel at 60 GHz was approximately linear in dB;

- Polarization mismatch： It was presented in [112] that the relative orientation of the antennas is important when human posture does not change very much, while omnidirectional monopole antenna is more suitable when polarization mismatch is caused by random movements. However, an omnidirectional antenna might raise more security problems because it may cause interference to other BANs.

Therefore, to ensure the stability of the link, introducing relay nodes is a promising solution, which not only shortens the long distance paths, but also reduces the changes of relative positions of antennas. Thus, a multi-hop method is proposed to overcome the shortcomings in the aforementioned studies. In [113], only two-hop links for different applications were considered, and it has been concluded that given an appropriate threshold for every link, the multi-hop approach can offer reliable links and also more valuable information about human movement at the same time, and the simultaneous state of the hops forms the state of the whole network. Therefore, it is worth investigating a whole body area network with repeater y GHz H , ’ k , channel modelling in a network at 60 GHz has not been discussed in the literature to date. Although a three-state Frichman model was used to describe the channel state at 2.45GHz in [114] and a Markov model was simply employed to describe the single on-body link states at 60 GHz in [108], neither the Frichman model nor the Markov model can simply satisfy the requirement of multi-hop channel modelling at 60 GHz.

In this chapter, a representative model is proposed to describe the states of these multi-hop on-body channels for different movement scenarios. In addition, power control is another vital factor needed to be considered to extend the lifespan of these repeater nodes. Two typical networks were selected to represent some daily and specialised military and medical

applications. Figure 7.1 shows the repeater nodes and transceiver placements for different applications, henceforth denoted as Network 1 and Network 2.

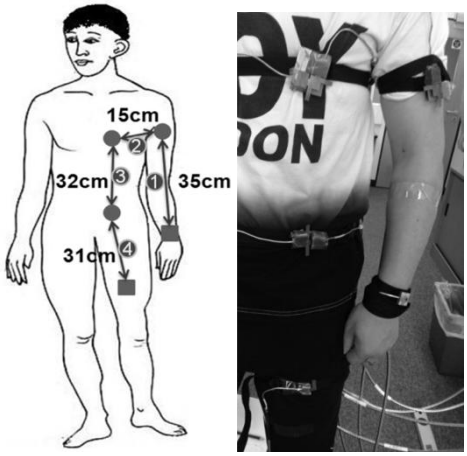

(a)

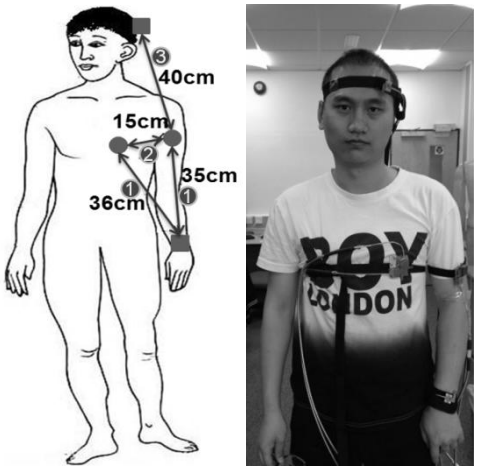

(b)

Figure 7.1 (a) Network 1 (b) Network 2

7.2 Measurement Setup

The measurement of movements for each network lasted 300 seconds and 30000 sample points were collected. Two types of SIW Vivaldi array antennas proposed in Chapter 4 were used as

shown in Figure 7.2. Each antenna had B - , B

y dB beamwidth perpendicular to the body surface. The conformal distance along the body of each link is also marked in Figure 7.1

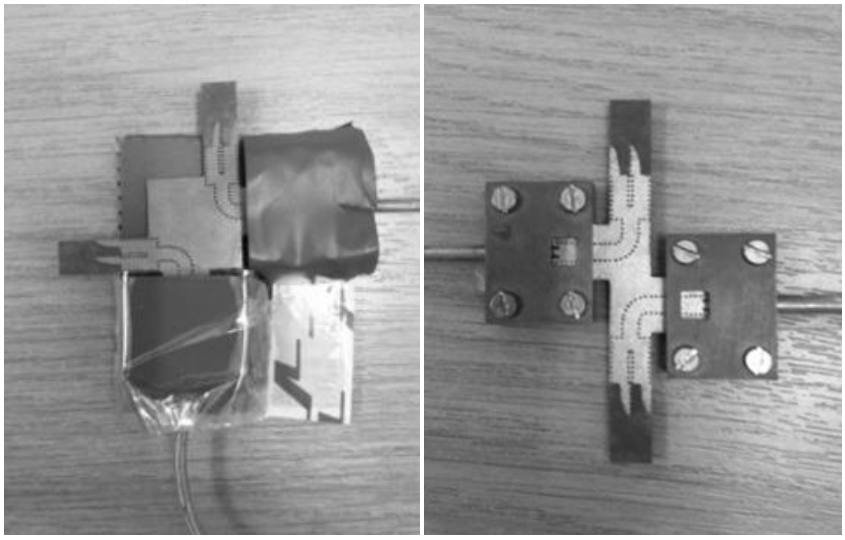

Figure 7.2 Structure of mounted antennas

Three scenarios were considered for the two networks: random movements for Network 1 (including walking, eating, typing, and exercising), crawling like a soldier (backwards and forwards) and random movements for Network 2. The speed of these movements was neither too fast nor too slow, and each set of movements was repeated 5-6 times every minute in each scenario. Links in Network 1 are marked from channel 1 to channel 4, respectively, as shown in Figure 7.1 (a). Although there are 4 links in Network 2, they are considered as three channels shown in Figure 7.1 (b), because selection diversity is employed to eliminate the severe fading effect caused by the arm moving.

7.3 Measurement Results

The measured data of the three movement scenarios is shown in Figure 7.3. For the case of Network 1 in Figure 7.3 (a), the chest to abdomen link (Link 3) is the strongest link among all the links as expected, because the positions of the antennas are relatively static in a predominant light-of-sight condition. Link 4 (abdomen to thigh) is the second strongest link most of the time, but occasionally suffers from serious fading due to the turning movements and running. Furthermore, Link 1 (wrist to upper arm) is the most stable link although the signal level is relatively low due to the long distance between transceivers. Finally, Link 2 from chest to upper arm is the worst one. Humans often raise their arms in daily movements, which will cause a non-line-of-sight condition, thus shadowing is frequent for this link, which explains that there are more fast variations in Link 2.

In the case of Network 2, two movement scenarios were investigated: crawling like a soldier and random upright movements. Figure 7.3 (b) shows the crawling case and it was found that all links suffered from deep fading, which we believe is caused by multipath fading due to the proximity of the floor and shadowing. The results are in accord with a previous multi-hop investigation in [113]. However, thanks to the selection diversity combining approach for Link 1, the signal level is much better than the other two links. Similarly, Link 2 is still the most unstable link and the signal strength is very weak. It is even worse than the same link in Network 1. Fast fading ocurring in all of the three links is caused by multi-path and reflection due to the short distance between body surface and ground floor. This also can explain why Link 3 experiences many rapid variations, although the average signal strength remains at a good level. In the case of random movement for Network 2, all three links are stronger than the

crawling case. Again, Link 2 is the most unstable link comparing to the other two links and Link 1 is improved because of the selection diversity combining process.

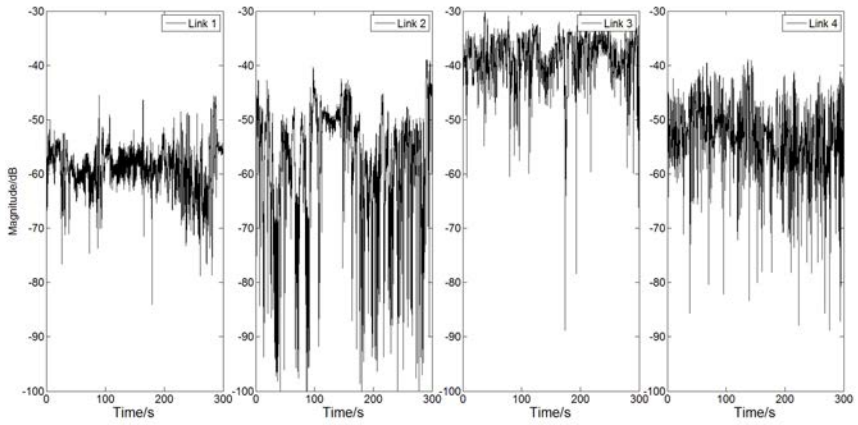

(a)

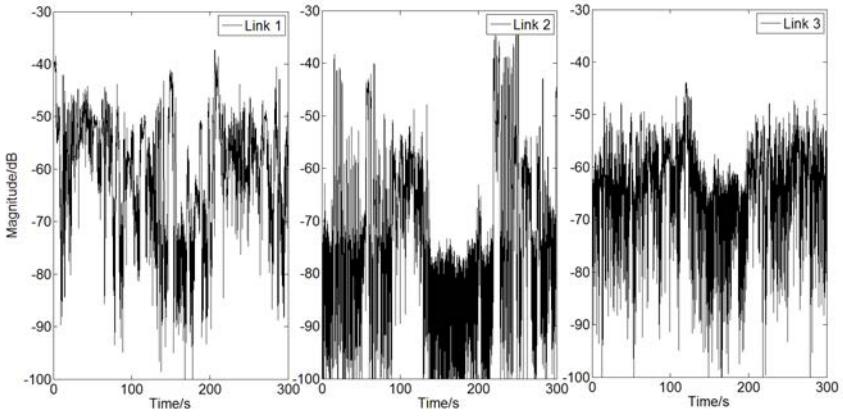

(b)

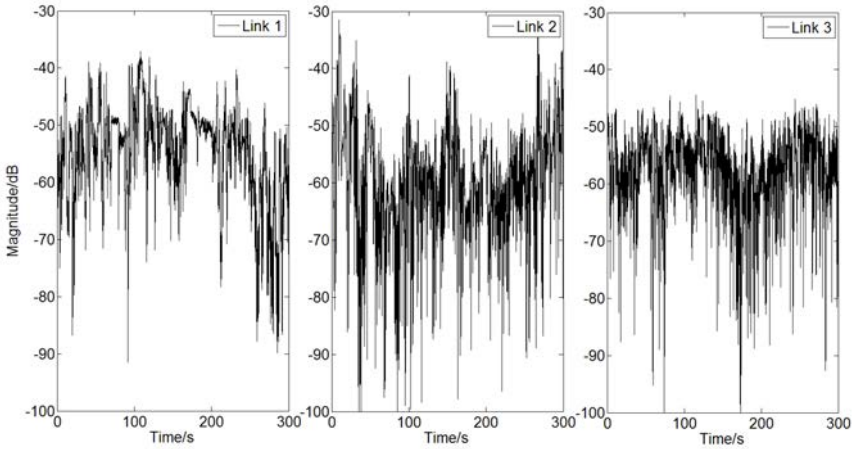

(c)

Figure 7.3 Measured signals with time variation (a) random movements for Network 1 (b) crawling for Network 2 (c) random movements for Network 2

7.4 Network State and Adaptive Power Control

To model the network state, we require system thresholds to specify every link state, and thus the state of the overall networks can be known accordingly. The 2-state Makov model is commonly used to describe a single channel state, but to better describe the on-state duration, a 3-state or even 4-state model was proposed to analyse a single channel. In this research a 2-state model per link is adopted because the overall network state incorporating all links in the network would result in an unwieldy, highly complex model. Therefore, the simplest description of a single link channel state is chosen, which is having an on and an off state. Thus, a sixteen-state model is generated for Network 1 and an eight-state model is generated for Network 2, respectively. Each link is described in terms of an individual binary variable: Y for the on state and N for the off state. The sixteen combinations for the Network 1 and the eight combinations for Network 2 are shown in Table 7.1 and 7.2, respectively. In addition, the joint-state of the networks is assigned a particular number, which can identify a particular state of the network. Among all of them, the joint-state 15 is the most interesting as it indicates every link in the network is in the on state simultaneously. According to the previous discussion, Channel 2 is the most unstable channel, so joint-state 11 is very important in the coming discussion.

Table 7.1 Joint-state of Network 1

Single Channel State: On for Y, Off for N				**Joint-state**
Channel 1	Channel 2	Channel 3	Channel 4	
N	N	N	N	0
N	N	N	Y	1
N	N	Y	N	2
N	N	Y	Y	3
N	Y	N	N	4
N	Y	N	Y	5
N	Y	Y	N	6
N	Y	Y	Y	7
Y	N	N	N	8
Y	N	N	Y	9
Y	N	Y	N	10
Y	N	Y	Y	11
Y	Y	N	N	12
Y	Y	N	Y	13
Y	Y	Y	N	14
Y	Y	Y	Y	15

Table 7.2 Joint-state of Network 2

Single Channel State: On for Y, Off for N			**Joint-state**
Channel 1	Channel 2	Channel 3	
N	N	N	0
N	N	Y	1
N	Y	N	2
N	Y	Y	3
Y	N	N	4
Y	N	Y	5
Y	Y	N	6
Y	Y	Y	7

A simple fixed threshold was applied in Chapter V, which was taken to be 10 dB below the median path loss value. The threshold does not only specify the channel state, but also can imitate the effect of transmit power control. Since power control is a crucial factor that will affect the transceiver node battery lifespan, it is considered that applying an adaptive power control algorithm would improve the channel state and optimize the usage of transmit power. It is assumed that to satisfy the criterion of 10^{-6} BER quadrature phase shift keying (QPSK) modulation should be employed with a SNR of 11dB. Usually, several parameters can be used to estimate the quality of a link, such as Packet Reception Ratio (PRR), Received Signal Strength Indication (RSSI), Link Quality Indicator (LQI) and so on. However, in the experiment, due to the limited number of VNA port interfaces and their direct measurement

capabilities, only SNR is used to estimate the measured results, instead of the other traditional estimators.

WBAN GHz, ' y causing a long separation to occur between transceivers, the signal might not be detected because of the limitation of maximum transmitter power and the limited measurement dynamic range. It is assumed to use a typical transceiver that maximum QPSK transmit output power is 16.5 dBm based on product (PRS1021) from Peraso Technologies Inc. Therefore, a two piecewise model can simply describe the relationship between the SNR and transmit power:

$$P_T(t) = \begin{cases} 16.5\text{dBm}, & if\ SNR < -5.5dB \\ P_{adaptive}(t), & otherwise \end{cases} \quad (7\text{-}1)$$

when SNR is smaller than -5.5dB, which mean the path loss is over 87.1 dB, the T_{max} (the maximum QPSK transmit output power) is needed to achieve the best SNR. $P_{adaptive}$ is the adaptive controlled power under the proposed algorithm below.

Initially, the transmit power is arbitrarily set at 0 dBm which can ensure the link is likely to be on-state. Then the received SNR of the packet is compared to the target SNR and the difference between them is determined. Finally, the transmit power for the next packet depends on the value of d that represents difference of SNR between measured and target. If the absolute value of d is smaller than maximum transmit power, then the transmit power is adjusted from 0 to d, otherwise transmit power needs to be kept at the maximum value to maintain the SNR at an acceptable level.

Algorithm: Adaptive power control

Sample rate: 1 point per 10ms

Packet size: 10 points (100ms)

$P_T(t)$: transmit power

$P_R(t)$: received power

P_N: noise power

SNR_{Target}: target SNR

SNR_R : received SNR

d: difference of SNR between measured and target

/* Adaptive algorithm*/

$P_T(0)$=0 dBm //The transmit power at original state

SNR_R=(P_R-P_N) dB

d=minimum(SNR_R(5t-4:5t+5)- SNR_{Target}); // t is time

/* the worst SNR for packet k*/

if |d|< T_{max}

$P_T(t)$= $P_T(0)$-d

/*transmit power for the k+1 packet*/

else

$P_T(t)$= T_{max}

It is assumed that an OFDM (Orthogonal Frequency Division Multiplexing) wireless communication system is used. A superframe containing desired data carries various messages that may be used in route searching, power adjusting, specifying buffering time and so on. However, the time cost for these messages is of the order of a few ns according to a draft IHP-60 GHz protocol [108], which is very short, compared to our measurements. Therefore, it is assumed that only 10 sampling points are carried by one packet. In addition, the time window

in this algorithm is 100 ms, because it is long enough to record a single change of body movement in daily life.

By using this transmission power control algorithm, the link quality is maintained and also the transmit power is reduced. In addition, the link can never be off unless the transmit power requirement is limited by the hardware, and this simple algorithm is employed to determine the state of each link.

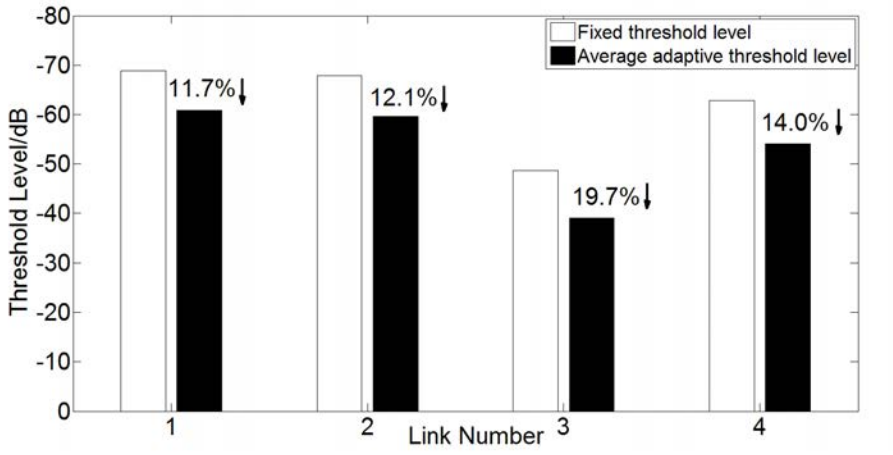

(a) Random movements for Network 1

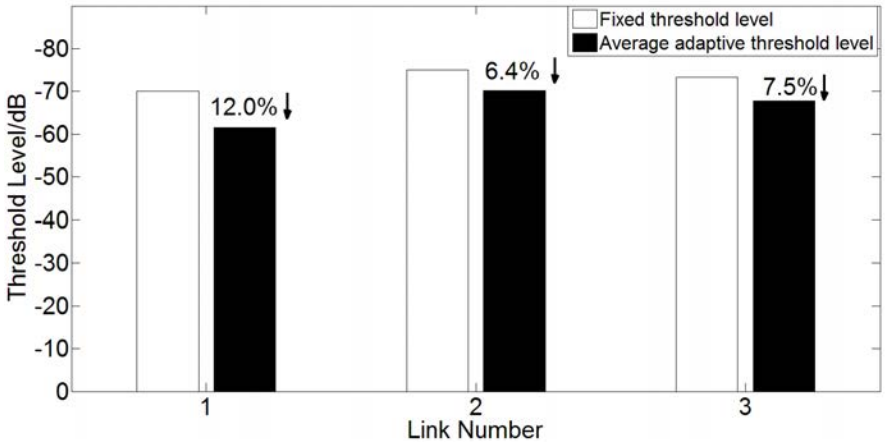

(b) Crawling for Network 2

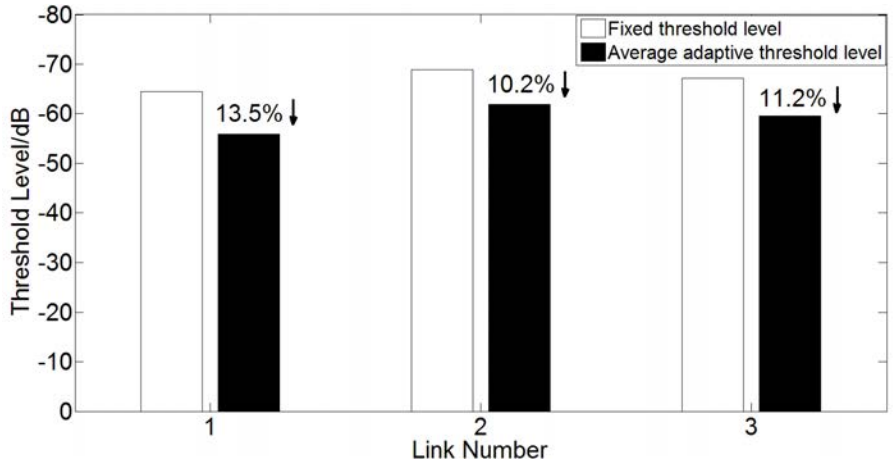

(c) Random movements for Network 2

Figure 7.4 The comparison of threshold level between fixed and adaptive threshold (a) random movements for Network 1 (b) crawling for Network 2 (c) random movements for Network 2

Comparison between the fixed (10 dB below the median value) and adaptive threshold is discussed below. The overall power saving is shown in Figure 7.4. It is found that this approach can save over 10% of energy for all links except the case of crawling, because the link quality is so poor that transceivers have to provide full-powered work most of the time. Therefore, the energy saving in the case of crawling is small, which can inform protocol designers to pay more attention to this kind of action for military applications. Alternatively, the node placement, or path directivity might need to be further employed. Figure 7.5 presented the comparison of joint-state with adaptive threshold and fixed threshold.

Figure 7.5 (a) indicates that Network 1 is much more stable when adaptive threshold is applied. The state of all links remaining in the on-state occurs over 90% of the time. Unlike the fixed threshold case, the joint states from 0 to 12 rarely arise in the case of adaptive threshold.

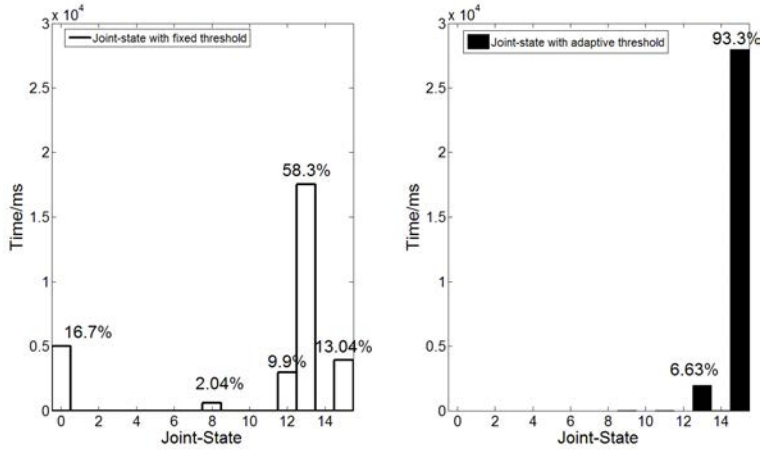

(a)

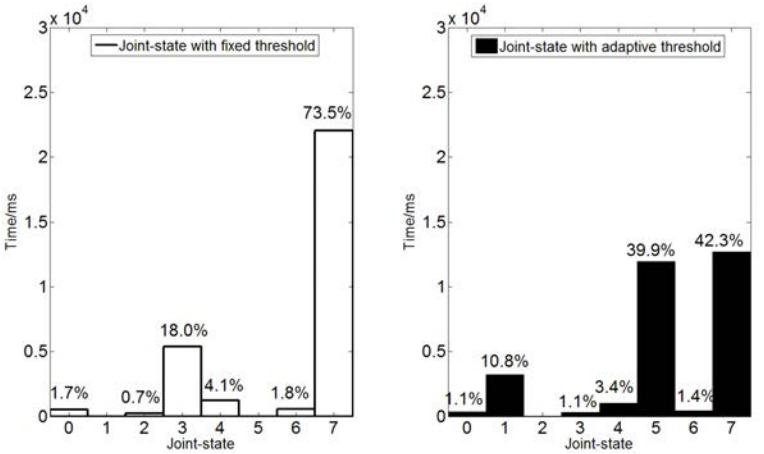

(b)

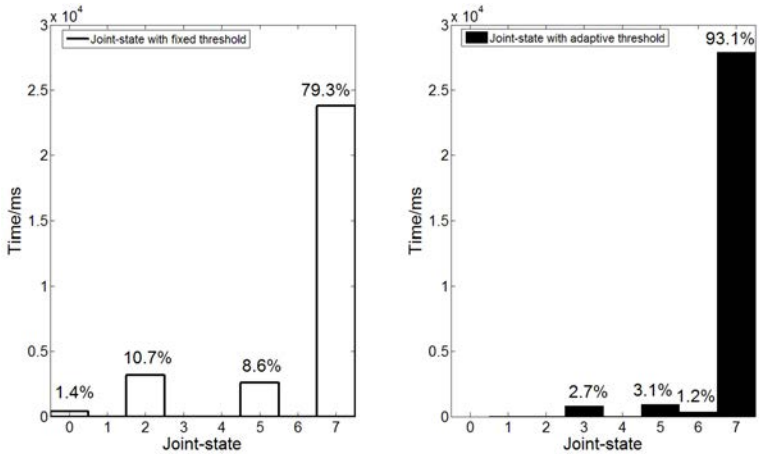

(c)

Figure 7.5 The comparison of joint-state with adaptive threshold and fixed threshold (a) random movements for Network 1 (b) crawling for Network 2 (c) random movements for Network 2

Similarly, in the case of random movements for Network 2 shown in Figure 7.5 (c), the network keeps staying a stable state most of the time when the adaptive threshold is employed. However, the crawling case is very different from the other two. Although applying adaptive threshold can save energy for each link as shown in Figure 7.4 (b), the network becomes unstable because the undesired joint-state 5 happens as much as the desired dominant joint-state 7 as shown in Figure 7.5 (b) and the stable time of network (joint-state 7) decreases from 79.5% to 42.3% of entire measurement. Therefore, given the limited improvement on the energy saving but significant reduction on network stability, the proposed algorithm makes things worse in the crawling case. Moreover, it is observed that Link 2 is the most unstable link among all these links, thus, a store and forward switch with a suitably dimensioned memory buffer should be considered in the chest node or upper arm node to hold and re-transmit the data during periods when link 2 is in the on state.

The empirical cumulative distribution functions (CDFs) of the durations of joint states with adaptive thresholds in different scenarios are shown in Figure 7.6. Moreover, Figure 7.7 depicts the state transition probabilities. In the case of Network 1(Figure 7.6 (a) and Figure 7.7 (a)) state 13 is very short-lived and the network predominantly switches between states 13 and 15. State 15 dominates most of the time.

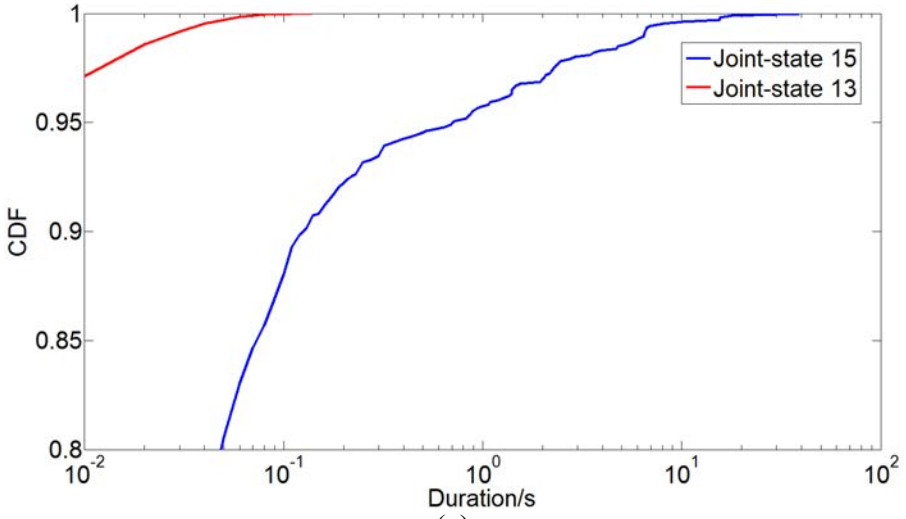

(a)

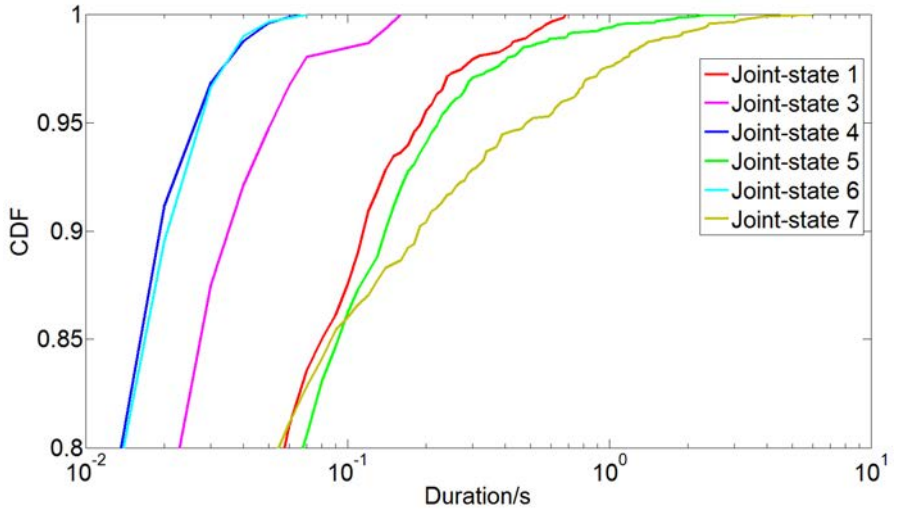

(b)

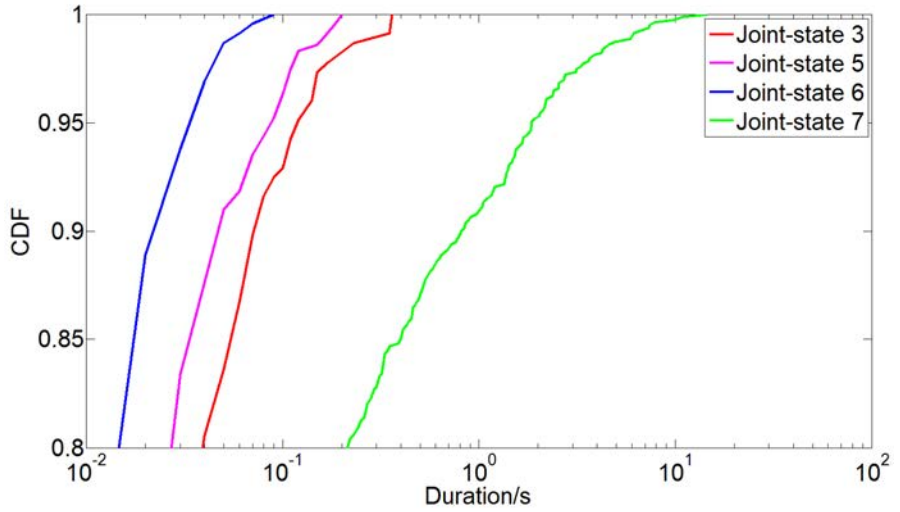

(c)

Figure 7.6 CDFs of the durations of joint state at different scenarios (a) random movements for Network 1 (b) crawling for Network 2 (c) random movements for Network 2

Figure 7.6 (b) also demonstrates that the crawling case is the most unstable scenario among the three. The network state mainly keeps switching between joint-states 5 and 7 comparing with the other joint states shown in Figure 7.7 (b). The durations of states 7 and 5 are the longest and second longest among all joint states, respectively. Joint- ’ 700 ms, and over 99% of durations of state 3, 4 and 6 are shorter than 100 ms. In addition, it is likely that once the network is in joint-state 1, it will remain the same state more than switching to other states. Furthermore, the figure provides quantitative information on how long data should be locally buffered before it is re-transmitted.

Finally, the random upright movements for Network 2 are described in Figure 7.6 (c), which is very similar with random movements for Network 1. With the proposed algorithm, the duration of joint-state 7 is able to last over 14s, while the rest joint-state have very short life spans and rarely occur and none of them lasts over 100 ms. Moreover, the other joint-states will be switched to the dominate state rapidly rather than staying according to Figure 7.7 (c).

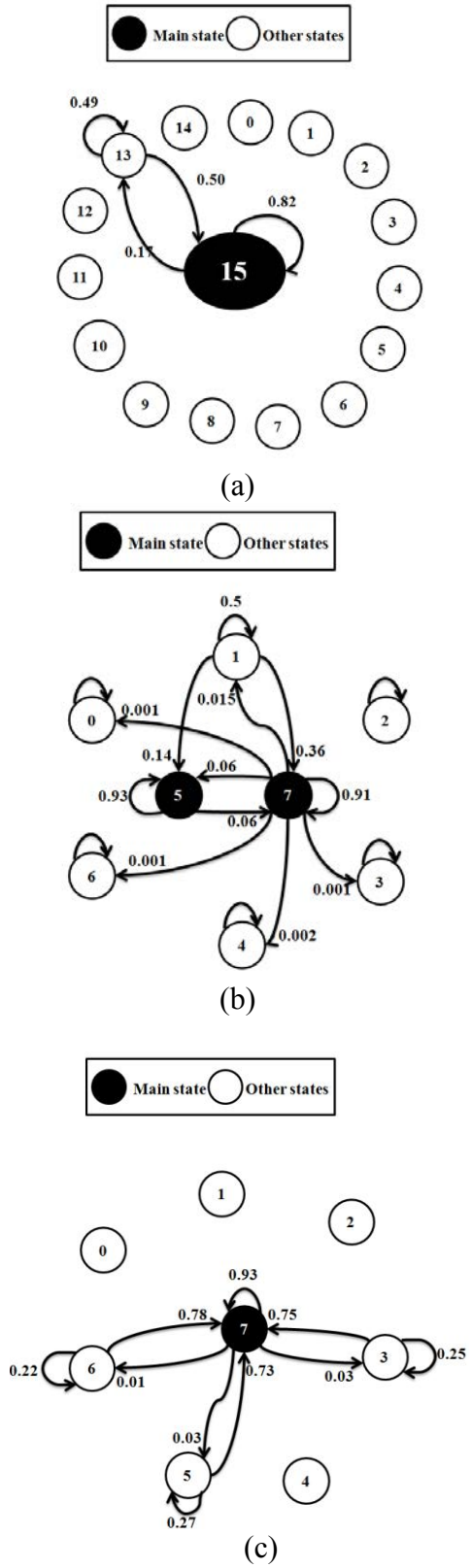

Figure 7.7 Transition probabilities of joint-state model for (a) random movements for Network 1 (b) crawling for Network 2 (c) random movements for Network 2

7.5 Summary

In this Chapter, a channel modelling method for on-body communication at millimetre-wave frequency is presented. Also, an eight-state model and a sixteen-state model are used to describe the network states, respectively. Moreover, the power control is also considered to extend the battery life of the repeater nodes. Through the statistical analysis of joint states, the conclusion can be reached that: by applying an appropriate power control method, it is possible to establish a stable network for medical, military and entertainment applications at 60 GHz band. The network state also is affected by the nature of human posture and activity, so it may be helpful in indentifying posture and activity.

CHAPTER 8

CONCLUSIONS AND FUTURE WORK

8.1 Conclusions

Recently, 60 GHz technology has been proposed for adoption in wireless body area networks because of its various merits, such as small RF components, low visibility and interference, a wide available spectrum (57-64 GHz), high data rates and so on, and researchers have conducted some investigations on both antennas and propagation for body area networks at the 60 GHz band. It is found that unlike the situations at lower frequencies 60 GHz radio can achieve better power control to not only extend battery life but also minimise the interference from other devices, and provide enhanced physical layer privacy and security. Therefore, this frequency band is highly suitable for certain applications such as military and medical ones, where privacy and security are paramount. However, complex antenna beam scanning and high efficiency antenna design are still a big challenge for body-worn applications at the 60 GHz band. Low profile and low cost antennas need to be adopted to establish reliable high capacity on-body single links. As discussed in Chapter 2, antenna design and propagation investigations for BANs at this mm-wave band have so far been related to single on-body links, and to the best acknowledge of the author, there has been no work on multi-hop on-body links at the 60 GHz band to date. Therefore, both on-body worn antennas and propagation characteristics for multi-hop WBANs are presented in this thesis for the first time.

A medium-gain SIW Vivaldi antenna and a two element Vivaldi array were proposed for on-body multi-hop communication at 60 GHz. Due to the requirement for multi-hop networking both of these antennas were designed with bidirectional layout and perpendicular layout, and they achieved about 12 dB gain, end-fire radiation pattern and wide impedance bandwidth. Propagation studies showed that the bidirectional antenna can establish stable multi-hop links for the belt to chest and chest to head paths except when the test subject was imitating a soldier in the slightly lifted prone position on the ground with the antennas mounted at the front of the body, while the perpendicular layout antenna was found to be highly suitable for diversity technology as discussed in Chapter 5 and it was also a key part to form a specific on-body network with stable links.

Different two-hop links under different movement scenarios were studied. Results showed that with the help of the designed antennas, stable two-hop links can be established, except for some highly time-variable links such as the Belt-Wrist link. These measurements indicated that omni-directional radiation pattern antennas should be used on the wrist due to the large range of hand movements, or pattern diversity technique can be employed to overcome the severe shadowing caused by hand movements. Therefore, a radiation pattern diversity technique for on-body communication at 60 GHz was investigated. Results showed that although some branches of certain links were correlated, the diversity technique could still bring essential improvements to the received signals. For instance, with the help of pattern diversity technique, the combined signal achieved at least 5 dB diversity gain, even up to 14 dB related to some highly variable links. In addition, the average signal strength was improved and there are almost no instances of the signals being below the noise floor any more.

Modelling the characteristics of multi-hop on-body channels at 60 GHz was first introduced with a simple thresholding method. Only one representative two-hop link with three movement scenarios was investigated. Although due to the limitations on antenna placements

y ’ ,

described the on-body channel intermittency well at 60 GHz. Therefore, the method was applied to describe more complex on-body networks. A representative model was developed to describe the states of an on-body network considering the power controlling issue at the same time. With the proposed method of thresholding and adaptive power control, the state of on-body network became more stable and considerable power savings were demonstrated. Additionally, more valuable information (unlike for a single link or some two-hop links) could be found in multi-hop on-body networks, which can be potentially used by both hardware designers and protocol designers to develop the devices and protocols for 60 GHz on-body communication systems. For instance, the different durations of the network states can provide some information regarding to time buffering at the repeater node. Finally, based on the work of this thesis, some suggestions can be given, as well as the advantages and disadvantages of WBANs at different frequencies (Table 8.1):

- The on-body antenna design should meet the different requirements for different positions on the body. The trade-off between the beamwidth and gain depends on the desired coverage area. For an on-body network, the beamwidth parallel to body surface should be much wider than that perpendicular to body surface, and a medium gain is required to maintain the energy around human body.

- The multi-hop networks with nodes on the head or the wrist can suffer from instability compared to the rest of the node placements. Diversity techniques or

beam-reconfigurable antennas can be employed to overcome this shortcoming. Beam pattern diversity is preferred because it is able to enlarge the signal coverage area.

- Due to the instability of some links in wireless body area networks at 60 GHz, power control and channel modelling are critical factors that might affect the battery life of on-body sensors. In addition, the buffering issue at each node should be considered because of the intermittency of the network at 60 GHz.

Table 8.1 The advantages and disadvantages of WBAN at different frequencies

Frequency	2.45 GHz	UWB	60 GHz
Spectrum availability	Congested	Congested	Under-utilised
Data rates	Mbps	Gbps	Gbps
Covertness	Not good	Good (Low power spectral density)	Excellent
Interference	High	Reduced interference to narrowband systems	Reduced interference (High path loss & atmospheric absorption)
Frequency reuse	Low	Low	High
Radiation control	Very limited	Limited	Good (Narrow antenna beamwidth & small antenna array)
Form factor	Bulky	Bulky	Small
Antenna efficiency	Low	Low	High

8.2 Future Work

Although wearable antenna design and on-body channel characterization at 60 GHz have been studied in this thesis, there are still many challenges left as future work:

1. Advanced antennas for WBAN at 60 GHz

Antennas are one of the most important parts of the entire on-body communication system. Beam-reconfigurable antennas at 60 GHz should be developed to meet the demand of highly variable channels. They should be easy to be manufactured and mounted on human body at the same time.

2. Interference in the on-body network at 60 GHz

Due to the limitation of VNA based measurement system, the interference among different hops within the same on- y k ' . Further studies of mutual interference within the same WBAN need to be conducted in the future to inform MAC protocol designers.

3. Modelling protocols for WBAN at 60 GHz

Further works on protocol design can be done. This thesis can help protocol designer to consider how much buffering memory is needed to hold data packets at each repeater node, and how long time the signals should be held.

4. Power control

Although an adaptive threshold method has been proposed for battery saving, due to the unpredictable human movements a more efficient power control algorithm is needed. A highly efficient feedback control algorithm is required to maintain the desired link quality. For 60 GHz, it is better to combine a practical system and the rigorous control-method, therefore, more real-world experiments about power control is needed.

APPENDIX I

LIST OF PUBLICATIONS

Refereed Publications

1. X L, Y I N y , P S H , “ -hop Channel Modeling at 60 GHz for On- y ” , th European Conference on Antenna and Propagation, pp.2286-2289, The Netherlands, April, 2014. (One of the five best paper prize)

2. X. Li, Y. I. Nechayev, C.C. Constantinou and P. S. Hall, “B band SIW Vivaldi Antenna Array for On- y ” , LAP .

3. X L, Y I N y , , “ y networks at microwave versus mm- ” IEEE -S International Microwave Workshop Series on RF and Wireless Technologies for Biomedical and Healthcare Applications, Dec 8-10,2014, London.

4. Y I N y , , X L, P S H , “ z Non-stationary On- y GHz”, Antennas and Propagation, *under review.*

5. X L, Y I N y , P S H “B y A N k GHz” *in preparation.*

6. X L, X Y W, Y N y , , P S H , “B SIW A ” IEEE A tennas and Wireless Propagation Letters, *in preparation*.

APPENDIX II

BROADBAND SIW TO COAXIAL CABLE ADAPTER

A new 60 GHz coaxial to SIW adaptor is proposed, with low insertion loss over a wide bandwidth. This adaptor is low cost, compact, lightweight and easy to manufacture and optimize. The operating principle of the proposed adapter is to modify the coaxial cable in a manner that breaks the azimuthal symmetry of its modal fields and feeds a broadband taper in a conductor-backed coplanar waveguide (CB-CPW) y ' modal fields to those of a SIW, *over a very short transition length*. The operation and design of each section are discussed below.

Transition structure

The TEM mode electric field distribution of a coaxial cable is radially polarized and thus possesses azimuthal symmetry, whereas the TE_{10} dominant mode of a post walled SIW has a linearly polarized mode with the electric field perpendicular to the coplanar walls and parallel to the posts. In order to break azimuthal symmetry of the coaxial cable fields, a short half-cylinder section of cable is removed as depicted in Figure II. 1. The post-to-post width of the SIW is selected as $W_4 = 2.6$ mm and the spacing is s = 0.7 j λ , ensure energy leakage from the waveguide is minimized. The modified semi-rigid coaxial cable outer and inner conductor diameters are 2.2 mm and 0.5 mm respectively, and the

y $\varepsilon_r = 1.6$. The half cylinder was machined on a CNC milling machine to a dimensional tolerance of 50 μm. This cable is connected to a 0.508 mm thickness RT/Duroid 5880 substrate ($\varepsilon_r = 2.2$). The length, L, of the half-cylinder segment has been found to significantly affect the connector scattering parameters, and was empirically determined through a numerical optimization in CST Microwave Studio® to be L = 2 mm, i.e.

y 5 λ H ,

have dimensions suitable for geometrically matching to this structure length as well. The slot length, m (see Figure II. 1), needs to be made as short as possible to achieve the best insertion loss and impedance match, given the modified semi-rigid cable dimensions. Considering the SIW width, W = 2.6 mm, the distance between the edges of two slots, W_3 (see Figure II. 1), should not exceed the diameter of outer conductor of the cable; otherwise, it cannot maintain electrical contact with the substrate and useful S-parameters cannot be obtained. The values of parameters n, g and W1 are also fixed in order to maintain good electrical contact between the cable and substrate. Thus our numerical optimization of the return and insertion losses is confined to their dependence on the length of the slot, m, and half cylinder length, L.

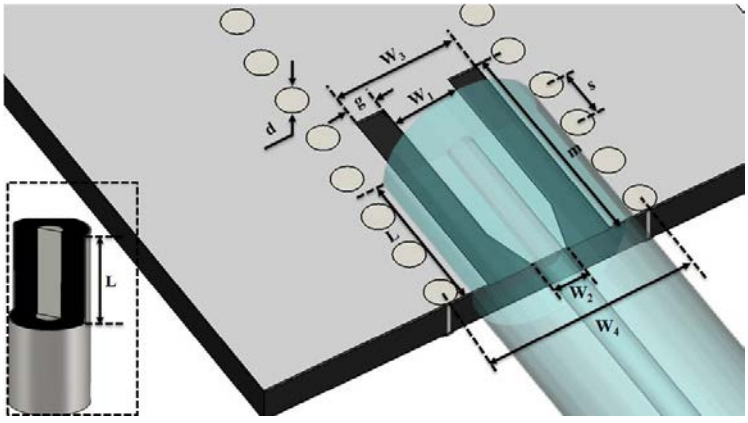

Figure II.1 The geometry of the modified coaxial cable and the coaxial-to-SIW adaptor

The length of the slot should not be either too long or too short. The transition region should

be provided for the fringing field to couple nearly all the incident energy into the SIW. This indicates that the length of the upper CPW wall slots is a critically sensitive parameter in jointly optimizing both the return and insertion losses.

Figure II. 1 depicts the geometry of a CB-CPW. The initial tapered section is used to achieve better impedance matching. Table.1 shows the numerically optimized geometrical dimensions of the feeding structure for a center frequency of 60 GHz.

TABLE I. The Optimized Dimensions Of The Proposed Transition

Parameters	d	s	g	m	L	W_1	W_2	W_3	W_4
Value(mm)	0.4	0.7	0.4	3	2	0.9	0.5	1.7	2.6

Electric Field Distribution

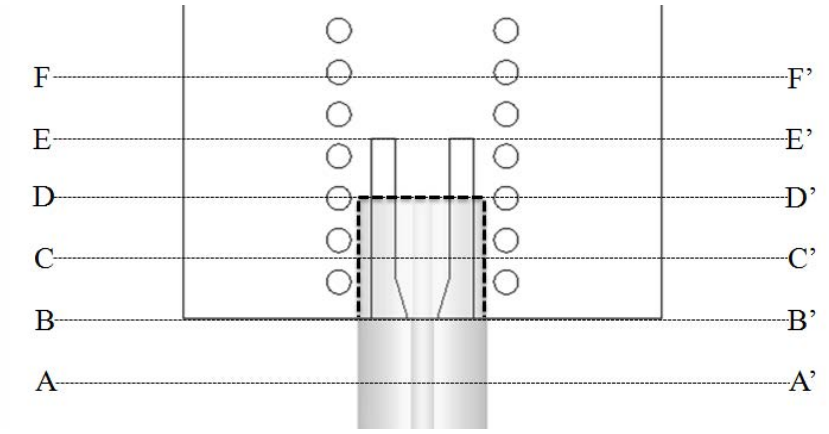

(a)

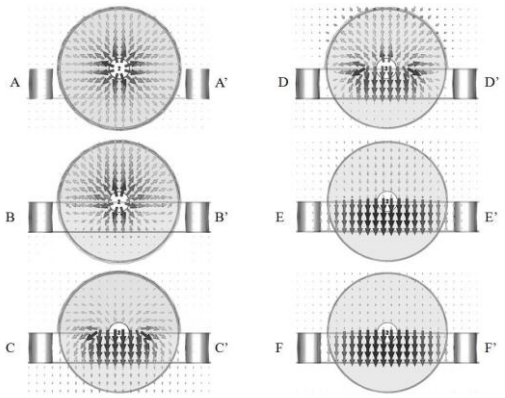

(b)

Figure II. 2 Structure of the proposed coaxial cable-to-SIW transition: (a) top view (b) the E-field distribution at the six cross-sections.

Figure II. 2 shows the simulated electric field amplitude and direction cross-sectional distribution in a number of planes from the coaxial cable to the SIW. Section A-A' shows the axially symmetric E-field in the coaxial cable. The gradual symmetry breaking in the E-field spatial distribution starts at section B-B', where the lower section of modified cable touches the substrate. The predominantly radial E-field rapidly transforms to a predominantly vertical E-field from section B-B' to section D-D' where the coaxial cable ends. The slotted coplanar waveguide transition segment must not terminate before the coaxial cable ends, because the fringing fields at section D-D' are still quite strong. By section E-E' it can be seen that the E-field has almost totally been converted to the SIW TE_{10} modal E-field. The spacing between successive cross-sections adopted in the simulations is 1 mm long and the phase is chosen at each cross-section as to show the biggest amplitude of the E-field.

Mechanical Assembly of Adapter Enclosure

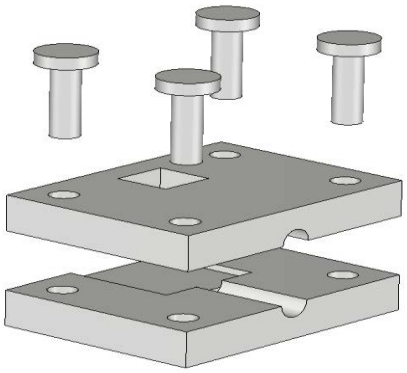

Figure II. 3 3D cut-out of supporting block

In order to provide good electrical contact between the coaxial cable and the CB-CPW, as well as to ensure the mechanical rigidity of the proposed adapter, a machined metal block is employed. Its overall volume is 25 mm × 15 mm × 6 mm and is much smaller than most connector blocks typically encountered at 60 GHz. Figure II.3 shows a 3D cut-out view of the connector schematic, which provides mechanical support and ensures a good electrical contact between the cable and substrate by clamping the two objects firmly together.

There is an open rectangular hole in the block situated directly above the region where the fringing fields play a significant role (extending a little beyond the area covered by the footprint of cross-sections DD' to EE' in Figure II. 2). This open cavity ensures that fringing fields over the exposed part of the slots are not shorted out. The choice of an open rather than a closed cavity is made to avoid introducing resonances in the connector transfer function around 60 GHz and thus improve its broadband impedance match, at the risk of giving rise to unwanted small radiation losses, which were not observed experimentally.

LIST OF REFERENCES

[1] http://en.wikipedia.org/wiki/Body_area_network

[2] Campbell, P., Current population reports (population projections: States, 1995–2025), pp. 25–1131. Census Bureau, 2005.

[3] http://healthcare-economist.com/2006/01/30/trends-in-health-care

[4] J. Kim and Y. Rahmat-S , "I y: , , z ," *IEEE Trans. Microw. Theory Tech.*, vol. 52, pp. 1934 – 1943, Aug. 2004.

[5] U , S , H , H , S , B , K k, K S , "O A WBAN", *International Journal of Communication Systems* 982–999, 2010. doi:10.1002/dac.1100.

[6] K , Y N y , P H , "P -body ," *IEEE Antennas and Propagation Society Int. Symp.*, vol. 3A, pp. 475 – 478, July. 2005.

[ ] H , P S , "A B y ", *International Workshop on Antenna Technology: Small and Smart Antennas Metamaterials and Applications*, pp. 41–44, 2007.

[8] M. Hanson, H. Powell, A. Barth, K. Ringgenberg, B. Calhoun, J. Aylor, and J. Lach, "B y k : ," *Computer*, vol. 42, pp. 58 –65, Jan. 2009.

[9] IEEE standard 802.15.3c-2009. http://standards.ieee.org/findstds/standard/802.15.3c-2009.html. [Online; accessed 17-August-2013].

[10] IEEE standard 802.11ad. http://en.wikipedia.org/wiki/Wireless_Gigabit_Alliance. [Online; accessed 17-August-2013].

[11] Millimeter waves may be the future of 5G phones. http://spectrum.ieee.org/telecom/wireless/millimeter-waves-may-be-the-future-of-5g-phones. [Online; accessed 18-August-2013].

[12] Akhoondzadeh-Asl, L.; Hall, P.S.; Nechayev, Y.; Khan, I., "Depolarization in On-Body Communication Channels at 2.45 GHz," *Antennas and Propagation, IEEE Transactions on* , vol.61, no.2, pp.882,889, Feb. 2013.

[13] Akhoondzadeh-Asl, L.; Nechayev, Y.; Hall, P.S.; Constantinou, C.C., "Parasitic Array Antenna With Enhanced Surface Wave Launching for On-Body Communications," *Antennas and Propagation, IEEE Transactions on* , vol.61, no.4, pp.1976,1985, April 2013.

[14] Alomainy, A.; Yang Hao; Owadally, A.; Parini, C.G.; Nechayev, Y.; Constantinou, C.C.; Hall, P.S., "Statistical Analysis and Performance Evaluation for On-Body Radio Propagation With Microstrip Patch Antennas," *Antennas and Propagation, IEEE Transactions on* , vol.55, no.1, pp.245,248, Jan. 2007.

[15] Cotton, S.L.; Conway, G.A.; Scanlon, W.G., "A Time-Domain Approach to the Analysis and Modeling of On-Body Propagation Characteristics Using Synchronized Measurements at 2.45 GHz," *Antennas and Propagation, IEEE Transactions on*, vol.57, no.4, pp.943,955, April 2009.

[16] Cotton, S.L.; Scanlon, W.G., "Characterization and Modeling of the Indoor Radio Channel at 868 MHz for a Mobile Bodyworn Wireless Personal Area Network," *Antennas and Wireless Propagation Letters, IEEE*, vol.6, no., pp.51,55, 2007.

[17] Cotton, S.L.; Scanlon, W.G., "Channel Characterization for Single- and Multiple-Antenna Wearable Systems Used for Indoor Body-to-Body Communications," *Antennas and Propagation, IEEE Transactions on*, vol.57, no.4, pp.980,990, April 2009.

[18] Cotton, S.L.; Scanlon, W.G.; Conway, G.A., "Autocorrelation of signal facing in wireless body area networks," *Antennas and Propagation for Body-Centric Wireless Communications, 2009 2nd IET Seminar on* , vol., no., pp.1,5, 20-20 April 2009.

[19] Cotton, S.L.; Scanlon, W.G., "An experimental investigation into the influence of user state and environment on fading characteristics in wireless body area networks at 2.45 GHz," *Wireless Communications, IEEE Transactions on* , vol.8, no.1, pp.6,12, Jan. 2009.

[20] Cotton, S.L.; Scanlon, W.G.; Guy, J., "The $\kappa - \mu$ Distribution Applied to the Analysis of Fading in Body to Body Communication Channels for Fire and Rescue Personnel," *Antennas and Wireless Propagation Letters, IEEE* , vol.7, no., pp.66,69, 2008.

[21] Fort, A.; Desset, C.; Wambacq, P.; Biesen, L.V., "Indoor body-area channel model for narrowband communications," *Microwaves, Antennas & Propagation, IET*, vol.1, no.6, pp.1197,1203, Dec. 2007.

[22] Hu, Z.H.; Nechayev, Y.I.; Hall, P.S.; Constantinou, C.C.; Yang Hao, "Measurements and Statistical Analysis of On-Body Channel Fading at 2.45 GHz," *Antennas and Wireless Propagation Letters, IEEE* , vol.6, no., pp.612,615, 2007.

[23] Jian Zhang; Smith, D.B.; Hanlen, L.W.; Miniutti, D.; Rodda, D.; Gilbert, B., "Stability of Narrowband Dynamic Body Area Channel," *Antennas and Wireless Propagation Letters, IEEE* , vol.8, no., pp.53,56, 2009.

[24] Katayama, N.; Takizawa, K.; Aoyagi, T.; Takada, J.-i.; Huan-Bang Li; Kohno, R., "Channel model on various frequency bands for wearable Body Area Network," *Applied Sciences on Biomedical and Communication Technologies, 2008. ISABEL '08. First International Symposium on* , vol., no., pp.1,5, 25-28 Oct. 2008.

[25] Khan, I.; Nechayev, Y.I.; Hall, P.S., "On-Body Diversity Channel Characterization," *Antennas and Propagation, IEEE Transactions on*, vol.58, no.2, pp.573,580, Feb. 2010.

[ ] I K , Y I N y , P S H "S -order statistics of measured on-body y ", *Microwave and Optical Technology Letters*, 51(10):2335–2337, 2009.

[27] Nechayev, Y.I.; Hall, P.S.; Constantinou, C.; Yang Hao; Alomainy, A.; Dubrovka, R.; Parini, C.G., "On-body path gain variations with changing body posture and antenna position," *Antennas and Propagation Society International Symposium, 2005 IEEE* , vol.1B, no., pp.731,734 vol. 1B, 2005.

[28] Nechayev, Y.I.; Hu, Z.H.; Hall, P.S., "Short-term and long-term fading of on-body transmission channels at 2.45 GHz," *Antennas & Propagation Conference, 2009. LAPC 2009. Loughborough* , vol., no., pp.657,660, 16-17 Nov. 2009.

[29] Nechayev, Y.I.; Hall, P.S.; Hu, Z.H., "Characterisation of narrowband communication channels on the human body at 2.45 GHz," *Microwaves, Antennas & Propagation, IET* , vol.4, no.6, pp.722,732, June 2010.

[30] Smith, D.B.; Zhang, J.; Hanlen, L.W.; Miniutti, D.; Rodda, D.; Gilbert, B., "Temporal correlation of dynamic on-body area radio channel," *Electronics Letters* , vol.45, no.24, pp.1212,1213, November 19 2009.

[31] Tai, K.; Harada, H.; Kohno, R., "Channel Modeling and Signaling of Medical Implanted Communication Systems and a Step to Medical ICT," *Mobile and Wireless Communications Summit, 2007. 16th IST*, vol., no., pp.1,5, 1-5 July 2007.

[32] Takizawa, K.; Aoyagi, T.; Hamaguchi, K.; Kohno, R., "Performance evaluation of wireless communications through capsule endoscope," *Engineering in Medicine and Biology Society, 2009. EMBC2009. Annual International Conference of the IEEE*, vol., no., pp.6897,6900, 3-6 Sept. 2009.

[33] Bin Zhen; Minseok Kim; Takada, J.-i.; Kohno, R., "Characterization and Modeling of Dynamic On-Body Propagation at 4.5 GHz," *Antennas and Wireless Propagation Letters, IEEE*, vol.8, no., pp.1263,1267, 2009.

[34] Hall, P.S.; Yang Hao; Nechayev, Y.I.; Alomainy, A.; Constantinou, C.C.; Parini, C.; Kamarudin, M.R.; Salim, T.Z.; Hee, D.T.M.; Dubrovka, R.; Owadally, A.S.; Wei Song; Serra, A.; Nepa, P.; Gallo, M.; Bozzetti, M., "Antennas and propagation for on-body communication systems," *Antennas and Propagation Magazine, IEEE* , vol.49, no.3, pp.41,58, June 2007.

[35] Alomainy, A.; Yang Hao; Davenport, D.M., "Parametric Study of Wearable Antennas with Varying Distances from the Body and Different On-Body Positions," *Antennas and Propagation for Body-Centric Wireless Communications, 2007 IET Seminar on* , vol., no., pp.84,89, 24-24 April 2007.

[36] Klemm, M.; Kovcs, I.Z.; Pedersen, G.F.; Troster, G., "Novel small-size directional antenna for UWB WBAN/WPAN applications," *Antennas and Propagation, IEEE Transactions on*, vol.53, no.12, pp.3884,3896, Dec. 2005.

[37] See, T.S.P.; Zhi Ning Chen, "Experimental Characterization of UWB Antennas for On-Body Communications," *Antennas and Propagation, IEEE Transactions on*, vol.57, no.4, pp.866,874, April 2009.

[38] Alomainy, A.; Hao, Y.; Parini, C.G.; Hall, P.S., "Comparison between two different antennas for UWB on-body propagation measurements," *Antennas and Wireless Propagation Letters, IEEE*, vol.4, no., pp.31,34, 2005.

[39] Chahat, N.; Zhadobov, M.; Sauleau, R.; Ito, K., "A Compact UWB Antenna for On-Body Applications," *Antennas and Propagation, IEEE Transactions on*, vol.59, no.4, pp.1123,1131, April 2011.

[40] Alomainy, A.; Sani, A.; Rahman, A.; Santas, J.G.; Yang Hao, "Transient Characteristics of Wearable Antennas and Radio Propagation Channels for Ultrawideband Body-Centric Wireless Communications," *Antennas and Propagation, IEEE Transactions on* , vol.57, no.4, pp.875,884, April 2009.

[41] Abbasi, Q.H.; Sani, A.; Alomainy, A.; Yang Hao, "Arm movements effect on ultra wideband on-body propagation channels and radio systems," *Antennas & Propagation Conference, 2009. LAPC 2009. Loughborough*, vol., no., pp.261,264, 16-17 Nov. 2009.

[42] Alomainy, A.; Hao, Y.; Hu, X.; Parini, C.G.; Hall, P.S., "UWB on-body radio propagation and system modelling for wireless body-centric networks," *Communications, IEE Proceedings-* , vol.153, no.1, pp.107,114, 2 Feb. 2006.

[43] Alomainy, A.; Sani, A.; Rahman, A.; Santas, J.G.; Yang Hao, "Transient Characteristics of Wearable Antennas and Radio Propagation Channels for Ultrawideband Body-Centric Wireless Communications," *Antennas and Propagation, IEEE Transactions on* , vol.57, no.4, pp.875,884, April 2009.

[44] Fort, A.; Ryckaert, J.; Desset, C.; De Doncker, P.; Wambacq, P.; Van Biesen, L., "Ultra-wideband channel model for communication around the human body," *Selected Areas in Communications, IEEE Journal on* , vol.24, no.4, pp.927,933, April 2006.

[45] Goulianos, A.A.; Brown, T.; Stavrou, S., "Power delay profile modelling of the ultra wideband off-body propagation channel," *Microwaves, Antennas & Propagation, IET*, vol.4, no.1, pp.62,71, January 2010.

[46] Van Roy, S.; Oestges, C.; Horlin, F.; De Doncker, P., "On-body propagation velocity estimation using ultra-wideband frequency-domain spatial correlation analyses," *Electronics Letters*, vol.43, no.25, pp.1405,1406, Dec. 6 2007.

[47] Zasowski, T.; Meyer, G.; Althaus, F.; Wittneben, A., "UWB signal propagation at the human head," *Microwave Theory and Techniques, IEEE Transactions on*, vol.54, no.4, pp.1836,1845, June 2006.

[48] Zasowski, T.; Wittneben, A., "Performance of UWB Receivers with Partial CSI Using a Simple Body Area Network Channel Model," *Selected Areas in Communications, IEEE Journal on* , vol.27, no.1, pp.17,26, January 2009.

[49] W J k , “ ”, York Wiley, 1974.

[5] L R K , “ R S q ,” P IRE, , , November 1954.

[51] Turkmani, A.M.D.; Arowojolu, A.; Jefford, P.A.; Kellett, C.J., "An experimental evaluation of the performance of two-branch space and polarization diversity schemes at 1800 MHz," *Vehicular Technology, IEEE Transactions on* , vol.44, no.2, pp.318,326, May 1995.

[5] K k , J H kk , K k k , “W ” , European Conference on Antennas and Propagation. pp. 1-6, 2006.

[53] Matthews, J.C.G.; Pettitt, G., "Development of flexible, wearable antennas," *Antennas and Propagation, 2009. EuCAP 2009. 3rd European Conference on*, vol., no., pp.273,277, 23-27 March 2009

[54] Massey, P.J., "Mobile phone fabric antennas integrated within clothing," *Antennas and Propagation, 2001. Eleventh International Conference on (IEE Conf. Publ. No. 480)*, vol.1, no., pp.344,347 vol.1, 2001

[55] Salonen, P.; Sydanheimo, L., "Development of an S-band flexible antenna for smart clothing," *Antennas and Propagation Society International Symposium, 2002. IEEE*, vol.3, no., pp.6,9, 16-21 June 2002

[56] Salonen, P.; Hurme, L., "A novel fabric WLAN antenna for wearable applications," *Antennas and Propagation Society International Symposium, 2003. IEEE*, vol.2, no., pp.700,703 vol.2, 22-27 June 2003

[57] Yuehui Ouyang; Karayianni, E.; Chappell, W.J., "Effect of fabric patterns on electrotextile patch antennas," *Antennas and Propagation Society International Symposium, 2005 IEEE* , vol.2B, no., pp.246,249 vol. 2B, 3-8 July 2005

[58] Klemm, M.; Locher, I.; Troster, G., "A novel circularly polarized textile antenna for wearable applications," *Wireless Technology, 2004. 7th European Conference on*, vol., no., pp.285,288, 11-12 Oct. 2004

[59] Salonen, P.; Rahmat-Samii, Y.; Hurme, H.; Kivikoski, M., "Dual-band wearable textile antenna," *Antennas and Propagation Society International Symposium, 2004. IEEE*, vol.1, no., pp.463,466 Vol.1, 20-25 June 2004

[60] Shih-Hsun Hsu; Kai Chang, "Ultra-thin CPW-fed rectangular slot antenna for UWB applications," *Antennas and Propagation Society International Symposium 2006, IEEE* , vol., no., pp.2587,2590, 9-14 July 2006

[61] Tronquo, A.; Rogier, H.; Hertleer, C.; Van Langenhove, L., "Robust planar textile antenna for wireless body LANs operating in 2.45 GHz ISM band,"*Electronics Letters* , vol.42, no.3, pp.142,143, 2 Feb. 2006

[62] Tronquo, A.; Rogier, H.; Hertleer, C.; Van Langenhove, L., "Applying textile materials for the design of antennas for wireless body area networks,"*Antennas and Propagation, 2006. EuCAP 2006. First European Conference on*, vol., no., pp.1,5, 6-10 Nov. 2006

[63] Hertleer, C.; Rogier, H.; Van Langenhove, L., "A TEXTILE ANTENNA FOR PROTECTIVE CLOTHING," *Antennas and Propagation for Body-Centric Wireless Communications, 2007 IET Seminar on*, vol., no., pp.44,46, 24-24 April 2007

[64] Qiang Bai; Langley, R., "Wearable EBG antenna bending," *Antennas and Propagation, 2009. EuCAP 2009. 3rd European Conference on*, vol., no., pp.182,185, 23-27 March 2009

[65] Bai, Q.; Langley, R., "Crumpled textile antennas," *Electronics Letters*, vol.45, no.9, pp.436,438, April 23 2009

[66] Zhu, S.; Langley, R., "Dual-band wearable antennas over EBG substrate," *Electronics Letters*, vol.43, no.3, pp.141,142, Feb. 1 2007

[67] Salonen, P.; Keskilammi, M., "SoftWear Antenna," *Military Communications Conference, 2008. MILCOM 2008. IEEE*, vol., no., pp.1,6, 16-19 Nov. 2008

[68] Salonen, P.; Rahmat-Samii, Y., "Textile Antennas: Effects of Antenna Bending on Input Matching and Impedance Bandwidth," *Aerospace and Electronic Systems Magazine, IEEE* , vol.22, no.12, pp.18,22, Dec. 2007

[69] Tanaka, M.; Jae-Hyeuk Jang, "Wearable microstrip antenna," *Antennas and Propagation Society International Symposium, 2003. IEEE*, vol.2, no., pp.704,707 vol.2, 22-27 June 2003

[70] Lea, A.; Ping Hui; Ollikainen, J.; Vaughan, R.G., "Propagation Between On-Body Antennas," *Antennas and Propagation, IEEE Transactions on*, vol.57, no.11, pp.3619,3627, Nov. 2009

[71] M.U. Rehman, Y. Gao, X. Chen, C.G. Parini, Z Y , B , J W Z " O - y k : E j " I *Loughborough Antennas and Propagation Conference, 2008*, pages 97– 100, 2008.

[ ] L Ak z *"Polarization behaviour of on-body communication channels at 2.45 GHz"*. PhD thesis, University of Birmingham, July 2011.

[73] Yener, A.; Yates, R.D.; Ulukus, Sennur, "Interference management for CDMA systems through power control, multiuser detection, and beamforming," *Communications, IEEE Transactions on* , vol.49, no.7, pp.1227,1239, Jul 2001

[74] Hanlen, L.W.; Miniutti, D.; Rodda, D.; Gilbert, B., "Interference in body area networks: Distance does not dominate," *Personal, Indoor and Mobile Radio Communications, 2009 IEEE 20th International Symposium on* , vol., no., pp.281,285, 13-16 Sept. 2009.

[5] L W H , , S , R , B G " -channel interference in body area networks with indoor measurements at 2.4 GHz: Distanceto- interferer is a poor " *International Journal of Wireless Information Networks*, pp.113–125, 2010.

[76] Zhang, A.; Hanlen, L.W.; Miniutti, D.; Rodda, D.; Gilbert, B., "Interference in body area networks: Are signal-links and interference-links independent?," *Personal, Indoor and Mobile Radio Communications, 2009 IEEE 20th International Symposium on* , vol., no., pp.456,460, 13-16 Sept. 2009.

[ ] , N , Z ,) "A B y W Commun W q "

[78] N , Z , R S , " -GHz textile antenna array for bodycentric ," *IEEE Transactions on Antennas and Propagation*, vol. 61, no. 4, pp. 1816–1824, Apr. 2013.

[79] N. Chahat, Z , R S , "W -fire textile antenna for onbody GHz," *IEEE Antennas Wirel. Propag. Letters*, vol. 11, pp. 799–802, 2012

[ ] G , A R ; , N ; L , ; Z , ; S , R "E -Fire Antenna for BAN at 60 GHz: Impact of Bending, On-B y P ", S y O O - Body Scenario. *Electronics* **2014**, *3*, 221-233.

[81] Chandra, D.; Shrivastava, P.; Rao, T.R., "Design of Antipodal Linear Tapered Slot Antenna using SIW at 60GHz for Gigabit Wireless communications," *Communications and Signal Processing (ICCSP), 2013 International Conference on* , vol., no., pp.88,91, 3-5 April 2013

[82] Brzezina, G.; Amaya, R.E.; Petosa, A.; Roy, L., "Broadband and compact Vivaldi arrays in LTCC for 60 GHz point-to-point networks," *Wireless and Microwave Technology Conference (WAMICON), 2014 IEEE 15th Annual*, vol., no., pp.1,5, 6-6 June 2014

[83] Wu, X.Y.; Akhoondzadeh-Asl, L.; Wang, Z.P.; Hall, P.S., "Novel Yagi-Uda antennas for on-body communication at 60GHz," *Antennas and Propagation Conference (LAPC), 2010 Loughborough*, vol., no., pp.153,156, 8-9 Nov. 2010

[84] Kovacs, I.; Pedersen, G.F.; Eggers, P.C.F.; Olesen, K., "Ultra wideband radio propagation in body area network scenarios," *Spread Spectrum Techniques and Applications, 2004 IEEE Eighth International Symposium on* , vol., no., pp.102,106, 30 Aug.-2 Sept. 2004.

[85] S. Dusara. *Radio-over-fibre systems for body-centric communication measurements*. PhD thesis, University of Birmingham, 2011.

[86] M , N , "I z GHz k ", IEEE A P , 5 , , - 3189, Dec. 2004.

[ ] Z k, , "W S W odel for the 60 GHz I R ", IEEE V , 5 , , : - 1277, 2005.

[ ] IEEE P 5, "W P A N k , G S - R " , , IEEE 5 -07-0584-01-003c)

[89] Collon , S , "I y -band characteristics of the 60 GHz ", IEEE W , , - 2406, Nov. 2004.

[ ] S L, S W G, B K, "S -Wave Channels for Short-Range Body-to-B y ", E A P , Barcelona, Spain, EuCAP, 12-16 April 2010

[91] Gallo, M.; Hall, P.S.; Qiang Bai; Nechayev, Y.I.; Constantinou, C.C.; Bozzetti, M., "Simulation and Measurement of Dynamic On-Body Communication Channels," *Antennas and Propagation, IEEE Transactions on*, vol.59, no.2, pp.623,630, Feb. 2011

[92] Khan, I.; Nechayev, Y.I.; Ghanem, K.; Hall, P.S., "BAN-BAN Interference Rejection With Multiple Antennas at the Receiver," *Antennas and Propagation, IEEE Transactions on*, vol.58, no.3, pp.927,934, March 2010.

[93] Hall, P.S.; Yang Hao; Nechayev, Y.I.; Alomainy, A.; Constantinou, C.C.; Parini, C.; Kamarudin, M.R.; Salim, T.Z.; Hee, D.T.M.; Dubrovka, R.; Owadally, A.S.; Wei Song; Serra, A.; Nepa, P.; Gallo, M.; Bozzetti, M., "Antennas and propagation for on-body communication systems," *Antennas and Propagation Magazine, IEEE* , vol.49, no.3, pp.41,58, June 2007.

[94] Wu, X.Y.; Akhoondzadeh-Asl, L.; Wang, Z.P.; Hall, P.S., "Novel Yagi-Uda antennas for on-body communication at 60GHz," *Antennas and Propagation Conference (LAPC), 2010 Loughborough*, vol., no., pp.153,156, 8-9 Nov. 2010.

[95]Orfanidis, S. J., Electromagnetic Waves and Antennas, Rutgers University, Feb. 2008

[96] Yan, L.; Hong, W.; Wu, K.; Cui, T.J., "Investigations on the propagation characteristics of the substrate integrated waveguide based on the method of lines," *Microwaves, Antennas and Propagation, IEE Proceedings*, vol.152, no.1, pp.35,42, 19 Feb. 2005.

[97] Abhijith, B.N.; Akhtar, M.J., "Optimization of Vivaldi antenna for microwave imaging applications," *Antennas and Propagation Society International Symposium (APSURSI), 2014 IEEE*, vol., no., pp.1596,1597, 6-11 July 2014.

[98] Pellegrini, A.; Brizzi, A.; Zhang, L.; Ali, K.; Hao, Y.; Wu, X.; Constantinou, C.C.; Nechayev, Y.; Hall, P.S.; Chahat, N.; Zhadobov, M.; Sauleau, R., "Antennas and Propagation for Body-Centric Wireless Communications at Millimeter-Wave Frequencies: A Review [Wireless Corner]," *Antennas and Propagation Magazine, IEEE* , vol.55, no.4, pp.262,287, Aug. 2013

[99] Deslandes, D.; Ke Wu, "Design Consideration and Performance Analysis of Substrate Integrated Waveguide Components," *Microwave Conference, 2002. 32nd European* , vol., no., pp.1,4, 23-26 Sept. 2002.

[100] Kai, T.; Hirokawa, J.; Ando, M., "A stepped post-wall waveguide with aperture interface to standard waveguide," *Antennas and Propagation Society International Symposium, 2004. IEEE*, vol.2, no., pp.1527,1530 Vol.2, 20-25 June 2004.

[101] Deslandes, D.; Ke Wu, "Integrated microstrip and rectangular waveguide in planar form," *Microwave and Wireless Components Letters, IEEE* , vol.11, no.2, pp.68,70, Feb. 2001.

[102] Simpson, J.J.; Taflove, A.; Mix, J.A.; Heck, H., "Computational and experimental study of a microwave electromagnetic bandgap structure with waveguiding defect for potential use as a bandpass wireless interconnect," *Microwave and Wireless Components Letters, IEEE* , vol.14, no.7, pp.343,345, July 2004.

[103] Wu, X.Y.; Hall, P.S., "Substrate integrated waveguide Yagi-Uda antenna," *Electronics Letters*, vol.46, no.23, pp.1541,1542, November 11 2010.

[104] Deslandes, D.; Ke Wu, "Analysis and Design of Current Probe Transition From Grounded Coplanar to Substrate Integrated Rectangular Waveguides," *Microwave Theory and Techniques, IEEE Transactions on*, vol.53, no.8, pp.2487,2494, Aug. 2005.

[105] Rod Waterhouse, Printed Antennas for Wireless Communications, John Wiley & Sons, 11 Mar 2008

[106] Puskely, J.; Mikulasek, T., "Compact wideband Vivaldi antenna array for microwave imaging applications," *Antennas and Propagation (EuCAP), 2013 7th European Conference on*, vol., no., pp.1519,1522, 8-12 April 2013.

[ ] X Y W "Antennas and propagation for body area networks at 60 GHz" PhD thesis, University of Birmingham, September 2013

[108] Nechayev, Y.I.; Xianyue Wu; Constantinou, C.C.; Hall, P.S., "Millimetre-wave path-loss variability between two body-mounted monopole antennas," *Microwaves, Antennas & Propagation, IET* , vol.7, no.1, pp.1,7, January 11 2013.

[109] Reusens, E.; Joseph, W.; Latre, B.; Braem, B.; Vermeeren, G.; Tanghe, E.; Martens, L.; Moerman, I.; Blondia, C., "Characterization of On-Body Communication Channel and Energy Efficient Topology Design for Wireless Body Area Networks," *Information Technology in Biomedicine, IEEE Transactions on* , vol.13, no.6, pp.933,945, Nov. 2009.

[110] I. Khan. *Diversity and MIMO for body-centric wireless communication channels*. PhD thesis, University of Birmingham, December 2009.

[111]L. Petrillo, T. Mavridis, J. Sarrazin, A. Benlarbi- P k “S On- y R GH z” IEEE Transactions on Antennas and Propagation, Vol. 63, No. 1 Jan. 2015

[ ] Y I N y , , X Y W , P S H , “De-polarization of On- y P z y GHz”, IEEE Transactions on Antennas and Propagation, Vol. 62, No. 12, Dec, 2014

[113] X L , Y I N y , P S H , “ -hop Channel Modeling at 60 GHz for On-body ” , The 8th European Conference on Antenna and Propagation, pp.2286-2289, April, 2014

[114] E. Reusens, W.Joseph, B. Latr´e, B. Braem, G. Vermeeren, E. T. Luc Martens, I. Moerman, and C. Blondia, "Characterization of On-Body Communication Channel and Energy Efficient Topology Design for Wireless Body Area Networks," IEEE Trans. Information Technology in Biomedicine, vol. 13, no. 6, pp. 933-945, 2009.

[115] Bereka, D.; Gopinath, A.; Sainati, B., "Design of a 60GHz integrated antenna on silicon substrate," *Antennas and Propagation Society International Symposium (APSURSI), 2014 IEEE*, vol., no., pp.1063,1064, 6-11 July 2014.

[116] Pan, H.K., "Dual-polarized Mm-wave phased array antenna for multi-Gb/s 60GHz communication," *Antennas and Propagation (APSURSI), 2011 IEEE International Symposium on* , vol., no., pp.3279,3282, 3-8 July 2011.

[117] Wu, X.Y.; Akhoondzadeh-Asl, L.; Wang, Z.P.; Hall, P.S., "Novel Yagi-Uda antennas for on-body communication at 60GHz," *Antennas and Propagation Conference (LAPC), 2010 Loughborough* , vol., no., pp.153,156, 8-9 Nov. 2010.

[118] Chahat, N.; Zhadobov, M.; Le Coq, L.; Sauleau, R., "Wearable Endfire Textile Antenna for On-Body Communications at 60 GHz," *Antennas and Wireless Propagation Letters, IEEE* , vol.11, no., pp.799,802, 2012

[119] Wu, X.Y.; Nechayev, Y.I.; Constantinou, C.C.; Hall, P.S., "Investigation of inter-user interference of wireless body area networks at 60 GHz," *Antennas and Propagation Society International Symposium (APSURSI), 2012 IEEE* , vol., no., pp.1,2, 8-14 July 2012.

[ ] X L , Y I N y , P S H , “ -hop Channel Modeling at 60 GHz for On- y ”, th European Conference on Antenna and Propagation, pp.2286-2289, April, 2014

[121] Y I N y , X W , , P S H " E B y P P G GH z" European Conference on Antenna and Propagation, pp.3397-3401, 2012.

[ ] W k , E , E G β G, "A 60 GHz OFDM Indoor Localization System Based on DTDOA", Processing.

[123] Hu, Z.H.; Nechayev, Y.I.; Hall, P.S.; Constantinou, C.C.; Yang Hao, "Measurements and Statistical Analysis of On-Body Channel Fading at 2.45 GHz," *Antennas and Wireless Propagation Letters, IEEE* , vol.6, no., pp.612,615, 2007.

[124] P.S. Hall, Y. Hao and Y.I. Nechayev et al, "Antenna and propagation for on-body communication systems," IEEE Antennas and Propagation Magazine, vol. 49, no. 3, pp. 41-58, 2007.

[125] A.R. Guraliuc, A.A. Serra, P. Nepa, G. Manara and F. Potorti, "Detection and classification of human arm movements for physical rehabilitation," 2010 IEEE Antennas and Propagation Society International Symposium (APSURSI), 2010.

[126] Zhen B, Patel M, Lee S, Won E, Astrin A (2008) TG6 technical requirements document (TRD) IEEE P802.15-08-0644- 09-0006. https://mentor.ieee.org/802.15

[ ] A, R A, H , S J, I J) "A review of channel modelling for wireless body area network in wireless medical " I : y communications. Saariselka, Finland

[128] K. Y. Yazdandoost and K. Sayrafian-P , " y k (BAN)," *Networks*, p. 91, 2009.

[129] Nechayev, Y.; Constantinou, C.; Swaisaenyakorn, S.; Rakibet, O.; Batchelor, J.; Hall, P.; Parini, C.; Hunt, J., "Use of motion capture for path gain modelling of millimetre-wave on-body communication links," *Antennas and Propagation (ISAP), 2012 International Symposium on* , vol., no., pp.987,990, Oct. 29 2012-Nov. 2 2012